Effect of Electroacidification on Ultrafiltration Performance and Physicochemical Properties of Soy Protein Extracts

by

Jana Skořepová

A thesis
presented to the University of Waterloo
in fulfillment of the thesis requirement for the degree of
Doctor of Philosophy
in
Chemical Engineering

Waterloo, Ontario, Canada, 2007

I hereby declare that I am the sole author of this thesis. This is a true copy of the thesis, including any required final revisions, as accepted by my examiners.

I understand that my thesis may be made electronically available to the public.

Abstract

A novel approach for the production of soy protein isolates was investigated integrating electroacidification and membrane ultrafiltration. The effect of electroacidification on the ultrafiltration performance and physicochemical properties of the soy protein extracts was obtained by comparing an electroacidified (pH 6) and a non-electroacidified (pH 9) soy protein extract.

The effect of membrane fouling on the permeate flux decline was studied in a hollow fiber and a dead end ultrafiltration system. Due to more significant membrane fouling, the permeate flux was always lower for the electroacidified extract, resulting in at least 1.5-fold increase in the total fouling resistance compared to the non-electroacidified extract. The total amount of protein deposited on the membrane surface during unstirred dead-end ultrafiltration was comparable (about 7 mg/cm^2) for both soy protein extracts. The discrepancy between the total fouling resistance and the protein deposition estimates was attributed to the formation of denser (less permeable) fouling deposit for the electroacidified extract, which was supported by scanning electron microscopy studies of fouled membranes.

The removal of carbohydrates and minerals was evaluated for direct ultrafiltration and two-stage discontinuous diafiltration using a hollow fiber system. The carbohydrate removal results were always consistent with the theoretical predictions, indicating that the carbohydrates were freely permeable across the membrane. In contrast, the minerals were partially retained by the membrane, but to a higher extent for the non-electroacidified extract, which demonstrated that the electroacidification pretreatment enhanced the mineral removal during the ultrafiltration. Incorporation of the diafiltration step improved the ash (mineral) and carbohydrate removal. Stronger electrostatic interactions between soy proteins, calcium/magnesium, and phytic acid (antinutrient) at alkaline pH resulted in less efficient removal of calcium, magnesium, and phytic acid during the ultrafiltration of the non-electroacidified extract compared to the electroacidified extract. Consequently, the soy protein isolates produced by electroacidification and the hollow fiber

ultrafiltration had a lower mineral and phytic acid content. The protein content was at least 88 % (dry basis), with or without the electroacidification pretreatment.

The study of the viscosity revealed that the electroacidification pretreatment reduced the viscosity of the soy protein extract, which resulted in a lower axial pressure drop increase during the ultrafiltration of the electroacidified extract compared to the non-electroacidified extract. Adjusting the pH of the electroacidified extract to 9 and the pH of the non-electroacidified extract to 6 had a great impact on the particle size distribution but only a marginal effect on the viscosity of the pH adjusted extracts. This indicated that the pH and the particle size distribution were not responsible for the viscosity difference between the electroacidified and the non-electroacidified soy protein extracts. It was proposed that the electroacidification pretreatment had some impact on the water hydration capacity of the soy proteins, which consequently affected the viscosity.

Acknowledgements

I would like to express my sincere thanks to my supervisor, Dr. Christine Moresoli, for giving me the opportunity to work on this project. I am very grateful for her invaluable advice, support, and encouragement that made completion of my thesis possible.

I would like to acknowledge the National Sciences and Engineering Research of Canada for funding and Agriculture and Agri-Food Canada for providing me the soy protein extracts. I also wish to thank Dr. Martin Mondor (Agriculture and Agri-Food Canada) for his help with the protein content analysis as well as his useful comments and suggestions about my work.

I wish to thank Mark Sobon (Civil Engineering) for his help with the mineral analysis, Nina Heinig (Chemistry) for her assistance with the scanning electron microscopy, Dr. Elizabeth Meiering (Chemistry) for allowing me using the dynamic light scattering instrument, and Dr. Milena Corredig (University of Guelph) for the samples of purified soy proteins.

Many thanks to my thesis reviewers, Dr. Raymond Legge, Dr. Xianshe Feng, Dr. Tong Leung, and Dr. Robert Lencki (University of Guelph), for their constructive and helpful feedback.

A big “Thank You” goes to all the people from my lab: Maja for being a wonderful friend, Dom and Joe for all their advice and help, Kela for his infectious enthusiasm (high-five!), Barbara and Laetitia for their help and contributions to my work, and the list would not be complete without mentioning Vic, Mary, Seung Mi, Amin, Rand, Ramila, Sonja, Stephanie, Magali, and many other people…it was a pleasure meeting all of you. I will never forget how much fun we had during bowling on Fridays…I will miss you guys a lot.

I would like to thank Sarah and Marc for providing me a home and a great deal of support during the last three months of finishing my degree. Writing my thesis with a cup of hot tea and their cat Spooky on my lap was definitely very calming.

My warmest thanks go to my family, especially my father Zdenek, my brother Petr, and my sister Daniela for their livelong support and care.

Finally…I can not possibly express how much I thank you, Petr, for being there for me…and all the great adventures we experienced in Canada (and before) and I hope there is many more to come.

LIST OF CONTENTS

LIST OF FIGURES

LIST OF TABLES

NOMENCLATURE

Roman letters

a	particle radius (m)
A	proportionality constant (mL/g)
A_M	membrane area (m^2)
c_B	solute concentration in bulk (kg/m^3 or g/mL)
c_R	protein concentration in the retentate (g/L)
c_F	protein concentration in the feed (g/L)
d	particle diameter (m)
F	Faraday constant (C/mol)
I	ionic strength (mol/m^3)
J_0	permeate flux at t = 0 ($L/m^2.h$ or m/s)
J_P	permeate flux ($L/m^2.h$ or m/s)
J_W	water flux ($L/m^2.h$ or m/s)
k	rate constant (s^{-1} or min^{-1})
l	length (m)
P_{in}	inlet pressure (Pa or psi)
P_{out}	outlet pressure (Pa or psi)
P_p	pressure on the permeate side (Pa or psi)
ΔP	axial pressure drop (Pa or psi)
R	gas constant (J/mol K)
R_F	resistance of fouling (m^{-1})
R_I	resistance of irreversible fouling (m^{-1})
R_M	clean membrane resistance (m^{-1})
R_R	resistance of reversible fouling (m^{-1})
R_T	total hydraulic resistance (m^{-1})
s	shape factor (-)
t	time (s or min)
T	temperature (K)
TMP	transmembrane pressure (Pa or psi)

u	electrophoretic mobility (m^2/V.s)
v	flow velocity (m/s)
VCR	volume concentration ratio (-)
V_F	initial feed volume (m^3)
V_P	cumulative permeate volume (m^3)
V_R	retentate volume (m^3)

Greek letters

α	specific cake resistance (m/kg)
ε	porosity (-)
ε_m	medium permittivity (C^2/N m^2)
ζ	zeta potential (V or mV)
η	dynamic viscosity (Pa.s)
η_P	dynamic viscosity of permeate (Pa.s)
υ_h	specific hydrodynamic volume (mL/g)
κ^{-1}	thickness of electrical double layer (m)
μ	kinematic viscosity (m^2/s)
ρ	particle density (kg/m^3)
φ	volume fraction (-)

1

Research Aim and Outline

Soybeans contain about 40 % of protein (dry basis), the highest protein content among legumes and cereals, thus representing a great source of non-animal protein. Soy proteins are highly digestible and their amino acid profile is well-balanced to meet the requirements for human nutrition. Consumption of soy proteins has been associated with health benefits such as lower risk of coronary heart disease, which was recognized by the U.S. Food and Drug Association in 1999 through the authorization of a health claim for food products containing soy proteins. In addition to the nutritional benefits, soy proteins have good functional properties, including water and fat binding, thickening, gelling, emulsification, and foam formation, which impart the texture and mouth-feel properties of the finished foods. Soy protein ingredients are used in a variety of food applications including meat and dairy products, bakery, breakfast cereals, infant formulas, and beverage powders.

According to the protein content, soy protein ingredients are divided into grits and flours (about 60 % protein, dry basis), soy protein concentrates (70 % protein minimum, dry basis), and soy protein isolates (90 % protein minimum, dry basis). The conventional methods for the production of the soy protein concentrates and isolates involve the use of solvents, concentrated acids and alkali, or heat treatment. Such processing conditions can result in protein denaturation and loss of solubility, reducing the quality of the soy protein ingredients. In the production of soy protein isolates, large volumes of acid whey-like effluents are generated (containing relatively high quantities of proteineous material), which may impose a water pollution risk. Therefore, alternative methods that will preserve the protein functionality and at the same time, will be environmentally cleaner are sought after.

Membrane ultrafiltration presents an attractive and technologically viable solution. The advantages of membrane ultrafiltration for the production of soy protein concentrates or isolates include mild processing conditions (no use of concentrated acids or alkali and moderate temperatures). Research indicates that the concentration of soy proteins by membrane ultrafiltration results in products with improved solubility, superior functional properties, and lower phytic acid (antinutrient) content. The disadvantages of membrane processing include permeate flux decline due to membrane fouling, which requires cleaning or replacing the membrane. Yet, membrane ultrafiltration has commercial

application in the dairy industry for the fractionation of cheese whey and the concentration of milk for cheese production. The feasibility of membrane ultrafiltration for milk and whey processing, considering their complex composition (proteins, fat, carbohydrates, minerals), suggests that industrial application of membrane ultrafiltration for the production of soy protein concentrates and isolates is a realistic consideration.

This thesis investigates a novel approach for the production of soy protein isolates by a combination of electroacidification and membrane ultrafiltration. As illustrated in **Figure 1.1**, the process involves alkaline extraction of defatted soy flakes to obtain a soy protein extract at pH 9 (SPE 9). The pH of the soy protein extract is gradually adjusted to 6 during electroacidification, which is based on the use of bipolar membranes to split water into hydroxyl and hydrogen ions. In the electrical field, the hydrogen ions migrate towards the cathode, while acidifying the soy protein extract solution. The electroacidified soy protein extract (SPE 6) is subjected to membrane ultrafiltration for purification and concentration of soy proteins. Gradual acidification of the soy protein extract without the use of concentrated acids should minimize the loss of protein solubility due to protein denaturation, while membrane ultrafiltration should allow for the removal of undesirable low molecular weight components and yield a highly purified soy protein isolate.

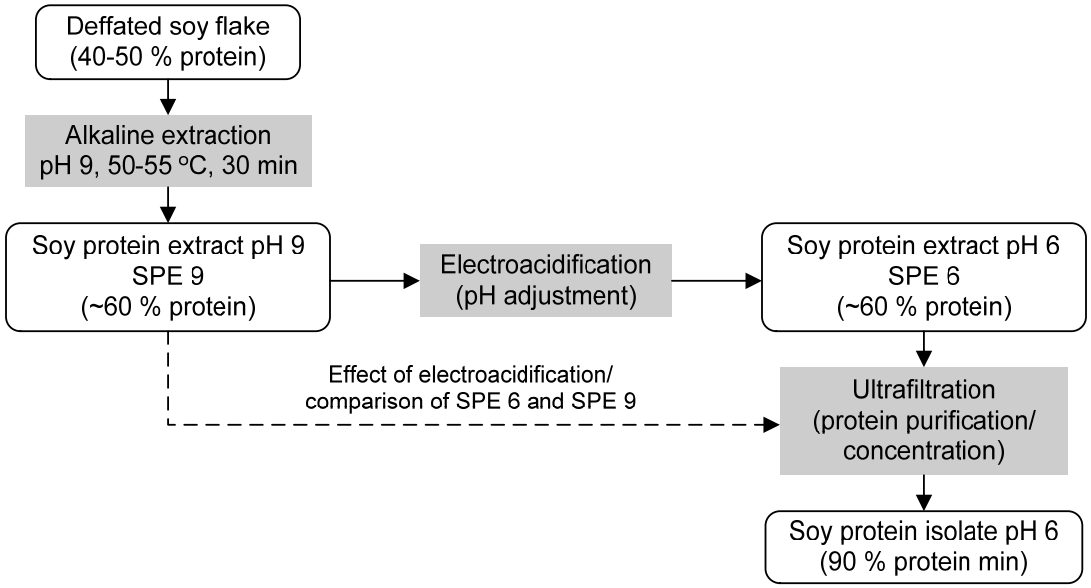

Figure 1.1 Production of soy protein isolates by electroacidification and ultrafiltration.

It should be noted that the alkaline extraction and electroacidification were not part of this study. The electroacidified and the non-electroacidified soy protein extracts were kindly provided by Agriculture and Agri-Food Canada. The objective of this work was to investigate the effect of electroacidification on the ultrafiltration performance by comparing the behavior of the electroacidified and non-electroacidified soy protein extract. The ultrafiltration performance was compared in terms of the efficiency of the carbohydrate, mineral, and phytic acid removal, the permeate flux decline and membrane fouling, and the axial pressure drop profile. The physicochemical properties (particle size distribution, zeta potential, viscosity) of the soy protein extracts were investigated.

Chapter 2 provides a theoretical background on the membrane ultrafiltration, the consideration of the electrostatic effects and their influence on the solute-solute and solute-membrane interactions, and characteristics of the soy proteins. The removal of carbohydrates, minerals, and phytic acid during the ultrafiltration of the soy protein extracts in a cross-flow (hollow fiber) system is discussed in Chapter 3. The permeate flux decline and the axial pressure drop increase observed during the hollow fiber ultrafiltration are further investigated in Chapters 4 and 5, respectively. Chapter 4 provides a detailed analysis of the membrane fouling in a dead-end ultrafiltration system, including the estimation of the fouling resistance, the morphology of the fouling deposits, and the quantification of protein and mineral deposition. Chapter 5 investigates the axial pressure drop increase during the hollow fiber ultrafiltration and considers the effect of electroacidification on the flow and physicochemical properties of the soy protein extracts. Chapters 3, 4, and 5 are organized in a publication format, having their own abstract, introduction, materials and methods, results and discussion, and conclusion. The most significant findings of this work are emphasized in Chapter 6, along with the recommendations for the future research.

2

Introduction

2.1 Ultrafiltration

Ultrafiltration is a pressure-driven membrane separation process that is used for concentration and purification of macromolecular solutions. The pore size of ultrafiltration membranes is typically characterized by molecular weight cut-off (MWCO), which indicates the molecular weight of a component with 90 % membrane retention. The MWCO of ultrafiltration membranes ranges between 1–1000 kDa. The components are mainly separated based on their molecular weight, but in some cases, the separation may be also governed by other factors (e.g., charge). Ultrafiltration can be operated in a dead-end or a cross-flow configuration, as illustrated in **Figure 2.1**.

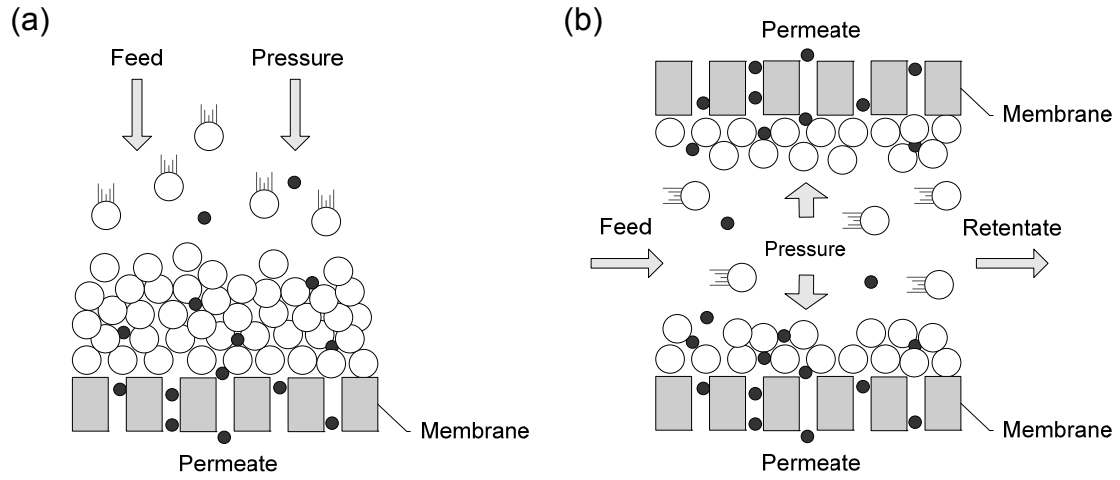

Figure 2.1 Dead-end (a) and cross-flow (b) configuration.

Convective forces induced by the pressure gradient across the membrane (transmembrane pressure) and the permeate flow bring the solutes towards the membrane surface. Components with a lower molecular weight than the membrane MWCO are transported across the membrane along with the solvent, whereas the larger components are retained by the membrane and may accumulate on the top. Membrane fouling is usually more pronounced in the dead-end configuration, where the flow is perpendicular to the membrane surface (**Figure 2.1** (a)). In contrast, membrane fouling is usually reduced in the cross-flow configuration, because the tangential flow removes some of the accumulated solutes from the membrane surface (**Figure 2.1** (b)). The feed refers to the stream, which enters the filtration process. The concentrated solution of the retained components collected on the upstream side of the membrane is called the retentate. The

stream, containing the low molecular weight components that passed through the membrane pores, is the permeate.

Dead-end ultrafiltration is usually performed in a cylindrical cell with a flat sheet membrane resting on a support grid or corrugated plate (**Figure 2.2**). The cell can be pressurized by compressed nitrogen or air. A magnetic stirring bar can be used to minimize membrane fouling and enhance the permeate flux. The device can be easily disassembled for cleaning and/or membrane replacement before the next operation. Ultrafiltration cells are especially suitable for laboratory scale applications such as research or process development.

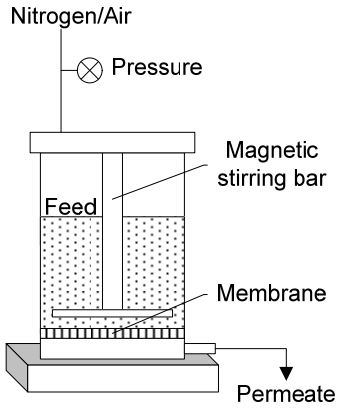

Figure 2.2 Dead-end ultrafiltration cell.

The most common examples of cross-flow systems include hollow fiber, flat sheet, and spiral wound membrane modules, which are mainly used for larger-scale industrial processing, including food and biotechnological applications. In this work, hollow fiber ultrafiltration will be considered. The membrane modules consist of a bundle of hollow fibers with a diameter ranging between 0.25 and 2.5 mm. The fibers are housed in a cartridge shell and fixed at both ends by an epoxy resin. The feed flows through the lumen of the fibers and the permeate passes through the fiber walls to the shell side. The small diameter of the hollow fibers provides high shear rates (4000–14000 s^{-1}) and low Reynolds numbers, typically between 500 and 3000, corresponding to laminar to turbulent flow regime. Advantages of hollow fiber membranes include high membrane packing density and low pumping costs when compared with other ultrafiltration modules [1,2].

2.1.1 Permeate flux

According to Darcy's law (2-1), the permeate flux (J_P) is a linear function of the transmembrane pressure (TMP):

$$J_P = \frac{TMP}{\eta_P R_T} \tag{2-1}$$

where η_P is the viscosity of the permeate and R_T is the total hydraulic resistance to flow. The resistance of the clean membrane is dependent on the porosity and thickness of the membrane and the morphology of the porous structure (pore tortuosity) [3]. The clean membrane resistance can be estimated by measuring the pure water flux as a function of transmembrane pressure and applying Eq. (2-1). During the filtration, retained components will accumulate on the top of the membrane or within the membrane pores, resulting in membrane fouling and increase in the hydraulic resistance. The total hydraulic resistance (R_T) then consists of the clean membrane resistance (R_M) and the resistance exerted by the fouling layer (R_F), which can be determined from the resistance-in-series model (2-2). The fouling resistance (R_F) can be further divided into two fouling components, the reversible (R_R) and irreversible (R_I) fouling resistance. The former takes into account the solutes, which are loosely deposited on the membrane surface and can be removed by rinsing the membrane with water. The latter involves strongly bound solutes, which can not be removed from the membrane without chemical cleaning.

$$R_T = R_M + R_F = R_M + R_R + R_I \tag{2-2}$$

The transmembrane pressure (TMP) in cross-flow ultrafiltration can be calculated, according to Eq. (2-3):

$$TMP = \frac{(P_{in} + P_{out})}{2} - P_p \tag{2-3}$$

where P_{in}, P_{out}, and P_p represent the pressure measured at the inlet and outlet of the membrane module and on the permeate side, respectively. As illustrated in **Figure 2.3**, the pressure difference between the module inlet and outlet is referred to as the axial pressure drop, i.e.:

$$\Delta P = P_{in} - P_{out} \tag{2-4}$$

The axial pressure drop is expected to increase during the filtration, as the concentration of the retained components and thereby, the viscosity of the retentate increases. Note that the permeate flux (through the pores of the membrane) is governed by the viscosity of the permeate (η_P), while the axial pressure drop (ΔP) will be a function of the retentate viscosity (η), i.e., the viscosity of the fluid flowing inside the fibers.

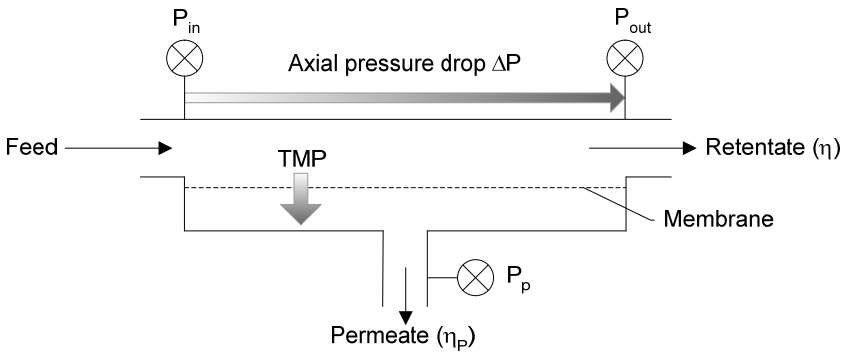

Figure 2.3 Transmembrane pressure and axial pressure drop in cross-flow ultrafiltration.

The permeate flux in ultrafiltration is often presented as a function of time or volume concentration ratio (VCR), defined as the initial feed volume to the retentate volume.

2.1.2 Membrane fouling

Ultrafiltration processes are usually operated at constant transmembrane pressure. The increase in the hydraulic resistance due to membrane fouling is associated with a permeate flux decline. A typical profile of the permeate flux is illustrated in **Figure 2.4** as a function of time.

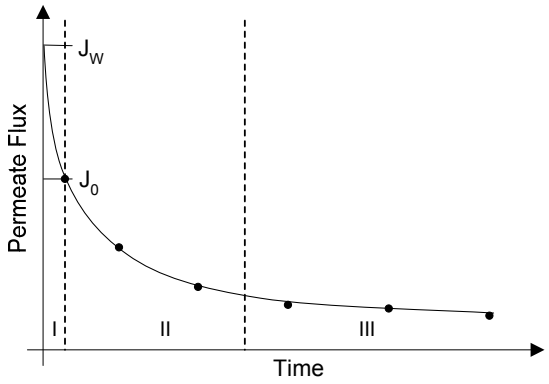

Figure 2.4 Permeate flux decline in ultrafiltration.

The permeate flux decline can be described in three stages. In the first stage of the operation, the permeate flux declines very rapidly due to concentration polarization, which refers to the concentration gradient that develops between the membrane surface and the bulk solution. The effect of concentration polarization can be obtained from the comparison of the pure water flux (J_W) and the initial permeate flux (J_P) at the same transmembrane pressure. In the second stage, the permeate flux declines mostly due to solute adsorption and deposition within the porous structure or the external surface of the membrane. The rate of the flux decline in this stage depends on the character of the solute-membrane and the solute-solute interactions. In the final stage, the flux may reach a steady state or may decrease slowly due to additional solute deposition or fouling layer consolidation [4].

Concentration polarization

Concentration polarization is the concentration gradient that develops between the membrane surface and the bulk solution. The solutes are constantly driven to the membrane surface by the permeate flow, and therefore the concentration of the retained components is higher at the membrane wall. The concentration gradient is a driving force for solute back diffusion to the bulk. At high permeate fluxes (e.g., initial stage of filtration), the rate of the convective flow is higher compared to the back diffusion, and the solutes readily accumulate on the membrane surface. The rate of the back diffusion is dependent on the solute properties (size, shape) and the viscosity of the aqueous phase [3]. Concentration polarization does not influence the sieving properties of the membrane but increases the resistance to the permeate flow. The effect of concentration polarization

is usually minimized in cross-flow systems due to the sweeping action of the tangential flow.

Protein adsorption and deposition

In ultrafiltration of protein-containing solutions, proteins tend to be the major foulants. Membrane fouling can be characterized by protein adsorption and deposition on the membrane surface. Proteins can adsorb or deposit on the external surface of the membrane (external fouling) or within the membrane pores (internal fouling). In ultrafiltration, external fouling is usually the predominant fouling mechanism. Pore plugging may occur, when the proteins are comparable in size to the dimensions of the membrane pores due to the protein entrapment at pore constrictions [2]. The presence of polar and non-polar functional groups within the protein amino acid sequence implies that proteins are capable of adsorbing to both hydrophobic and hydrophilic surfaces. In membrane ultrafiltration, it has been observed that proteins tend to adsorb and deposit more on hydrophobic than hydrophilic membranes [5,6]. Protein adsorption occurs as soon as the membrane surface and the protein solution come in contact, as a result of protein partitioning between the solid and the liquid phase. The amount of protein adsorption depends on the membrane material, protein properties (charge, hydrophobicity), and solution properties (pH, ionic strength) and can be estimated by exposing the membrane to the protein solution in static conditions (i.e., without permeate flow). Protein adsorption is considered irreversible, which may be explained by the size of the protein molecules. Proteins can interact with surfaces through electrostatic (coulombic) forces, polar and hydrophobic interactions, hydrogen bonding, and van der Waals forces, which can take place at multiple locations within the protein polypeptide chain. Although, formation and disruption of individual bonds may be a dynamic process, to break all connections at once is very unlikely [7].

Protein deposition involves additional protein that becomes associated with the membrane surface due to the convective flow. Multiple layers of protein may form on the membrane surface, depending on the strength of intermolecular interactions. It is likely that the porosity (void space) of the fouling deposit decreases closer to the membrane surface due to cake consolidation. Therefore, the upper part of the deposit (close to the bulk) may be less strongly bound and easier to remove during cleaning than the protein

layers in the proximity of the membrane surface. Protein deposition will be mostly controlled by the protein-protein interactions, which depend on the solution pH and ionic strength [4]. One can expect that the amount of protein deposition will be also governed by the protein concentration in the concentration polarization layer. The morphology of the fouling deposits will be likely affected by the strength and reversibility of the protein-protein interactions, given by the physicochemical characteristics of the protein.

Depending on the size of the pores within the fouling deposit, protein adsorption and deposition may increase the retention of the smaller solutes, thus reducing the efficiency of solute separation. Both permeate flux decline and lower selectivity have a negative effect on the overall performance of the filtration process. Careful selection of operating parameters (TMP, shear rate, concentration, pH, ionic strength) is necessary to minimize the effect of membrane fouling.

2.1.3 Diafiltration

Diafiltration is an ultrafiltration process, which involves pure solvent (water/buffer) addition to the retentate to replace the solvent which permeated through the membrane. In protein purification, diafiltration can be used as an effective method for removing low molecular weight impurities. The solvent addition may also reduce the amount of membrane fouling and improve the solute separation by reducing the solute-solute interactions in the retentate [8]. Diafiltration can be operated in a discontinuous or continuous mode. In discontinuous operation, the feed solution is first concentrated by conventional ultrafiltration, diluted back to the initial feed volume, and re-ultrafiltered. Several concentration/dilution cycles can be performed until the concentration of impurities drops to an acceptable level. In continuous operation, the solvent is added to the retentate at the same rate as the permeate flow, thus keeping the retentate volume and the concentration of the retained components constant. The concentration of impurities decreases in proportion to the amount of solvent added. The solvent consumption to reach the same level of purification is higher for the continuous operation, but this may be compensated by the higher permeate flux compared to the discontinuous operation [1].

2.2 Electrostatic effects

2.2.1 Electrical double layer and zeta potential

Protein molecules are complex biopolymers composed of 20 different amino acids linked by peptide bonds in a sequence, which is unique for each protein. In an aqueous solution, the proteins fold into a three-dimensional structure stabilized by covalent (disulfide bridges) and/or non-covalent bonding (hydrophobic and electrostatic interactions, hydrogen bonding, van der Waals forces). The polar and charged (hydrophilic) amino acids tend to be exposed on the protein surface, where they can interact with the surrounding molecules of water, while the non-polar (hydrophobic) amino acids are hidden in the protein core. The protein net charge is determined by the protonation of acidic and basic amino acid residues, which is dependent of the pH of the solution. The isoelectric point of a protein is the pH, at which the protein carries a zero net charge [9].

Protein molecules are typically several nanometers in size, which categorizes them as colloids (i.e., particles between 1–1000 nm). Due to high surface to volume ratio, the surface properties of colloidal particles or macromolecules, such as the surface charge, play an important role in overall characteristics of colloidal dispersions (e.g., stability, rheology). The surface charge influences the distribution of ions in solution around the particles. If the particles are negatively charged, positively charged ions (counter-ions) will be attracted to their proximity, resulting in the formation of an electrical double layer (**Figure 2.5**).

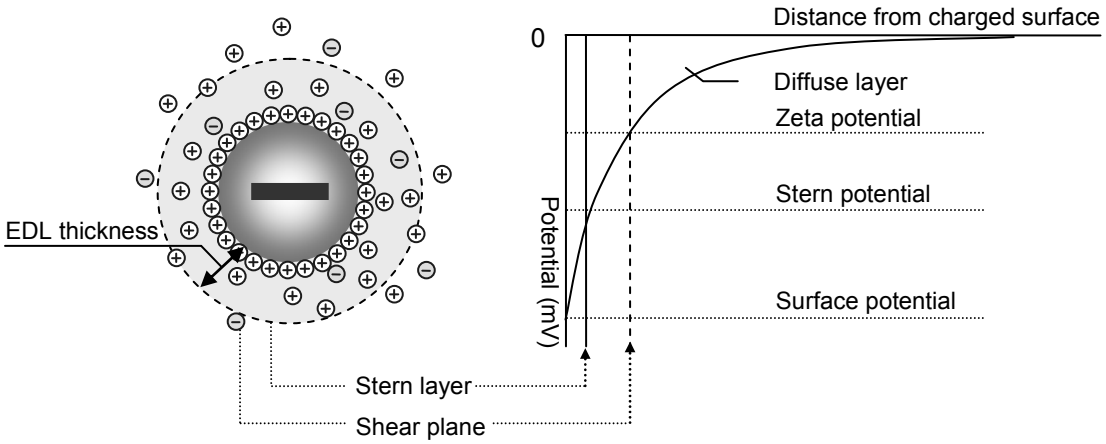

Figure 2.5 Electrical double layer (EDL) and electrical potential in the vicinity of negatively charged colloid.

The inner Stern layer is formed by the counter-ions in immediate contact with the charged surface. The counter-ions in this region are strongly bound to the surface and partially neutralize the negative charge. Outside the Stern layer, electrostatic forces are thus reduced and the counter-ions can move more freely around the particle. The surface charge gives rise to an electrical potential between the surface and the bulk solution. The potential difference is the highest at the particle surface and gradually decreases with increasing distance from the surface (**Figure 2.5**). When a charged particle moves in solution (e.g., sedimentation, electrophoresis), the Stern layer and the inner part of the diffuse layer remain associated with the surface during the particle movement. The boundary defining ions that move with the particle as a single entity is called the shear plane (or the slipping plane). The electrical potential at the shear plane is known as the zeta potential. It should be noted that the situation illustrated in **Figure 2.5** is oversimplified for proteins, which can not be described as rigid spheres with evenly distributed surface charge, and is only used to explain the concept of the double layer formation.

The thickness of the double layer depends on the type and concentration of electrolytes in solution and decreases with increasing ionic strength according to Eq. (2-5):

$$\kappa^{-1} = \sqrt{\frac{\varepsilon_m RT}{F^2 2I}} \tag{2-5}$$

where κ^{-1} is the thickness of the double layer, ε_m is the medium permittivity, R is the gas constant, T is the temperature, F is the Faraday constant, and I is the ionic strength [10].

2.2.2 DLVO theory

Colloidal particles in dispersion constantly move by a random Brownian motion, resulting from collisions with molecules of the surrounding medium. The stability of colloidal dispersions can be predicted from the Derjaguin-Landau-Verwey-Overbeek (DLVO) theory, which determines the total interaction energy of two approaching particles as a function of their separation distance. The total interaction energy is evaluated from the contributions of electrostatic repulsion and van der Waals attraction. The former arises from the double layer overlap between two approaching particles and acts as an energy barrier, preventing the particles from agglomeration or flocculation. If the electrostatic repulsive forces are weak (e.g., due to low surface charge) and the kinetic energy of the colliding particles is high enough to overcome the energy barrier, the particles will agglomerate due to van der Waals attractive forces (**Figure 2.6**). This type of agglomeration is considered irreversible, because the particles do not have sufficient energy to escape from the primary energy minimum (min 1).

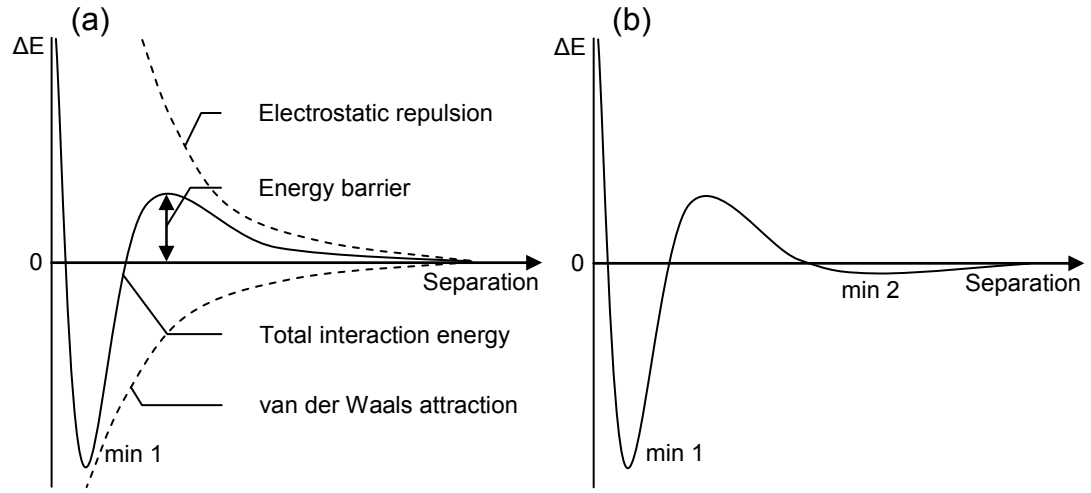

Figure 2.6 Total interaction energy calculated from the contributions of repulsive and attractive forces (a), with illustration of the secondary minimum (b).

The stability of colloidal dispersions is affected by physicochemical parameters such as pH or ionic strength. Increasing electrolyte concentration reduces the surface charge (due to double layer compression) and electrostatic repulsive forces, thus favoring agglomeration of the particles. At intermediate ionic strength, the total interaction energy may display a secondary energy minimum (min 2), as illustrated in **Figure 2.6** (b). This occurs when the double layer is partially reduced but still effective at short particle separation. The secondary minimum is much shallower than the primary minimum and as a result, particle agglomeration may be reversed (e.g., by stirring) [10].

The concept of the total interaction energy is often used to explain phenomena where interparticle interactions play an important role. Although the DLVO theory considers only the contributions of electrostatic repulsion and van der Waals attraction, the total interaction energy related to proteins may involve other forces, e.g., hydrophobic interactions, hydration forces. The strength of interparticle forces will be considered in the following sections to explain some characteristics of the soy protein dispersions used in this work.

2.2.3 Determination of zeta potential

The determination of the zeta potential (at the shear plane) can be used to describe the stability of a colloidal dispersion. For a protein solution, zeta potential is positive at low pH and negative at high pH, passing through zero at the protein isoelectric point. The electrostatic repulsion between the protein molecules is minimal at the isoelectric point, resulting in protein aggregation and eventually, precipitation. The zeta potential (ζ) is usually determined by measuring the electrophoretic mobility (u) of charged particles/proteins in an applied electric field and evaluated from Eq. (2-6):

$$u = \frac{2\varepsilon_m}{3\eta}\zeta \cdot f(\kappa a) \tag{2-6}$$

where ε_m and η are the permittivity and the dynamic viscosity of the medium, respectively. The correction factor $f(\kappa a)$ depends on the ratio of the particle radius (a) to the thickness of the double layer (κ^{-1}) [11].

The electrophoretic mobility can be estimated by laser Doppler velocimetry. Light from a laser source is split into an incident beam and a reference beam. The incident

beam passes through the sample to illuminate the dispersed particles, whereas the reference beam is directed around the sample. The particle movement due to the applied electric field causes a frequency shift in the light that is scattered by the particles. The frequency shift, obtained by comparing the frequency of the reference beam with that of the scattered light, is proportional to the velocity at which the particles migrate.

2.3 Soy proteins

2.3.1 Soybean composition

The soybean is native to China, where it has been cultivated as a source of dietary protein and oil for thousands of years. The plant was introduced to North America in the mid-18th century and since then the cultivation of soybeans has grown enormously. Today, the U.S. is the top soybean producer, accounting for at least 40 % of the total world production. Other leading soybean producers include Brazil, Argentina, and China. According to the American Soybean Association, Canada was the world's sixth largest soybean producer in 2006 [12]. The protein content of dry soybeans is about 40 %, which is the highest compared to other legumes (20–30 %) and cereal crops (8–15 %). For this reason, soybeans can produce more protein per unit land area than any other agricultural crop. Despite the high protein content, the soybean is mainly cultivated for oil, which accounts for about 20 % of its dry weight. The remaining soybean constituents include carbohydrates and minerals (or ash), accounting for about 35 and 5 % (on dry basis), respectively. Soybean carbohydrates contain soluble mono-, di-, and oligosaccharides (e.g., glucose, sucrose, raffinose and stachyose) and insoluble polysaccharides (cellulose, hemicellulose, pectin). The minerals are mainly composed of sulfates, phosphates, and carbonates, which implies that oxygen is a major component of ash. Other major minerals include potassium, phosphorus, magnesium, sulfur, calcium, chlorine, and sodium. Soybeans also contain small amounts of vitamins and phenolic compounds (e.g., isoflavones).

The defatted soybean meal, a by-product of oil production, contains at least 50 % of protein and is mainly used as animal feed. Only a small part of the protein-rich meal is used for human consumption, which relies primarily on animal protein foods. However, from the development of the first soy protein products (flours, concentrates, and isolates)

in the 1960s, their production for human consumption has been steadily increasing and with the ever-growing world population, the trend is expected to continue [13].

2.3.2 Soy proteins as food ingredients

Soy protein products are used as food ingredients due to their nutritional and functional properties. Soy proteins are highly digestible and contain all essential amino acids in sufficient quantities to meet human nutritional requirements, although the amount of sulfur-containing (methionine and cysteine) amino acids is lower than in animal protein sources [14]. Soy protein ingredients not only improve the nutritional quality of food products, but also modify their physical and sensory characteristics (e.g., texture, firmness, mouth-feel), which in turn affect customer satisfaction with the food products. The functional properties of soy proteins include water absorption and binding, viscosity (or thickening), gelation, elasticity, emulsification, fat absorption, and foaming. Most of these functional applications require highly soluble soy protein ingredients, which at the same time facilitates their incorporation into moist food products. Soy protein ingredients are used for the production of infant formulas, beverages, soups and gravies, meat extenders, dairy analogs, whipped toppings, and bakery items.

2.3.3 Characterization of soy proteins

Soy proteins can be classified as metabolic and storage proteins. The former include structural proteins and metabolic enzymes involved in cellular functioning. The latter represent about 85 % of the total protein content and act as a source of nitrogen during seed germination [15]. Storage proteins are globulins with an average isoelectric point at pH 4.5–4.8. The major constituents include β-conglycinin and glycinin, accounting for about 28 and 40 % of all storage globulins. Soy proteins can be also categorized according to sedimentation coefficients determined by ultracentrifugation. Four to five fractions are often identified in the sedimentation profile of soy proteins, depending on the ionic strength. These fractions are designated as 2, 7, 9, 11 and 15S (in Svedberg units). The 2S fraction contains small proteins such as α-conglycinin and trypsin inhibitors, representing about 20 % of total extractable protein. The 7S fraction contains β- and γ-conglycinin, lipoxygenase, and lectins. At low ionic strength ($I < 0.2$)

β-conglycinin forms a dimer with a sedimentation coefficient of 9–10S [16]. The 11S and 15S fractions correspond to pure protein, the former consisting of glycinin and the latter representing its polymerized form. The 15S fraction accounts for about 10 % of total extractable protein [13]. The isoelectric point (pI) and amino acid composition for the two major soy proteins, β- conglycinin and glycinin, is shown in **Table 2.1**. Both proteins have relatively similar amino acid composition, with the highest content of glutamic acid, followed by aspartic acid, leucine, and arginine.

β-conglycinin is a trimeric glycoprotein with a molecular mass around 180–210 kDa, and a carbohydrate content between 4 and 5 %. The molecule of β-conglycinin contains three protein subunits, α (57–76 kDa), α' (57–83 kDa), and β (42–53 kDa), assembled in random combinations. The molecular structure of β-conglycinin contains no disulfide bonds. Glycinin is a dodecamer composed of two identical hexamers, consisting of three basic (~20 kDa) and three acidic (~40 kDa) subunits. The acidic (A) and basic (B) subunits are connected by a single disulfide bond, resulting in a general structure A-S-S-B [13]. The molecular mass of glycinin is 300–350 kDa. In contrast to β-conglycinin, glycinin contains only a small amount of sugar and about 4–6 times more methionine and cysteine (**Table 2.1**). From the nutritional perspective, glycinin may be more valuable than β-conglycinin [15].

In addition to nutritional differences, β-conglycinin and glycinin have slightly distinct functional properties. Glycinin is more heat stable but less soluble in salt solutions than β-conglycinin. Gels prepared from glycinin tend to be firmer and more stable than those of β-conglycinin. On the other hand, β-conglycinin offers better emulsifying capacity and emulsion stability than glycinin. The differences in functional properties of the two proteins are likely caused by the differences in the heat stability, conformational stability, surface hydrophobicity, and the extent of disulfide bond formation [13,15].

Table 2.1 Isoelectric points (pI) and amino acid composition of β-conglycinin and glycinin in amino acid % per 100 g protein.

Protein	pI	Trp	Lys	His	Arg	Asp	Thr	Ser	Glu	Pro	Gly	Ala	Cys	Val	Met	Ile	Leu	Tyr	Phe
β-conglycinin	4.8	0.3	7.0	1.7	8.8	14.	2.8	6.8	20.	4.3	2.9	3.7	0.3	5.1	0.3	6.4	10.	3.6	7.4
Glycinin	6.4	1.5	5.7	2.6	8.9	13.	4.1	6.5	25.	6.9	5.0	4.0	1.7	4.9	1.3	4.9	8.1	4.5	5.5

From García et al. [15].

2.3.4 Antinutritional factors in soy

The presence of antinutritional factors in the soy protein products diminishes their nutritional quality and their use as food ingredients. Antinutritional factors include substances that interfere with digestion or reduce the bioavailability of nutrients. The most important antinutritional components in soybeans are trypsin inhibitors, lectins, lipoxygenase, oligosaccharides, and phytic acid. These components are not only specific to soybeans but are commonly found in other legumes and plant sources. Soybeans contain two types of trypsin inhibitors, Bowman-Birk (8 kDa) and Kunitz inhibitor (21 kDa), which belong to the 2S fraction. As their name suggests, trypsin inhibitors inhibit trypsin (protease) activity, thus reducing protein digestibility and amino acid bioavailability. Lectins (or hemagglutinins) are proteins which can bind to carbohydrate-containing receptors on cell membranes and thus, interfere with the metabolic processes. Lipoxygenase is an enzyme that has the ability to catalyze hydroperoxidation of polyunsaturated fatty acids, resulting in the formation of fatty-acid hydroperoxides. These products can be further degraded into various volatile compounds, including ketones, aldehydes, alcohols, and acids, which may cause undesirable flavors of the soy-based foods. Trypsin inhibitors, lectins and lipoxygenase are usually inactivated by heat treatment during soybean processing [13,15].

Oligosaccharides, raffinose and stachyose, are associated with flatulence and abdominal discomfort after consumption of soybeans or soy-based foods. Raffinose (trisaccharide) and stachyose (tetrasaccharide) consist of sucrose linked with one and two galactose units, respectively, through α-galactosidic linkage. These oligosaccharides can not be metabolized in humans due to the absence of α-galactosidase, an enzyme that can hydrolyze α-galactosidic linkages. Anaerobic fermentation of these oligosaccharides by microflora in the small intestine results in gas production [13,15].

Phytic acid (myo-inositol hexakis phosphate) is a natural component of plant seeds, mostly occurring in the form of calcium-magnesium-potassium salt. The chemical structure of phytic acid is shown in the Appendix (Chapter 8). In legumes and cereals, phytic acid accounts for about 85 % of total phosphorus [17]. In general, phytic acid is considered an antinutrient, because it may limit the bioavailability of minerals and proteins. Phytic acid is a strong chelating agent for a variety of metal ions (e.g., Ca^{2+}, Mg^{2+}, Zn^{2+}, Fe^{2+}), forming

insoluble and indigestible mineral complexes. The molecule of phytic acid can also associate with proteins and carbohydrates through electrostatic interactions or hydrogen bonding, which may have a detrimental effect on the solubility and bioavailability of these nutrients [17,18].

2.3.5 Soy protein products

Soy protein products can be divided into flours and grits, concentrates and isolates based on their protein content (**Table 2.2**). In conventional processing, soybeans are first cleaned, dried, cracked, and dehulled. Before flaking, dehulled soybeans have to be conditioned to a moisture content of 10–11 % at 65–70 °C. Soy flakes are defatted by hexane extraction. The residual solvent is removed by exposing the soy flakes to steam, which is followed by a toasting process at 100–105 °C to inactivate enzymes associated with antinutritional effects [13]. The soy flours, concentrates, isolates are prepared from the defatted soy flakes.

Table 2.2 Composition of soy protein products (in % on dry basis)*

Constituent	Defatted flours and grits	Concentrates	Isolates
Protein	56–59	65–72	90–92
Fat	0.5–1.1	0.5–1.0	0.5–1.0
Crude fiber	2.7–3.8	3.5–5.0	0.1–0.2
Ash	5.4–6.5	4.0–6.5	4.0–5.0
Carbohydrates**	32–34	20–22	3–4

* Adopted from Liu, K. [13]. ** By difference.

Soy flours and grits are prepared by grinding the defatted flakes. Soy protein concentrates are produced by three basic methods: (1) acid leaching which involves washing the defatted soy flake with dilute acid at pH 4.5; (2) aqueous ethanol extraction; and (3) protein denaturation by moist heat followed by water extraction [14]. The purpose of all three methods is to make the protein insoluble and then remove the water-soluble carbohydrates [19]. Soy protein isolates are conventionally produced by alkaline extraction (pH 7–10) of the defatted flakes at mild temperatures (30–65 °C). The insoluble material, containing mostly polysaccharides (fiber), is removed by centrifugation. The protein solution is acidified

to pH 4.5–4.8 to precipitate the protein. The precipitate is separated by centrifugation, washed, neutralized (pH 6.5–7.0), and spray-dried. The neutralization step is sometimes excluded to produce soy protein isolates in their isoelectric form [13,19].

2.4 Membrane processing

2.4.1 Ultrafiltration

Membrane separation processes offer an alternative to the conventional production of soy protein concentrates and isolates. Using an ultrafiltration membrane with appropriate pore size, soy proteins can be separated from the low molecular weight components such as carbohydrates (including mono-, di-, and oligosaccharides) and minerals. The production of soy protein isolates by isoelectric precipitation requires the use of concentrated acids and alkali (for neutralization), which often causes irreversible protein denaturation due to local pH extremes [20]. Acid-precipitated soy protein isolates have relatively high mineral and phytic acid contents. Large volume of acid waste is generated during the multiple washings of the precipitated protein, resulting in higher capital costs for the waste treatment. In contrast, ultrafiltration has been shown to produce soy protein concentrates and isolates with higher solubility and improved functional properties [21,22]. Depending on the membrane pore size, ultrafiltration can also preserve proteins that normally do not precipitate at pH 4.5 (whey proteins), resulting in potentially higher protein yields than those achieved during the conventional isoelectric precipitation [23,24]. The removal of minerals and phytic acid during ultrafiltration is dependent on the pH of the soy protein extracts [24,25]. Stronger electrostatic interactions between soy proteins, minerals, and phytic acid or reduced solubility of minerals and phytic acid at alkaline pH can cause higher retention of these components by the membrane [24,25]. Omosaiye et al. [25] showed that the removal of phytic acid during ultrafiltration of soybean water extracts increased from 27 to 65 %, when the pH was lowered from 10 to 6.7. The solubility characteristics of calcium and magnesium phytates depend on the pH and the molar ratio of calcium/magnesium to phytic acid [26,27]. The solubility of calcium and magnesium phytates typically decreases above pH 5, with the maximum precipitation obtained at the molar ratio of calcium/magnesium to phytic acid between 4 and 6. The solubility of calcium, magnesium, and phytic acid in complex food systems will also depend on the type and concentration of other minerals, polyionic compounds (protein and

fiber), and the processing history of the product [26]. The 11S (glycinin) fraction of the soy proteins is known to associate with calcium and magnesium ions, which may be important for maintaining the protein structure [28,29]. Wallace et al. [30] reported that the amount of calcium bound to soy proteins increased with increasing pH between 7 and 11. Grynspan et al. [31] investigated the interactions between soy proteins, calcium, and phytic acid. At low pH (below pI of soy proteins), strong electrostatic interactions occur between the positively charged soy proteins and the negatively charged phytic acid. At pH above 6.5 (above pI of soy proteins), calcium ions mediate interactions between the negatively charged soy proteins and phytic acid, resulting in a ternary complex formation without protein precipitation. At higher pH values, the solubility of soy proteins remains high, but the solubility of phytate and calcium decreases due to calcium phytate precipitation. The ternary complex formation and the solubility profiles of soy proteins, calcium, and phytic acid are again dependent on the relative concentrations of individual components. The study of Omosaiye et al. [25] indicates that for optimal separation of the soy proteins from the phytic acid, ultrafiltration should be performed at a neutral pH, when the conditions for the ternary complex formation or the precipitation of mineral phytate are limited.

Ultrafiltration performance is usually affected by membrane fouling, which results in a permeate flux decline, longer filtration times, and more frequent membrane cleaning to maintain a stable operation [1,2].

2.4.2 Electroacidification

Electroacidification or bipolar-membrane electrodialysis is a novel technique that has been recently proposed for production of soy protein isolates [32,33]. Bipolar membrane consists of three components, a cation-exchange membrane, an anion-exchange membrane, and a hydrophilic interface separating the two membranes. In an electrical field, water dissociates at the hydrophilic interface, resulting in H^+ and OH^- migration in the direction of oppositely charged electrodes. **Figure 2.7** shows a schematic of an electroacidification cell, which can be composed of several compartments separated by cation-exchange membranes (CEM) and bipolar membranes (BPM). Thus, the soy protein extract (SPE) circulated in the compartment on the cationic side of the bipolar membrane becomes slowly acidified. Simultaneously, the ash content of the soy protein extract is reduced, as the positively

charged minerals migrate through the cation-exchange membrane towards the cathode. For the production of soy protein isolates, the soy protein extract is circulated in the cell until the pH reaches the isoelectric point (pH 4.5–4.8) and protein precipitation occurs.

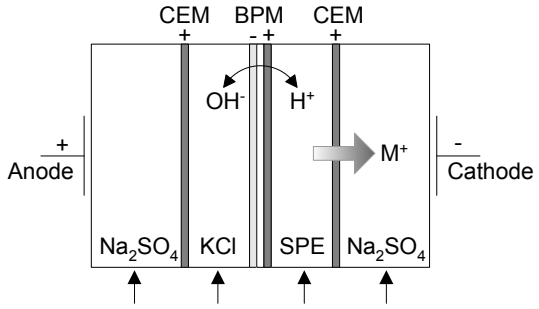

Figure 2.7 Electroacidification of soy protein extracts (SPE), adopted from [32]. CEM and BPM represent a cationic exchange membrane and a bipolar membrane, respectively.

In electroacidification, the pH is lowered gradually without the use of concentrated acids, resulting in soy protein isolates with higher solubility and lower ash content. Compared to the conventional isoelectric precipitation, electroacidification is more time-consuming but the water consumption is reduced by reusing the effluents generated during the process. However, gradual precipitation of proteins results in severe fouling of the bipolar membranes, increasing the cell resistance and thus, decreasing the process efficiency [33].

2.5 Electroacidification and ultrafiltration

A novel approach, integrating electroacidification and membrane ultrafiltration, for the production of soy protein isolates has been recently proposed [34,35]. The first step involves alkaline extraction of soy proteins from defatted soy flake. The pH of the alkaline soy protein extract (SPE 9) is adjusted to 6 by electroacidification (resulting in SPE 6), followed by membrane ultrafiltration for purification and concentration of soy proteins (**Figure 2.8**).

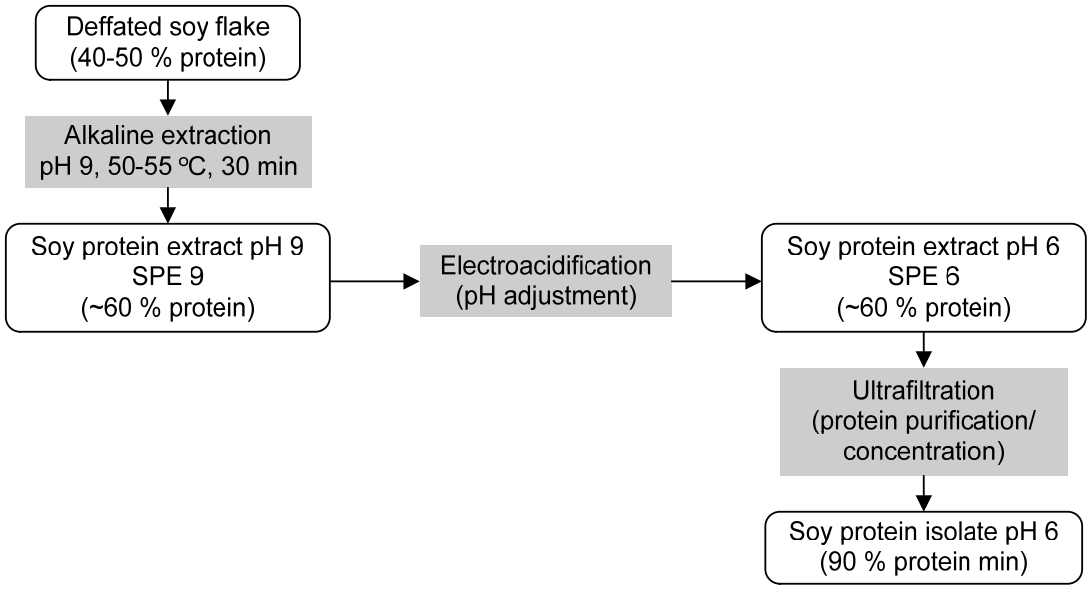

Figure 2.8 Production of soy protein isolates by electroacidification and ultrafiltration.

Preliminary work considered ultrafiltration of the soy protein extract in a dead-end system using a 100 kDa regenerated cellulose membrane, stirred conditions and constant transmembrane pressure of 30 psi [34]. The soy protein extract obtained by alkaline extraction was subjected to electroacidification to pH 7 and 6. The effect of electroacidification on the ultrafiltration performance was compared for the electroacidified soy protein extracts at pH 7 and 6 and the non-electroacidified soy protein extract at pH 9. Electroacidification of the soy protein extracts resulted in more significant membrane fouling (maximum at pH 7, intermediate at pH 6, and minimum at pH 9). Analysis of the hydraulic resistance showed that most of the fouling was due to cake layer formation. The ash removal was 72.9, 64.5, and 55.1 % at pH 6, 7, and 9 respectively, indicating that electroacidification enhanced the removal of minerals during ultrafiltration. Mineral analysis showed that the concentration of calcium and phosphorus (phytic acid) increased during the ultrafiltration at pH 7 and 9, which was attributed to the ternary complex formation between soy proteins, calcium, and phytic acid at pH above 6.5. In contrast, the removal of calcium and phosphorus was considerably improved during the ultrafiltration of the soy protein extract at pH 6, yielding a soy protein concentrate with superior composition and improved solubility. The comparison with a soy protein concentrate produced by the conventional acid precipitation at pH 4.5 showed that the two products had a similar ash content and solubility profile but the water consumption was twice as much during the conventional process.

Subsequent work investigated the membrane fouling of the electroacidified soy protein extract at pH 6 (SPE 6) and the non-electroacidified soy protein extract at pH 9 (SPE 9) in low shear (flat sheet) and high shear (hollow fiber) tangential flow ultrafiltration [36,37]. The analysis of the hydraulic resistance by the resistance-in-series model and the comparison of the fouling components (reversible and irreversible fouling) revealed that there was at least a 20-fold decrease in the reversible fouling for the low shear tangential flow system compared to the dead-end system. Additional improvement was obtained in the hollow fiber system, where the reversible fouling decreased about 100-fold compared to the dead-end system [37].

Comparison of the ultrafiltration performance for SPE 6 and SPE 9 during the hollow fiber ultrafiltration also indicated a more significant permeate flux decline for SPE 6 compared to SPE 9, which was attributed to more significant irreversible fouling [37]. The soy protein isolates obtained by ultrafiltration of SPE 6 and SPE 9 to VCR 6.5 contained about 87 % protein (dry basis) which was about 4 % less than predicted, assuming that protein is fully retained by the membrane and other components are freely permeable. The lower protein content was explained by insufficient removal of carbohydrates and minerals and protein loss due to adsorption and deposition on the membrane surface.

2.6 Project objectives

The overall objective of this work is to investigate the effect of electroacidification on the ultrafiltration of soy protein extracts. Two types of soy protein extracts will be used, an electroacidified soy protein extract at pH 6 (SPE 6) and a non-electroacidified soy protein extract at pH 9 (SPE 9). The specific objectives are:

1. To evaluate the efficiency of the carbohydrate and mineral removal in a hollow fiber ultrafiltration system, with the focus on the removal of calcium, magnesium, and phytic acid.

2. To assess the potential of a discontinuous diafiltration in the hollow fiber ultrafiltration system to enhance the removal of carbohydrates and minerals and reduce membrane fouling.

3. To investigate membrane fouling in a dead-end ultrafiltration system in order to identify the factors responsible for the permeate flux decline during ultrafiltration of the electroacidified and the non-electroacidified soy protein extract.

4. To determine the effect of electroacidification on the axial pressure drop profile during the hollow fiber ultrafiltration.

5. To examine the effect of electroacidification on the physicochemical properties of the soy protein extracts.

2.7 Selection of operating parameters

During the operation in a total recycle mode, i.e., when both the retentate and the permeate are recycled to the feed tank (**Figure 2.9**), it is often observed that the permeate flux increases linearly with increasing transmembrane pressure (TMP) up to a certain point, beyond which the flux becomes pressure-independent. This is due to the accumulation of the retained solutes near the membrane surface and possible consolidation of the fouling deposit at higher pressures. The pressure, at which the permeate flux starts leveling off, depends on the operating parameters (feed composition, concentration, shear rate), the properties of the retained solutes (diffusivity), and the hydrodynamic conditions within the membrane module [2]. The permeate flux-TMP profile is often used to determine appropriate conditions (transmembrane pressure, shear rate, feed concentration) for operation in the concentration mode, i.e., when the permeate is withdrawn.

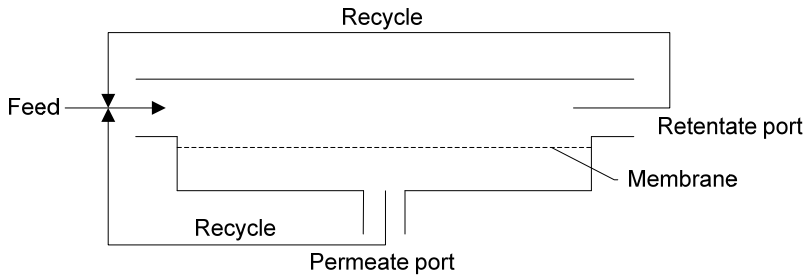

Figure 2.9 Operation in the total recycle mode.

The operating parameters for the ultrafiltration of soy protein extracts in the hollow fiber system were selected in a previous study by Vaughan [37]. The permeate flux-TMP profile obtained at various feed concentrations during the operation in the total recycle mode is shown in **Figure 2.10**. As expected, the permeate flux for pure water increased linearly with the transmembrane pressure. The permeate flux during the ultrafiltration of the soy protein extracts was linear at lower pressures but became pressure-independent at higher pressures. The magnitude of the steady state flux in the pressure-independent region was dependent on the type of feed, electroacidified or non-electroacidified, and the feed concentration. From the lower steady state flux, it was concluded that SPE 6 had a higher fouling tendency than SPE 9. The pressure, at which the flux started leveling off, was approximately 6 psi for SPE 6 and 10 psi for SPE 9. The steady state flux generally decreased with increasing feed concentration, as a result of more significant membrane fouling. The shape of the permeate flux-TMP profile was similar for all feed concentrations except for the 2 % w/w SPE 6 solution, for which the flux increased linearly up to 6 psi, followed by a sudden decrease, resulting in a steady state flux, which was lower than that obtained for the more concentrated SPE 6 solutions. It was proposed that around the transmembrane pressure of 6 psi, the fouling deposit underwent a structural rearrangement, resulting in a lower porosity and permeate flux. However, it was not clear why this behavior only occurred at the 2 % w/w concentration and not at the higher concentrations for SPE 6.

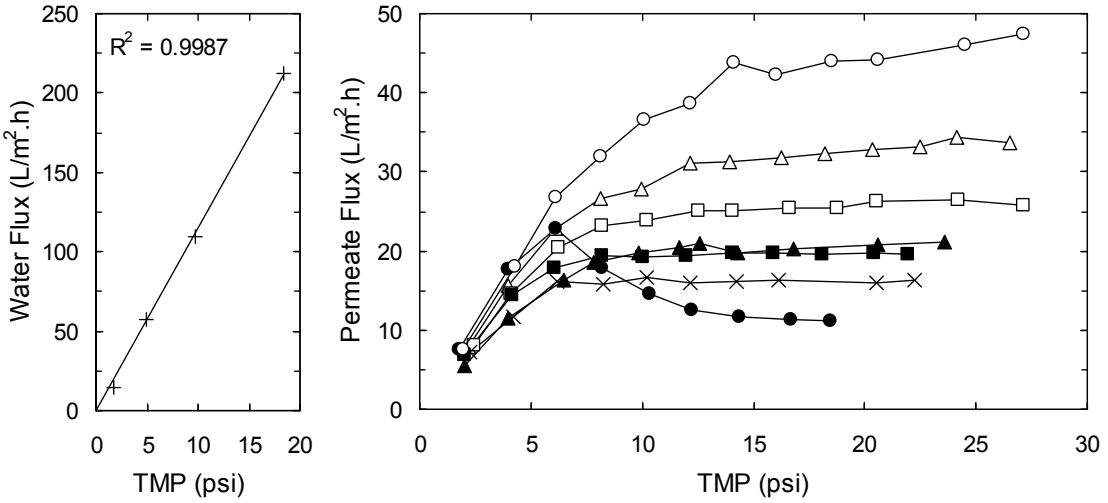

Figure 2.10 Permeate flux-TMP profile obtained at various feed concentrations during ultrafiltration of soy protein extracts in the total recycle: (+) pure water; (●) SPE 6, 2 % w/w; (▲) SPE 6, 4 % w/w; (■) SPE 6, 6 % w/w; (×) SPE 6, 8 % w/w; (○) SPE 9, 2 % w/w; (△) SPE 9, 4 % w/w; (□) SPE 9, 6 % w/w. MWCO = 100 kDa, shear rate = 8000 s^{-1}, T = 25 °C. Adopted from [37].

Ultrafiltration in the concentration mode should be operated at the knee of the permeate flux-TMP curve for an efficient process. This corresponds to a transmembrane pressure around 4-6 psi for SPE 6 and 6–10 psi for SPE 9, depending on the feed concentration (**Figure 2.10**). To compare the filtration behavior of both soy protein extracts at the same operating conditions, the transmembrane pressure was selected at 6 psi. To minimize the effect of membrane fouling and the increase in retentate viscosity at higher concentrations, it was decided to perform the concentration filtration experiments at 2 % w/w total solids for the feed.

For the selection of the shear rate, the recommendation of the supplier of the hollow fiber membrane module (GE Healthcare) was to operate at a minimum shear rate of 8000 s^{-1} for minimization of membrane fouling. To determine whether the permeate flux may be improved at higher shear rate, the permeate flux-TMP profile was obtained for ultrafiltration of 2 % w/w soy protein extract solution in the total recycle at 8000 and 10000 s^{-1}. The results in **Figure 2.11** show that no flux improvement was achieved during the operation at 10000 s^{-1} and therefore, the lower shear rate was selected for further experiments.

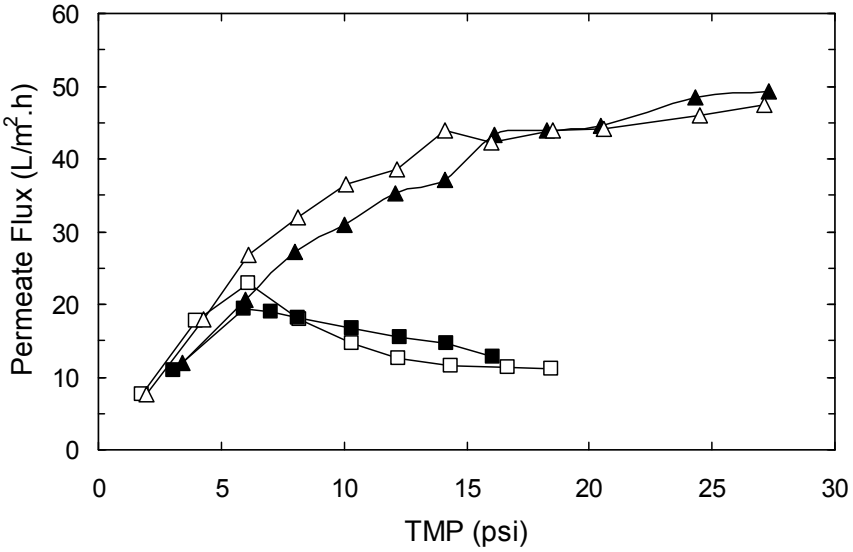

Figure 2.11 Permeate flux-TMP profile obtained at various shear rates during ultrafiltration of soy protein extract in the total recycle: (□) SPE 6, 8000 s^{-1}; (■) SPE 6, 10000 s^{-1}; (△) SPE 9, 8000 s^{-1}; (▲) SPE 9, 10000 s^{-1}. MWCO = 100 kDa, feed concentration = 2 % w/w, T = 25 °C. Adopted from [37].

Consequently, ultrafiltration of the soy protein extracts in the concentration mode was investigated with a feed concentration of 2 % w/w (total solids), a transmembrane pressure of 6 psi, and a shear rate of 8000 s^{-1}.

3

Carbohydrate and Mineral Removal during the Production of Low-Phytate Soy Protein Isolate by Combined Electroacidification and High Shear Tangential Flow Ultrafiltration*

In this work, soy protein isolates were produced by a combination of electroacidification and high shear tangential flow hollow fiber ultrafiltration with a 100 kDa membrane under constant pressure. The filtration performance was evaluated by comparing the filtration time and the final product composition for an electroacidified (pH 6) and a non-electroacidified (pH 9) soy protein extract. The removal of carbohydrates during the filtration was always consistent with the theoretical predictions (based on free permeability assumption) for both the electroacidified and the non-electroacidified feeds. A higher removal of calcium, magnesium, and phytic acid was achieved during the filtration of the electroacidified feed compared to the non-electroacidified feed. However, the electroacidification pretreatment had a negative impact on the permeate flux and resulted in more significant membrane fouling with correspondingly longer filtration times. A discontinuous diafiltration enhanced the removal of carbohydrates and minerals, thus yielding a product with higher protein content but did not result in the improvement of the permeate flux for the electroacidified feed.

*Adapted from J. Skorepova, C. Moresoli. J. Agric. Food Chem., 55 (2007) 5645.

3.1 Introduction

Plant materials, such as soy, represent an attractive source of dietary protein that is abundant and available at relatively low cost. In terms of nutritional quality, purified soy proteins can be considered equivalent to animal proteins [14,38]. Additional benefits associated with the consumption of soy proteins in sufficient quantities include a lower risk of coronary heart disease, which was recognized by the U.S. FDA in 1999 through the approval of a health claim for soy proteins. This recognition has resulted in an increased demand for soy protein containing products [39]. Besides the nutritional benefits, soy proteins also provide excellent functional properties, which stabilize and improve the texture of food products. Functional properties are affected by the composition of soy proteins, the presence of antinutritional factors, and processing conditions [40,41]. Soy proteins are mainly composed of storage proteins (~ 85 %) and tend to precipitate at pH 4.5–4.8 (isoelectric point, pI). Their major components are β-conglycinin and glycinin with molecular masses of 180–210 and 300–350 kDa, respectively [15].

Soy protein concentrates (70 % protein minimum, dry basis) and isolates (90 % protein minimum, dry basis) are generally obtained by the removal of oligosaccharides and minerals from defatted soy flour. Since the 1970s, membrane ultrafiltration has been investigated for the production of soy protein ingredients with superior properties and low antinutrient content [8,42]. The soy protein extract comes into contact with a membrane that separates the protein from other components based on the differences in molecular size. In comparison to isoelectric precipitation, membrane ultrafiltration is considered to be gentler to the proteins and tends to preserve their native structure [22]. In addition, ultrafiltration may recover proteins that do not precipitate at pH 4.5 (whey proteins), which could also improve the functional properties [23,24]. Rao et al. [22] reported improved solubility for soy protein concentrate produced by ultrafiltration when compared to acid-precipitated soy protein isolate. The ultrafiltered soy protein concentrate produced more stable emulsions, although the ability to form emulsions was less effective.

Membrane filtration systems have also contributed to the understanding of the interactions between phytic acid, calcium, magnesium, and proteins and to the development of low phytic acid soy protein products. Phytic acid is generally considered an important

antinutritional factor in soy products as it may limit the bioavailability of minerals and proteins [17,43]. However, recent work attributed also positive effects to phytic acid through anticarcinogenic and antioxidant effects [44]. Phytic acid contains six phosphate groups that are negatively charged over a wide range of pH and can interact with other electrostatically charged species such as multivalent cations, proteins, and starch [18]. In the context of protein-phytic acid interactions, it appears that pH and the content of calcium and magnesium play an important role in modulating these interactions. A ternary complex between negatively charged protein and phytic acid is facilitated by multivalent cations at pH above 6.5, whereas at lower pH the formation of this complex is limited [31,45]. Also at pH above 5, phytic acid is known to form insoluble salts with calcium or magnesium, depending on their concentration, which may compete with the formation of the ternary complex. The effect of pH on phytate solubility was exploited in the production of soy protein concentrates with enhanced mineral removal and improved solubility profiles [25,34]. Omosaiye et al. [25] reported a 65 % phytic acid removal at pH 6.7 compared to 43 and 27 % at pH 8 and 10, respectively, during direct ultrafiltration to VCR 5. Improved phytic acid removal (92 % at pH 6.7 and above 80 % at pH 8 and 10) was achieved at all three pH values by two-stage discontinuous diafiltration. What differentiates calcium and magnesium interactions with soy proteins is still unknown as limited information on magnesium was found. A study comparing the aggregation-dissociation process of soy protein isolate induced by calcium and/or magnesium chlorides reported a higher turbidity when calcium was used, suggesting different aggregation mechanisms for each cation [46].

A novel approach, integrating electroacidification and membrane ultrafiltration, for the production of soy protein concentrates/isolates has been recently developed [34-36]. In electroacidification, hydrogen ions generated by electrodissociation of water can be used to acidify the soy protein extract solution. The pH can be lowered at a controlled rate without the use of concentrated acids, which was shown as a more protein friendly approach [33]. In the work of Mondor et al. [34,35], the proteins, initially extracted from defatted soy flake at pH 9, were subjected to electroacidification and the pH was adjusted from 9 to 7 or 6. Subsequent ultrafiltration of the soy protein extracts in a dead-end system with a 100 kDa membrane was associated with membrane fouling, being maximum at pH 7, intermediate at pH 6, and minimum at pH 9. Analysis of the hydraulic resistance revealed that most of the

fouling (92–98 %) was due to the cake layer formation, suggesting that operation in a tangential flow ultrafiltration system, where the cake buildup is minimal, would be more suitable. Despite the higher membrane fouling, electroacidification to pH 6 enhanced the mineral and phytic acid removal, thus producing a soy protein concentrate with superior composition and improved solubility [34]. The mineral removal was 72.9 % at pH 6 compared to 55.1 % at pH 9. The phytic acid content decreased at pH 6, whereas it increased for both pH 7 and 9 final products.

In this study, the potential of a high shear tangential flow hollow fiber system operated in a concentration or a discontinuous diafiltration mode was investigated for the production of soy protein isolates (90 % protein minimum, dry basis). The effect of electroacidification on the filtration performance was assessed by comparing the most promising electroacidified soy protein extract at pH 6 (SPE 6) to the non-electroacidified soy protein extract at pH 9 (SPE 9). The efficiency of carbohydrate removal, mineral removal, and protein retention is presented. Particular emphasis is given to the phytic acid, calcium, and magnesium content of the final product. The permeate flux profile, as the filtration proceeded, is also reported and discussed in the context of the fouling behavior, feed pretreatment, and protein retention.

3.2 Materials and methods

3.2.1 Feed preparation

Lyophilized soy protein extracts containing approximately 60 % protein, 30 % carbohydrates, and 10 % ash were provided by Agriculture and Agri-Food Canada (Saint-Hyacinthe, QC, Canada). Details on the preparation of the soy protein extracts and the electroacidification process can be found in Mondor et al. [34]. The filtration feed consisting of SPE 6 or SPE 9 was obtained as follows: 2 % w/w SPE solution was prepared by mixing a preweighed amount of SPE powder with Nanopure water (resistivity > 17.5 MΩ-cm) from a Barnstead water purification system (Dubuque, IA). The suspended SPE was stirred at room temperature for 1–2 h to allow rehydration. The suspension was then centrifuged at 15300 g for 15 min using a Beckman Coulter L7-35 ultracentrifuge (Mississauga, ON, Canada) to remove any insoluble solids, and the supernatant was used as the feed solution for subsequent filtration. All experiments were performed with a feed volume of approximately 1.5 L.

3.2.2 Experimental setup

Ultrafiltration experiments were performed with a hollow fiber membrane unit purchased from GE Healthcare (Baie d'Urfe, QC, Canada). The membrane was made of polysulfone with a nominal molecular weight cutoff (MWCO) of 100 kDa. The chemical structure of polysulfone is shown in the Appendix (Chapter 8). The module was 30 cm long and consisted of 50 fibers, each having an inner diameter of 1 mm. The membrane area was 420 cm^2. The feed was pumped into the system (**Figure 3.1**) by a progressing cavity pump (Moyno Inc., Springfield, OH), and the flow rate was measured by a flowmeter. The pressure was monitored at the feed and the retentate side with two pressure transducers. The transmembrane pressure (TMP) was controlled on the retentate side by a manual pinch valve. The flowmeter, pressure transducers, and manual pinch valve were purchased from Cole Parmer Canada Inc. (Anjou, QC, Canada). A sampling valve was installed on the retentate side to allow for sample collection during the filtration experiments. The permeate was collected in a reservoir, and the flux was measured by weighing the permeate at specified time intervals. The balance (Ohaus Corp., Pine Brooks, NJ) and the pressure transducers were connected to a PC running Labview 7.1. To compensate for the temperature increase due to pumping, the feed tank was placed in an ice bath and the temperature of the feed was maintained constant (25 ± 1 °C).

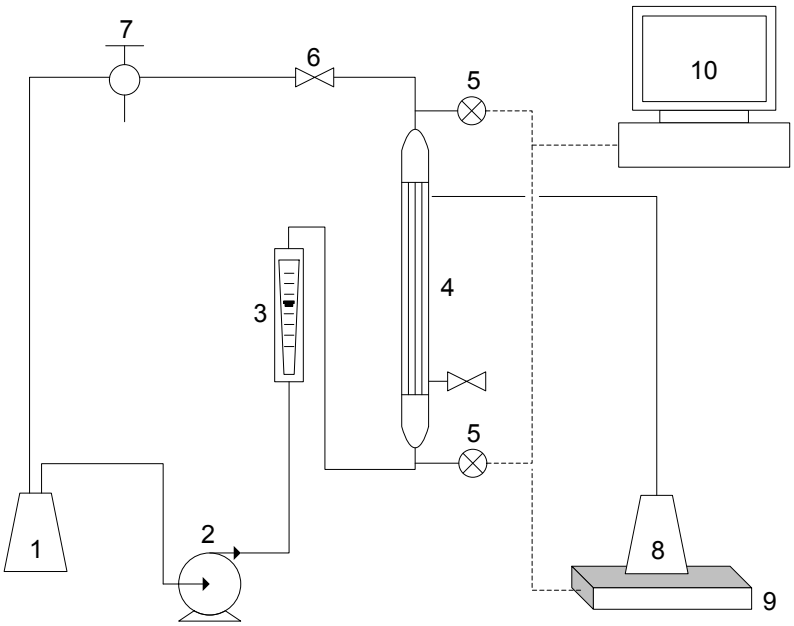

Figure 3.1 Schematic diagram of the filtration unit: 1-feed tank, 2-pump, 3-flowmeter, 4-membrane, 5-pressure transducers, 6-pinch valve, 7-sampling valve, 8-permeate container, 9-balance, and 10-PC/software.

3.2.3 Ultrafiltration experiments

Both SPE 6 and SPE 9 were subjected to two types of experiments, direct ultrafiltration (UF) and two-stage discontinuous diafiltration (DDF). The volume concentration ratio (VCR) given by Eq. (3-1) was used as a governing parameter to control the concentration extent during the filtration:

$$VCR = \frac{V_F}{V_R} = \frac{V_F}{V_F - V_P} \qquad (3\text{-}1)$$

V_F, V_R, and V_P are the feed, the retentate, and the permeate volume, respectively. VCR was determined by weighing the feed and the permeate and using the density of water to convert to volume.

In direct UF, the feed (~1.5 L) was concentrated in one step to VCR 4.5. In DDF, the feed (~1.5 L) was concentrated to VCR 2 (stage 1), then diluted to the original volume with Nanopure water, and re-concentrated to VCR 4 (stage 2). The filtrations were performed under identical operating conditions: temperature, 25 °C; TMP, 6 psi (41.4 kPa); flow rate, 2.4 L/min, corresponding to the shear rate of 8000 s^{-1}. Therefore, stage 1 of DDF provided

practically a replicate of direct UF up to VCR 2. The permeate flux profile and the composition of the retentate samples collected up to VCR 2 should be the same for both filtrations. Assuming all non-protein solutes were freely permeable, direct UF (VCR 4.5) and DDF (VCR 2, dilution, VCR 4) should result in a removal of 78 and 88 % of these solutes, respectively. During the filtration, samples of the retentate were taken at specific time points to investigate the changes in the composition. At the end of the filtration, samples of the final retentate and permeate were collected, lyophilized (SuperModulyo, Thermo Electron Corp., Waltham, MA), and kept for further analysis.

3.2.4 Analytical methods

Total solids and carbohydrates

The concentration of total solids (TS) was determined gravimetrically by drying the samples (1 mL) at 100 °C overnight. The carbohydrate concentration was determined by phenol-sulfuric acid assay modified from Fox et al. [47] using glucose standards (20–160 μg/mL). The procedure consisted of adding 25 μL of standard and sample into separate microtiter plate wells and then adding 25 μL of 5 % w/w phenol solution and 125 μL of concentrated sulfuric acid to each well. The microtiter plate was wrapped in DuraSeal (Diversified Biotech, Boston, MA) and placed in an 80 °C oven for 30 min. The absorbance was read on Multiskan Ascent microtiter plate reader (Labsystems, Helsinki, Finland) at 492 nm. The carbohydrate content on dry basis was determined as a ratio of the carbohydrate concentration to the TS concentration (× 100).

Protein

The protein concentration in the retentate samples (collected during the filtration) and the final permeate was determined according to the Bradford protein assay (Standard Procedure for Microtiter Plates, Bio-Rad Laboratories, Mississauga, ON, Canada) using purified β-conglycinin and glycinin as protein standards (provided by M. Corredig, University of Guelph, ON, Canada). The standard solutions were prepared by combining β-conglycinin and glycinin in a ratio of 1:1.4, which corresponds with the actual distribution of these two protein fractions in the soy proteins [15]. The Bradford assay enabled a fast analysis of the retentate samples (liquid) collected during the filtration (> 10). It was also used to analyze the permeate samples, which contained only small amounts of protein. The

protein content (dry basis) was determined as a ratio of the protein concentration to the TS concentration (× 100). The results obtained from the Bradford assay were verified for freeze-dried feed and final retentate samples with a LECO FP-428 nitrogen analyzer (LECO Corp., St. Joseph, MI). The combustion unit was calibrated with EDTA as nitrogen standard. The nitrogen content was determined using a sample size of 50–125 mg and the protein content was expressed as total nitrogen (N) x 6.25 [34].

Moisture, ash, and mineral content

Freeze-dried samples of the feed (samples collected before filtration) and the final retentate and permeate were analyzed for moisture and ash contents. The moisture and ash contents were determined according to the methods derived from AOAC [48]. The ash residues were dissolved in 2 M HCl solution, and portions were used for mineral content analysis. Phosphorus was determined using the phospho-vanado-molybdate spectrophotometric method described in Analytical Methods Manual [49] with monobasic potassium phosphate standard. Magnesium and calcium contents were determined by inductively coupled plasma-optical emission spectrometry using Spectroflame Modula (FSM-08, Spectro Analytical Instruments, Kleve, Germany).

Unless stated otherwise, all analytical assays were performed in at least triplicates for each sample.

3.2.5 Numerical analysis

The increase of the protein concentration in the retentate during the filtration was quantified by fitting a first order kinetics equation to the experimental data:

$$c_R(t) = c_F \exp(kt) \tag{3-2}$$

where c_R (t) is the protein concentration in the retentate at time t, c_F is the feed concentration (at time 0), and k is the rate constant, representing the increase in protein concentration per unit time. Model fitting was performed with Microsoft Excel Solver function by minimizing the residual sum of squares.

3.2.6 Statistical analysis

The removal of total minerals (ash), calcium, phosphorus, and magnesium was compared for direct UF and DDF using a two-sample t-test (two tailed) as described by Montgomery [50] to determine whether there were any significant differences between the SPE 6 and SPE 9 feed. The removal of the components during direct UF and DDF was estimated from both the retentate and the permeate samples (each analyzed in triplicates).

3.3 Results and discussion

For this study, the operating TMP was selected from the permeate flux-TMP profile for a total recycle mode (both retentate and permeate recycled to the feed tank). During this operation, a typical concentration polarization effect was observed with an initial linear increase of the flux with TMP followed by a leveling off of the flux at TMP above 6 psi (41.4 kPa, **Figure 2.10**). On the basis of this analysis, the operating TMP of 6 psi was selected.

3.3.1 Composition profile during filtration

The concentration of TS, protein, and carbohydrates during stages 1 and 2 (DDF) for SPE 6 and SPE 9 is illustrated in **Figure 3.2** as a function of VCR. For clarity, the results of the direct UF of SPE 6 and SPE 9 are not shown as the composition profiles were similar to those observed in stage 1 of DDF (up to VCR 2).

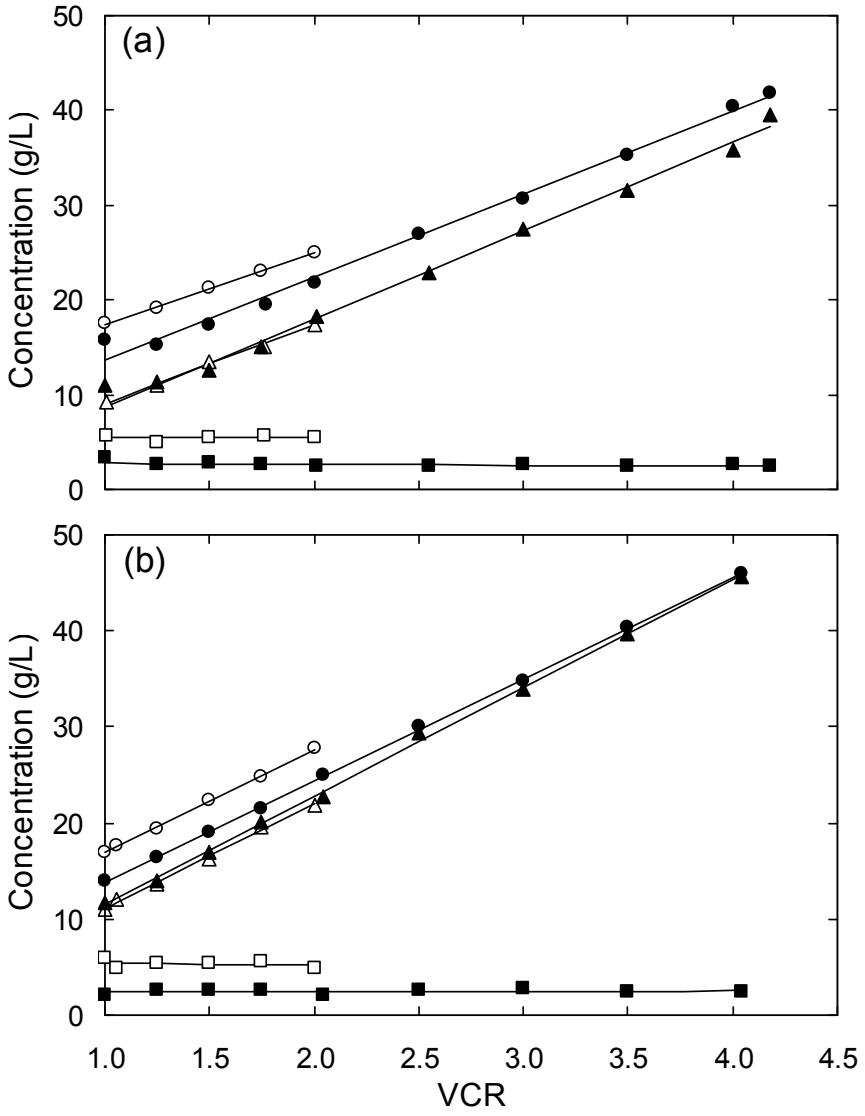

Figure 3.2 Effect of VCR on the retentate concentration of total solids (○,●), protein (△,▲), and carbohydrates (□,■) in DDF during stage 1 (open symbols) and stage 2 (closed symbols): (a) SPE 6 and (b) SPE 9. Protein determined by Bradford. MWCO = 100 kDa, TMP = 6 psi, shear rate = 8000 s^{-1}, T = 25 °C.

A 100 kDa membrane was used so that all proteins would be retained, whereas carbohydrates and minerals, the remaining components of the feed mixture, should be free to permeate through the membrane. A linear increase of the TS concentration in the retentate was observed for both the electroacidified and the non-electroacidified feeds. This increase was expected, because most of the TS were proteins (60 % initially in the feed). The TS concentration was lower for stage 2 of the DDF operation because about half of the

carbohydrates was removed in the permeate during stage 1. The concentration of the carbohydrates (smaller than the membrane MWCO) remained constant through the course of the filtration, indicating that the permeation of the carbohydrates across the membrane was not affected by the retention of the proteins. In contrast, the protein concentration increased with increasing VCR. The protein concentration profile was similar for both stages of DDF because the proteins were fully rejected by the membrane. The total rejection of the proteins by the membrane was confirmed by the analysis of the permeate, in which the protein concentration ranged between 0.049 and 0.155 mg/mL, accounting for about 0.7–3.1 % of TS in the permeate (**Table 3.1**).

Table 3.1 Composition of the feed, the final retentate, and the final permeate for direct UF and DDF of SPE 6 and SPE 9 [a]

Experiment	Sample	Volume (L)[b]	TS concentration (g/L)	% dry basis			Average total (%)
				Protein[c,d]	Carbohydrates[c]	Ash[c]	
SPE 6 Direct UF	Feed	1.421	18.0	55.2	33.3 ± 2.4	7.9 ± 0.1	96.4
	Retentate	0.315	52.0	91.6 ± 3.9	12.0 ± 2.3	4.2 ± 0.3	107.8
	Permeate	1.106	7.9	2.0 ± 3.0	73.8 ± 5.2	14.9 ± 5.0	90.7
SPE 6 DDF	Feed	1.406	18.0	55.2	32.4 ± 3.9	7.9 ± 0.1	95.5
	Retentate	0.336	42.0	94.6 ± 3.8	5.8 ± 3.3	3.5 ± 1.5	103.9
	Permeate 1	0.703	7.3	1.5 ± 2.9	55.5 ± 2.8	14.4 ± 0.9	71.4[e]
	Permeate 2	1.070	4.0	3.1 ± 5.6	51.1 ± 0.4	14.2 ± 3.7	68.4[e]
SPE 9 Direct UF	Feed	1.400	17.0	59.9	31.0 ± 1.7	9.4 ± 0.8	100.3
	Retentate	0.309	50.0	90.7 ± 3.1	10.4 ± 3.5	6.2 ± 4.9	107.3
	Permeate	1.091	6.7	0.7 ± 5.0	81.2 ± 4.1	18.5 ± 2.1	100.4
SPE 9 DDF	Feed	1.467	17.0	59.9	35.2 ± 4.8	9.4 ± 0.8	104.5
	Retentate	0.361	46.0	91.5 ± 1.7	5.3 ± 7.3	5.1 ± 0.1	101.9
	Permeate 1	0.738	6.7	1.1 ± 3.5	80.8 ± 2.3	16.6 ± 1.2	98.5
	Permeate 2	1.106	3.7	1.3 ± 6.2	55.9 ± 7.5	16.0 ± 1.5	73.2[e]

[a] Permeate 1 and 2 collected in DDF during stage 1 and 2, respectively. [b] Determined from mass using the density of water. [c] Mean ± relative standard error (n=3). [d] Feed and retentate determined by LECO (n=2); permeate determined by Bradford assay (n=3). [e] Indicates samples where the total composition differs from 100 % by more than 10 %.

The retention of proteins and the removal of carbohydrates during the filtration were also assessed through their respective mass fraction of the total solids. As expected, the protein content increased while the carbohydrate content decreased in direct UF and stage 1 of DDF (**Figure 3.3**).

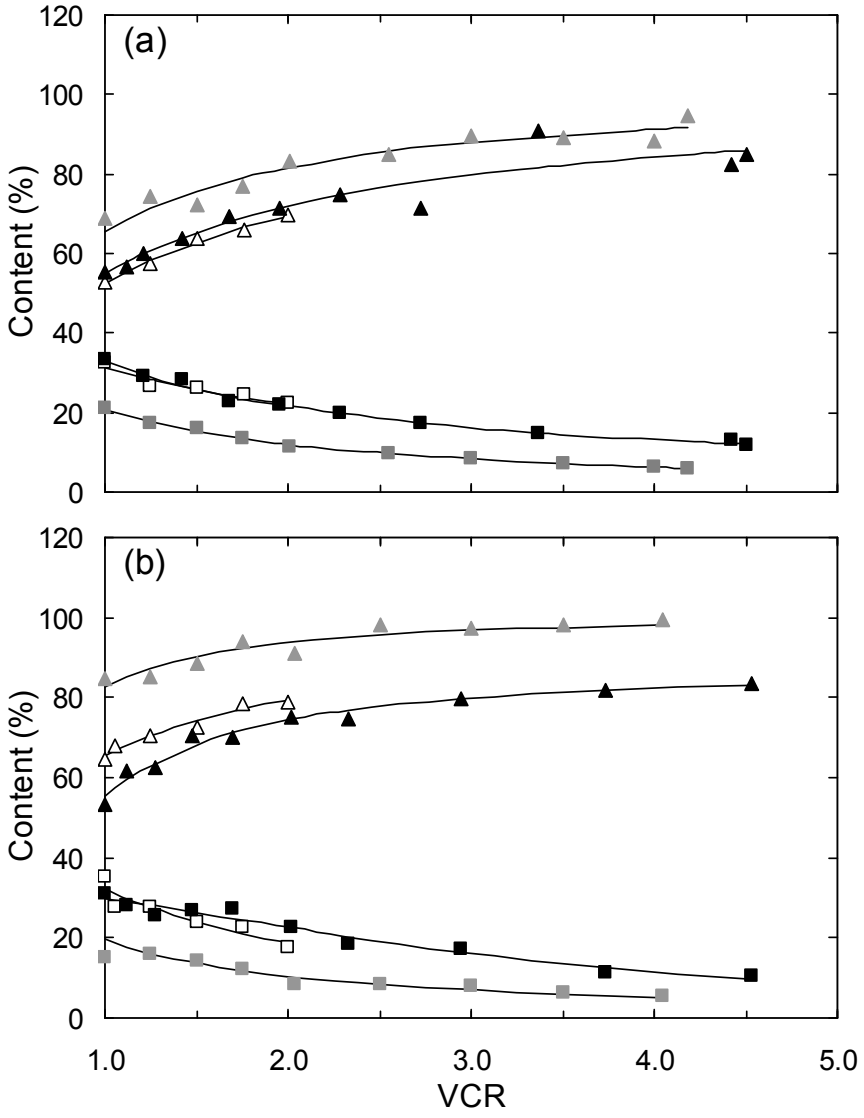

Figure 3.3 Protein (triangles) and carbohydrate (squares) content in retentate during direct UF (▲,■), stage 1 of DDF (△,□), and stage 2 of DDF (▲,■): (a) SPE 6 and (b) SPE 9. Protein determined by Bradford. MWCO = 100 kDa, TMP = 6 psi, shear rate = 8000 s^{-1}, T = 25 °C.

For both SPE 6 and SPE 9, the protein content appeared to level off above VCR 2.5 (direct UF). Such an observation agrees with previous results [24], when the amount of the permeable components remaining in the retentate decreases with the filtration

progress, resulting in a smaller change in the protein content. An additional removal of the non-protein solutes was achieved by DDF (stage 2) and resulted in a higher final protein content and a lower final carbohydrate content when compared to direct UF.

When considering the evolution with time of the protein concentration in the retentate for the direct UF operation, an exponential relationship was observed for both SPE 6 and SPE 9 (**Figure 3.4**). Similar behavior was also observed during the DDF operation (data not shown).

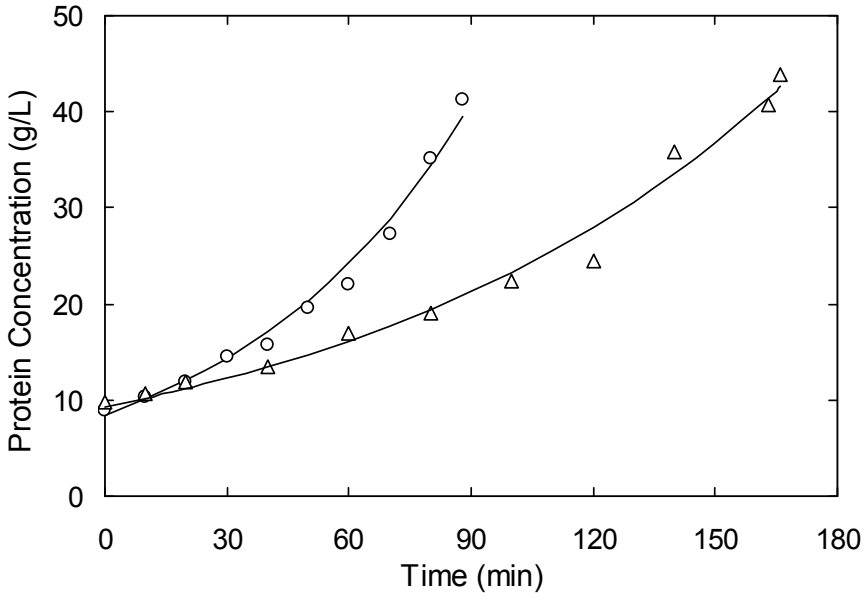

Figure 3.4 Protein concentration in retentate during direct UF and DDF as a function of time for SPE 6 (△) and SPE 9 (○). Solid line shows the fit based on the first order kinetics. Protein determined by Bradford. MWCO = 100 kDa, TMP = 6 psi, shear rate = 8000 s^{-1}, T = 25 °C.

The rate of the protein concentration increase was modeled using the first order kinetics (Eq. (3-2)), and the estimated rate constants (k) are presented in **Table 3.2**. A good fit was found between the model and the experimental data (R^2 values being in the range of 0.95–0.99). The rate constant, k, provides an estimate of how quickly the protein concentration increased during the filtration of SPE 6 and SPE 9 in direct UF or DDF modes. The values of the rate constant (k) for the electroacidified feed were always approximately half of those obtained for the non-electroacidified feed for both direct UF and DDF. In other words, the filtration time to reach the same final protein concentration (~40 g/L) was twice as long for the electroacidified feed compared to the non-

electroacidified feed, suggesting significant interactions between the proteins and the membrane at lower pH of the feed as will be discussed in subsequent sections.

Table 3.2 Rate constant (k) describing increase in protein concentration during direct UF and DDF of SPE 6 and SPE 9

Experiment	Rate constant, k (10^{-3} min^{-1})	
	SPE 6	SPE 9
Direct UF	9.2	17.6
DDF stage 1	7.8	13.7
DDF stage 2	7.8	15.0

3.3.2 Composition analysis of electroacidified and non-electroacidified soy protein isolates

In this study, proteins, carbohydrates, and ash were estimated by independent analytical techniques. The accuracy of the respective analytical techniques was assessed by computing the total mass balance for the feed, the retentate, and the permeate streams. As seen in **Table 3.1** (last column), the total mass balance accounted for 100 ± 10 % of the composition for most operations. Significant discrepancies for the permeate streams of the DDF operation are associated with the determination of the carbohydrate content. Assuming that the carbohydrates are freely permeable, an assumption supported by the concentration profile of the carbohydrates presented in **Figure 3.2**, the theoretical content of carbohydrates in the permeate should be at least 75 %. The carbohydrate content was calculated as the ratio of the carbohydrate concentration to the TS concentration. However, the TS concentrations in the feed or the retentate were much higher compared to the permeate samples (**Table 3.1**). For this reason, the carbohydrate content is associated with a higher experimental error compared to the feed or the retentate data. The removal of carbohydrates based on the retentate composition, indicates ~78 % for direct UF and ~89 % for DDF of both SPE 6 and SPE 9, which agrees with the theoretical expectations and results previously observed [24,42]. The effect of the feed electroacidification pretreatment and the mode of operation can be compared on the basis of the carbohydrate analysis for the retentate stream. The electroacidification pretreatment had a negligible effect on the carbohydrate content of the retentate for both

direct UF and DDF. For both feeds, the carbohydrate content of the retentate was reduced by 50 % for the DDF operation when compared to the direct UF operation.

Of utmost importance in this study is that a soy protein isolate (90 % protein, dry basis) was obtained for both operations, direct UF and DDF, and for both the electroacidified and the non-electroacidified feeds. Previous work with a dead-end system did not produce soy protein isolates after electroacidification pretreatment to pH 6 or 7 [34]. The protein content in the retentate determined by LECO analysis was on average above 90 % but the experimental error was significant (**Table 3.1**). Such estimates are higher than the theoretical predictions (~86 % for direct UF and ~92 % for DDF on dry basis) calculated using the protein content of the feed and assuming that all non-protein solutes are freely permeable. Although the protein content should be improved by ~7 % in DDF due to additional removal of carbohydrates and minerals, the analysis was unable to detect such differences in the two modes of operation.

The ash content (minerals intrinsically present in the SPE composition) was analyzed only at the end of the filtration when sufficient material was collected for the analysis. For both SPE 6 and SPE 9, the ash content in the retentate produced by direct UF decreased (**Table 3.1**), corresponding to a mineral removal of 64.1 % for SPE 6 and 59.0 % for SPE 9. By conducting two-stage DDF, the ash removal was enhanced to 71.8 % for SPE 6 and 63.8 % for SPE 9. For both direct UF and DDF, the mineral removal was lower than theoretical (based on free permeability assumption), indicating that the minerals were partially retained by the membrane. Although the mineral removal was similar for SPE 6 and SPE 9 during direct UF, a significantly higher mineral removal was achieved for SPE 6 compared to SPE 9 during DDF ($p < 0.1$). This could be attributed to the differences in the surface charge on the proteins at pH 6 and 9. Proteins at pH 9 possess a higher negative net charge, being further away from their isoelectric point, which could lead to a higher degree of electrostatic attraction to positively charged ions (minerals), compared to conditions at pH 6. A similar mineral removal effect was observed by Mondor et al. [34] during the dead-end ultrafiltration of the soy protein extracts with different pH values (6, 7, and 9). Kumar et al. [24] also indicated that during the ultrafiltration of soy flour suspension at pH 8, the minerals were partially retained, suggesting that they were either bound to the protein or in an insoluble form. In their

approach, a continuous diafiltration with 5 diavolumes (corresponding to > 99 % removal of all permeable components) was unable to achieve a complete removal of minerals, suggesting there could be a limit to mineral removal if the minerals were firmly bound to the protein or insoluble.

3.3.3 Phytic acid, magnesium, and calcium removal

The antinutritional nature of phytic acid and its known interactions with protein and divalent cations led us to investigate the removal of these components from SPE 6 and SPE 9 during direct UF and DDF. We decided to focus on magnesium (Mg) and calcium (Ca), because both are among the most abundant divalent minerals in soy products [14] and are known to form salts with phytic acid (phosphorus, P) [26,27,31]. Direct UF of the electroacidified feed (SPE 6) reduced magnesium, calcium, and phosphorus contents in the retentate when compared to the feed by a factor of 2.0, 1.5, and 1.4, corresponding to removals of 63, 55, and 50 %, respectively (**Table 3.3**). The two-stage diafiltration further improved the removal of all three components by 8, 11, and 7 % (for magnesium, calcium, and phosphorus, respectively) when compared to direct UF.

Table 3.3 Magnesium, calcium, and phosphorus (phytic acid) contents in feed and final retentate samples produced by direct UF and DDF

Extract	Sample	VCR	Content (mg/g dry powder)			Removal (%)[a]		
			Mg	Ca	P	Mg	Ca	P
SPE 6	Feed	1.0	4.40	5.98	7.54	-	-	-
	Retentate (UF)	4.5	2.26	3.99	5.53	63.1 ± 5.2	54.9 ± 4.0	50.3 ± 4.5
	Retentate	4.0	2.06	3.65	5.38	71.6 ± 1.8	65.9 ± 0.6	57.2 ± 2.2
SPE 9	Feed	1.0	2.80	3.34	4.91	-	-	-
	Retentate (UF)	4.5	2.54	4.20	6.85	40.9 ± 0.3	21.0 ± 3.2	11.0 ± 2.5
	Retentate	4.0	2.57	4.67	6.51	41.3 ± 1.5	14.4 ± 2.0	13.7 ± 2.3

[a] Expressed as mean ± range based on the mass balance calculations.

In contrast, both direct UF and DDF of the non-electroacidified feed (SPE 9) resulted in an increase of calcium and phosphorus contents in the retentate when compared to the feed. The overall removal of both components was marginal (11–21 %), indicating either

that the components are insoluble at pH 9 or that the degree of interactions between proteins, calcium, and phytic acid is higher at this pH. The difference in calcium and phosphorus removal between SPE 6 and SPE 9 was significant for both direct UF and DDF at $p < 0.05$.

Higher removal of calcium and phosphorus when the feed was electroacidified to pH 6 was previously observed by Mondor et al. [34] for the dead-end ultrafiltration system. The effects of phytate-calcium-soy protein interactions on the pH-solubility profiles of soy protein isolates were reported by Grynspan et al. [31], who noted an increased solubility of calcium, phytic acid, and protein just above pH 6.5. This solubility increase was attributed to the formation of a ternary complex. With increasing pH the solubility of protein kept on increasing while the solubility of calcium and phytic acid decreased, depending on their molar ratio. This observation suggests that for SPE 9, calcium and phytic acid are either associated with the protein via electrostatic forces or form an insoluble salt, both cases leading to the incapability of permeating through the membrane. In contrast, for the electroacidified feed at pH 6, the conditions for the formation of the ternary complex are limited (the proteins are negatively charged but less than at pH 9) and both calcium and phytic acid should be relatively soluble. The removal of calcium and phosphorus at pH 6 was still lower than the theoretical expectations based on free permeability (78 and 88 % for direct UF and DDF, respectively), indicating that both components are somewhat retained by the membrane but to a much lower extent than at pH 9.

In the context of the magnesium content, a higher reduction of magnesium was achieved in the final retentate for SPE 6 produced by direct UF and DDF when compared to SPE 9. The removal of magnesium was by 22 (direct UF) and 31 % (DDF) higher for SPE 6 than for SPE 9. The difference in magnesium removal between SPE 6 and SPE 9 was not as pronounced compared to the removals of calcium and phosphorus, which were closely correlated. Although both magnesium and calcium have been implicated in the context of protein-phytic acid interactions, our observations suggest that magnesium and calcium behave differently when contained in a soy protein mixture. This is especially obvious for the filtrations at pH 9, where the difference in the removal of magnesium compared to calcium and phosphorus becomes significant ($p < 0.05$). This could imply

that calcium has a higher affinity toward protein and/or phytic acid, which leads to more magnesium ions in a free form, able to permeate through the membrane.

3.3.4 The permeate flux characteristics of the electroacidified soy protein extract

The permeate flux profile and the filtration time to reach a desired VCR was used to investigate the process performance of the soy protein concentration. In direct UF, significant permeate flux decline was observed up to VCR 1.5 for both SPE 6 and SPE 9, indicating that most of the membrane fouling took place in the initial part of the filtration. After reaching VCR 1.5, the flux continued declining but at a lower rate. The permeate flux declined more seriously for SPE 6, with the final flux of ~6 $L/m^2.h$ (**Figure 3.5** (a)), which was half of the flux for SPE 9 reached at VCR 4.5 (**Figure 3.5** (b)). A more pronounced permeate flux decline for SPE 6 was also observed when using a dead-end and a low shear ultrafiltration system [34,36] and was attributed to the lower net charge of the proteins at pH 6 (closer to pI) compared to pH 9. As a result, the electrostatic repulsion forces become weaker, which would promote the formation of protein aggregates. Further analysis using a force balance on a given particle concluded that larger particles are more likely to deposit on the membrane surface and contribute to the cake layer formation [35]. Thus, the use of a high shear tangential flow hollow fiber system was unable to eliminate the higher fouling observed when the feed was electroacidified. The potential to improve the flux performance by a two-stage DDF was explored. It was hoped that a dilution step would reduce interactions between the proteins and other feed components involved in the membrane fouling [8]. Also, it was expected that lowering the concentration in the bulk solution could lead to solute desorption from the membrane surface, which would improve the permeate flux. However, the permeate flux did not increase after the water addition (stage 2 in DDF) regardless of whether the feed had been subjected to electroacidification or not. Due to more serious membrane fouling, both direct UF and DDF filtrations of SPE 6 required significantly more time compared to SPE 9 to achieve the same VCR (**Figure 3.5**, lower part). The total filtration time of the DDF operation was 264 min for SPE 6 compared to 147 min for SPE 9. These times were 1.6 and 1.7 times longer compared to direct UF of SPE 6 and SPE 9, respectively. Thus, the DDF operation with the dilution of the retentate at VCR 2 could

not disrupt the cake deposit on the membrane surface irrespective of the feed investigated in this study.

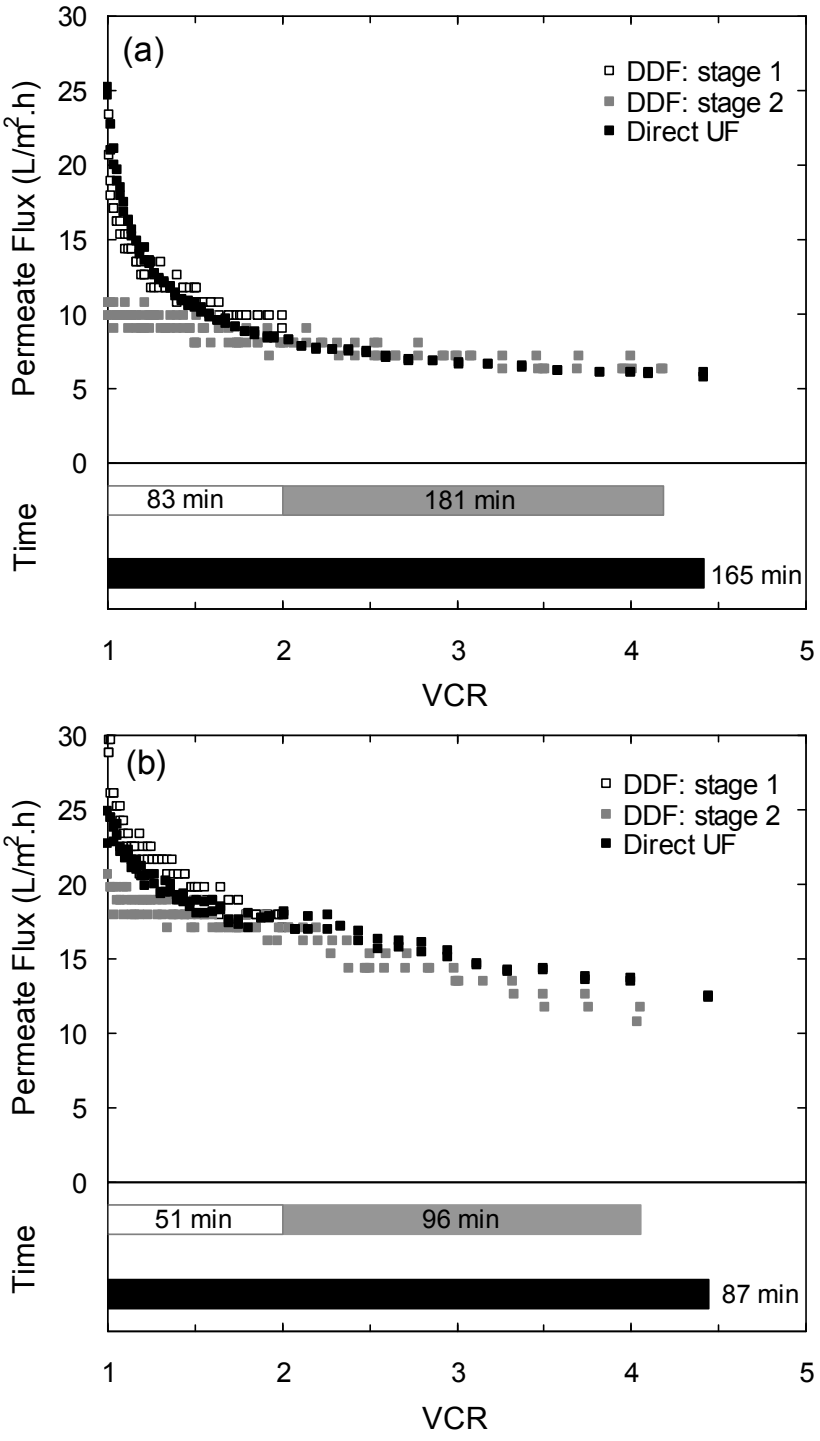

Figure 3.5 Permeate flux decline in direct UF and DDF as a function of VCR, with the filtration time indicated below: (a) SPE 6 and (b) SPE 9. MWCO = 100 kDa, TMP = 6 psi, shear rate = 8000 s^{-1}, T = 25 °C.

3.4 Conclusion

In this study, the suitability of using electroacidification for the production of soy protein isolates was investigated. We have demonstrated that soy protein isolates were obtained using a high shear tangential flow ultrafiltration system for a feed with or without electroacidification pretreatment and whether direct UF or discontinuous diafiltration was used. Carbohydrate analysis during the course of the filtration confirmed that carbohydrates behaved as freely permeable solutes. In contrast, magnesium, calcium, and phytic acid (antinutrient) were partially retained by the membrane. Electroacidification to pH 6 was beneficial in providing a higher removal of magnesium, calcium, and phytic acid when compared to the non-electroacidified feed at pH 9. A two-stage discontinuous diafiltration improved the carbohydrate removal (and thus increased the protein content) and the ash removal (including magnesium, calcium, and phosphorus) for the electroacidified feed. Despite the use of a high shear ultrafiltration configuration, the electroacidified feed at pH 6 was still characterized by higher fouling when compared to the non-electroacidified feed at pH 9. Future work will investigate the mechanisms responsible for the higher fouling observed for the electroacidified feed at pH 6.

4

Investigation of Membrane Fouling during Dead-End Ultrafiltration of Soy Protein Extracts*

Dead-end ultrafiltration experiments were carried out under unstirred conditions to investigate membrane fouling of an electroacidified (pH 6) and a non-electroacidified (pH 9) soy protein extract using 100 and 200 kDa polyethersulfone membranes. Due to more significant membrane fouling, the permeate flux was always lower for the electroacidified feed, resulting in longer filtration times. Evaluation of the fouling resistance components (by resistance-in-series model) showed that the magnitude of the reversible fouling was similar for both feeds but the irreversible fouling was more than 20 times higher for the electroacidified feed. The total amount of protein accumulated on the membrane (including reversible and irreversible fouling) was comparable for both feeds but protein deposition associated with the irreversible fouling was higher for the electroacidified feed. Examination of the fouled membranes by scanning electron microscopy showed that the electroacidified feed formed a denser and less permeable fouling deposit than the non-electroacidified feed. Adjusting the pH of the electroacidified feed to pH 9 decreased the membrane fouling significantly. A similar but opposite effect was observed with the non-electroacidified feed adjusted to pH 6, indicating that the pH of the feed was the most significant factor in the membrane fouling. Mineral deposition was correlated with protein deposition and did not appear to have a significant effect on the membrane fouling.

* Adapted from Skorepova, J., Moresoli C., submitted.

4.1 Introduction

In a previous study [51], the production of soy protein isolates was investigated by hollow fiber tangential flow ultrafiltration using an electroacidified soy protein extract at pH 6 (SPE 6) and a non-electroacidified soy protein extract at pH 9 (SPE 9). Comparing the filtration performance for the two soy protein extracts showed that electroacidification enhanced the removal of minerals (calcium, magnesium) and phytic acid but had a negative impact on the permeate flux, resulting in higher membrane fouling. This indicated that ultrafiltration at pH 6 reduces the protein-mineral-phytic acid interactions or the precipitation of calcium/magnesium phytate, both leading to improved separation of the minerals and the phytic acid from the soy proteins. Therefore, the objective of the current study was to characterize the higher membrane fouling observed for the electroacidified SPE 6 and to identify the components associated with fouling.

Due to their amphiphilic nature and large size, proteins are highly adhesive to solid surfaces and tend to be the major foulants in protein ultrafiltration [7,52]. Protein adsorption and deposition on the membrane surface increases the membrane resistance and results in the decline of the permeate flux. Protein adsorption is generally considered a thermodynamically driven process, which normally takes place under static conditions, and refers only to the protein that is directly bound to the membrane surface [53]. During ultrafiltration, where dynamic conditions exist, protein adsorption can still occur. In addition, the proteins are convectively carried to the membrane by the permeate flow and their accumulation near the membrane surface gives rise to concentration polarization. Higher concentration of proteins at the membrane surface may induce the formation of protein aggregates and their deposition/adsorption on the membrane. The degree of protein adsorption and deposition is mainly governed by protein-membrane and protein-protein interactions, respectively, which are driven by electrostatic, hydrophobic, and weak van der Waals forces. The predominant interactions will depend on the membrane material, the nature of the proteins, and the physicochemical conditions [4].

The strength and the nature of the electrostatic protein-membrane and protein-protein interactions are controlled by the solution pH and ionic strength. Many studies have shown that the permeate flux is minimal at the protein isoelectric point (pI) and

tends to increase either below or above the isoelectric point [4-6,54]. Palecek et al. [55] showed that the quasi-steady (long-term) flux during the filtration of five different proteins was directly proportional to the square of the protein charge density and independent of the protein molecular weight. Although the quasi-steady flux was quite similar for all five proteins at their pI (indicating similar resistance to flow), significant differences were observed in the sieving coefficients, suggesting a different structure and intermolecular spacing in the fouling deposit depending on the type of protein. In a subsequent study, Palecek and Zydney [56] showed that the permeability of the protein deposits decreased with increasing ionic strength (i.e., salt concentration). This was attributed to electrostatic shielding of the protein charge at higher ionic strength which would allow for protein re-structuring and tighter packing within the deposit. The correlation between a higher long-term flux and an increasing protein charge was also demonstrated by Huisman et al. [57] for filtration of bovine serum albumin (BSA) at various pH values. Mukai et al. [58] showed that the cake porosity during ultrafiltration of BSA at various pH values was minimal at the protein pI and increased with increasing zeta potential (i.e., protein charge) measured by electrophoretic light scattering. Menon et al. [59] pointed out the importance of electrolyte composition in protein (BSA) transmission through semipermeable ultrafiltration membranes due to changes in protein characteristics upon ion binding. At constant ionic strength but using different electrolytes ($NaClO_4$, NaCl, Na_2SO_4, $CaCl_2$, and CH_3COONa), protein transmission increased with increasing ion binding affinity and ion valence due to higher reduction of the protein charge and thus, the effective size (via compression of the electrical double layer). Marshall et al. [60] have shown that addition of only 8 mM ionic calcium caused a dramatic increase in the fouling resistance during ultrafiltration of β-lactoglobulin (milk whey protein) at neutral pH. This was attributed to calcium binding to carboxylic or other negatively charged groups, resulting in protein complex formation within the fouling deposit. Vetier et al. [61] found that calcium and phosphate salts contributed to the membrane fouling during microfiltration of milk. The amount of fouling increased after addition of calcium chloride which was believed to involve intermolecular links between calcium and proteins. Indeed, soy proteins (11S fraction in particular) in solution have the capability of binding calcium and magnesium ions. At low concentration, these minerals

might have a stabilizing effect on the structure of the 11S fraction [29]. Wallace et al. [30] have shown that the amount of calcium bound to the soy proteins increased with increasing pH between 7 and 11. As previously observed [51], direct tangential flow ultrafiltration of an electroacidified soy protein extract (SPE 6) to a volume concentration ratio of 4.5 with a 100 kDa membrane resulted in a 63, 55, and 50 % removal of magnesium, calcium, and phosphorus (phytic acid), respectively, compared to only 41, 21, and 11 % removal for ultrafiltration of the non-electroacidified soy protein extract (SPE 9) under the same operating conditions. This difference was explained by the formation of a ternary complex between soy proteins, magnesium/calcium, and phytic acid or by the precipitation of magnesium/calcium phytate which may occur at pH > 6.5. However, it is not clear whether magnesium, calcium and phosphorus also contribute to the membrane fouling during ultrafiltration of SPE 6 and SPE 9. The permeate flux is dictated by the thickness and the porosity of the fouling deposit. Chan et al. [62] provided a comprehensive review of microscopy and surface analysis techniques that can be used for characterization of protein fouled membranes. Scanning electron microscopy was used previously for characterization of the membrane fouling and/or elucidation of the fouling mechanisms [63-67].

In this work, ultrafiltration of soy protein extracts (SPE 6 and SPE 9) was performed in a dead-end system (without stirring) to permit a comprehensive examination of the membrane fouling. The reversible and irreversible membrane fouling components were evaluated by the resistance-in-series model. The reversible fouling, including the concentration polarization and part of the loosely attached deposit, was removed by rinsing the membrane with water. The remaining part of the deposit was considered as the irreversible fouling (due to adsorption and strongly attached foulants). The fouled membranes were examined by high-resolution field emission scanning electron microscopy (FESEM) which is suitable for examination of ultrafiltration membranes [66]. The amounts of protein (which was expected to be the major foulant), magnesium, calcium, and phosphorus deposited on the membrane were also determined. Phosphorus represents the content of phytic acid [18].

4.2 Materials and methods

4.2.1 Dead-end ultrafiltration

Unstirred dead-end ultrafiltration was performed in an Amicon filtration cell (model 8200, Amicon Inc., Beverly, MA, USA) with a volume capacity of 200 mL and a 28.7 cm^2 membrane surface area. The cell was pressurized with compressed nitrogen. Omega polyethersulfone (PES) membranes (Pall Corporation, Mississauga, ON, Canada) with a 100 and 200 kDa molecular weight cutoff (MWCO) supplied as flat sheets were used. The chemical structure of polyethersulfone is shown in the Appendix (Chapter 8). For each experiment, a new membrane piece was cut, placed in the cell, and pre-conditioned by rinsing it with 180 mL of Nanopure water (resistivity ~17.5 MΩ-cm, Barnstead water purification system, Dubuque, IA, USA). Lyophilized soy protein extracts (electroacidified SPE 6 and non-electroacidified SPE 9) containing approximately 60 % protein, 30 % carbohydrates, and 10 % ash (minerals) were obtained from Agriculture and Agri-Food Canada (Saint-Hyacinthe, PQ, Canada). The electroacidified SPE 6 and the non-electroacidified SPE 9 contained 0.44 % and 0.25 % magnesium (Mg), 0.60 % and 0.33 % calcium (Ca), and 0.75 % and 0.49 % phosphorus (P), respectively [51]. The major components of soy proteins are β-conglycinin (7S) and glycinin (11S) with molecular masses of 180–210 kDa and 300–350 kDa, respectively. Their average isoelectric point is at pH 4.5–4.8 [15]. The filtrations were performed with 50 mL of a ~2 % w/w SPE 6 or SPE 9 solution (prepared according to [51]) at room temperature (RT) and at constant transmembrane pressure of 30 psi (i.e., 206.8 kPa). The permeate flux was measured gravimetrically using an electronic balance (Adam Equipment Inc., Danbury, CT, USA) which was connected to a PC running Labview 7.1. Unless stated otherwise, the feed solution was concentrated to a volume concentration ratio (VCR) of 2.5 which was calculated as the initial feed volume to the retentate volume ratio.

4.2.2 Fouling layer resistance

According to Darcy's law, the permeate flux (J_P), expressed as the permeate volume (V_P) collected per unit time (t) per unit membrane area (A_M), is proportional to the transmembrane pressure (TMP) and inversely proportional to the permeate viscosity

(η_P) and to the total resistance (R_T). The total resistance can be divided into the clean membrane resistance (R_M) and the fouling layer resistance (R_F) according to Eq. (4-1). The clean membrane resistance is obtained from the pure water flux data collected as a function of transmembrane pressure before the filtration while the fouling resistance is determined at the end of the filtration as the difference between the total and the clean membrane resistance:

$$J_P = \frac{1}{A_M}\frac{dV_P}{dt} = \frac{TMP}{\eta_P R_T} = \frac{TMP}{\eta_P\left(R_M + R_F\right)} \tag{4-1}$$

Assuming the filtration proceeds in accordance with the conventional cake filtration theory, the fouling layer resistance (R_F) is proportional to the cake mass per unit membrane area (Eq. (4-2)):

$$R_F = \frac{\alpha c_B V_P}{A_M} \tag{4-2}$$

where α is the specific cake resistance and c_B is the solute concentration in the bulk. Substituting Eq. (4-2) into (4-1) and integrating provides:

$$\frac{t}{V_P} = \frac{\alpha c_B \eta_P}{2A_M^2 \Delta P} V_P + \frac{R_M \eta_P}{A_M \Delta P} \tag{4-3}$$

Plotting t/V_P versus V_P should yield a straight line and the slope is used to estimate the specific cake resistance (α).

The fouling layer resistance can be further partitioned into reversible (R_R) and irreversible (R_I) fouling:

$$R_T = R_M + R_F = R_M + R_R + R_I \tag{4-4}$$

To determine the fouling components, the membrane was rinsed at the end of the filtration with 25 mL of Nanopure water using a magnetic stirrer (supplied with the Amicon filtration cell) at 200 rpm for 3 min. After rinsing, the cell was emptied and the rinsing water was kept for further analysis. The cell was then filled with clean water and the water flux across the membrane was re-evaluated. This provided the sum of the clean membrane resistance and the resistance due to irreversible fouling. The resistance due to

reversible fouling was obtained from the difference between the total resistance and the resistances of the clean membrane and irreversible fouling.

The feed solution (i.e., before filtration) and the rinsing water, containing the solutes which were part of the reversible fouling, were analyzed for total solids and protein content. The total solids were determined gravimetrically by drying the samples (1 mL) at 100 °C overnight and the protein colorimetrically using Bradford Protein Assay (Standard Procedure for Microtiter Plates, Bio-Rad Laboratories, Mississauga, ON, Canada). Purified β-conglycinin (7S) and glycinin (11S) were used as protein standards (provided by M. Corredig, University of Guelph, ON, Canada). Standard solutions were prepared by combining the two proteins in a ratio of 1:1.4 which corresponds to their actual distribution in the soy proteins [15]. The total solids and protein recovered by rinsing the membrane with water represent the fraction of total solids and protein involved in the reversible fouling.

4.2.3 Mineral deposition

Samples (~7 cm^2) from the fouled membranes (after rinsing) were air-dried and ashed at 550 °C for 16 h in a muffle furnace. The ash residues were dissolved in 10 mL of 2 M HCl and analyzed for magnesium and calcium contents by inductively coupled plasma-optical emission spectrometry using Spectroflame Modula (FSM-08, Spectro Analytical Instruments, Kleve, Germany). Phosphorus was determined colorimetrically by phospho-vanado-molybdate method using monobasic potassium phosphate standard [49]. Since the mineral deposition was estimated using the fouled membranes after rinsing, the results represented the mineral content of the irreversible fouling layer.

4.2.4 Fouling layer morphology and protein deposition

The morphology of the fouling layer was studied by FESEM. For this purpose, filtrations were performed under identical operating conditions as described in Section 4.2.1 but only for 20 min duration. After each run, the membrane was removed from the system and two pieces (0.5 x 0.5 cm) were cut from the central membrane area. One of the pieces was rinsed with Nanopure water to remove labile solutes and then both pieces were fixed by soaking them for 3 h in 2.5 % glutaraldehyde prepared in 0.2 M phosphate

buffer (pH 7.2). The fixed membranes were serially dehydrated with 20–100 % v/v acetone solution, critical point dried, sputter-coated with 10–15 nm of gold (DESKII, Denton Vacuum Inc., Moorestown, NJ, USA), and observed by FESEM using LEO 1530 microscope (Carl Zeiss AG, Germany) at 5 kV of accelerating voltage.

The amount of protein deposited on the membranes after 20 min ultrafiltration was measured by a method derived from [66]. After the filtration, the membrane was gently rinsed with water, transferred to 10 mL of 5 % sodium dodecyl sulfate (SDS) solution, and incubated on a shaker for 5 h at RT. After the SDS incubation, the membranes looked clean, indicating protein desorption from the membrane. The solution was then analyzed for protein by BCA^{TM} protein assay (RT protocol, Pierce, Rockford, IL, USA) which is compatible with the 5 % SDS concentration. The protein standard was the mixed solution of purified β-conglycinin and glycinin in 1:1.4 ratio.

Statistical analysis was carried out according to Montgomery [50] using a two-sample t-test (two tailed) assuming an unequal variance to determine any significant differences in the results obtained for the different feeds (SPE 6 and SPE 9). Results are reported as mean ± standard error (SE) and the number of independent experiments (n) is indicated.

4.3 Results and discussion

4.3.1 Characteristics of the clean PES membranes

The resistance of the clean PES membranes was determined from the water flux measurements. The 100 kDa membrane had surprisingly a lower resistance (3.5×10^{11} m^{-1}, n = 19) than the 200 kDa membrane (4.5×10^{11} m^{-1}, n = 8). Although the difference was statistically significant ($p < 0.016$) due to the large n (number of tests), the variability between membranes cut from the same flat sheet was quite high, with the relative standard deviation up to 43 and 11 % for the 100 and the 200 kDa membrane, respectively. A similar membrane-to-membrane variability for the Omega PES membranes was also reported by Palecek et al. [55,56]. The FESEM micrographs of the clean membranes revealed morphological distinctions between the membranes (**Figure 4.1**). The 100 kDa membrane seemed rougher with pores forming within a network of

interlocking nodular structures. The pores of the 200 kDa membrane had various sizes with small to very large holes and the surface between them was very smooth.

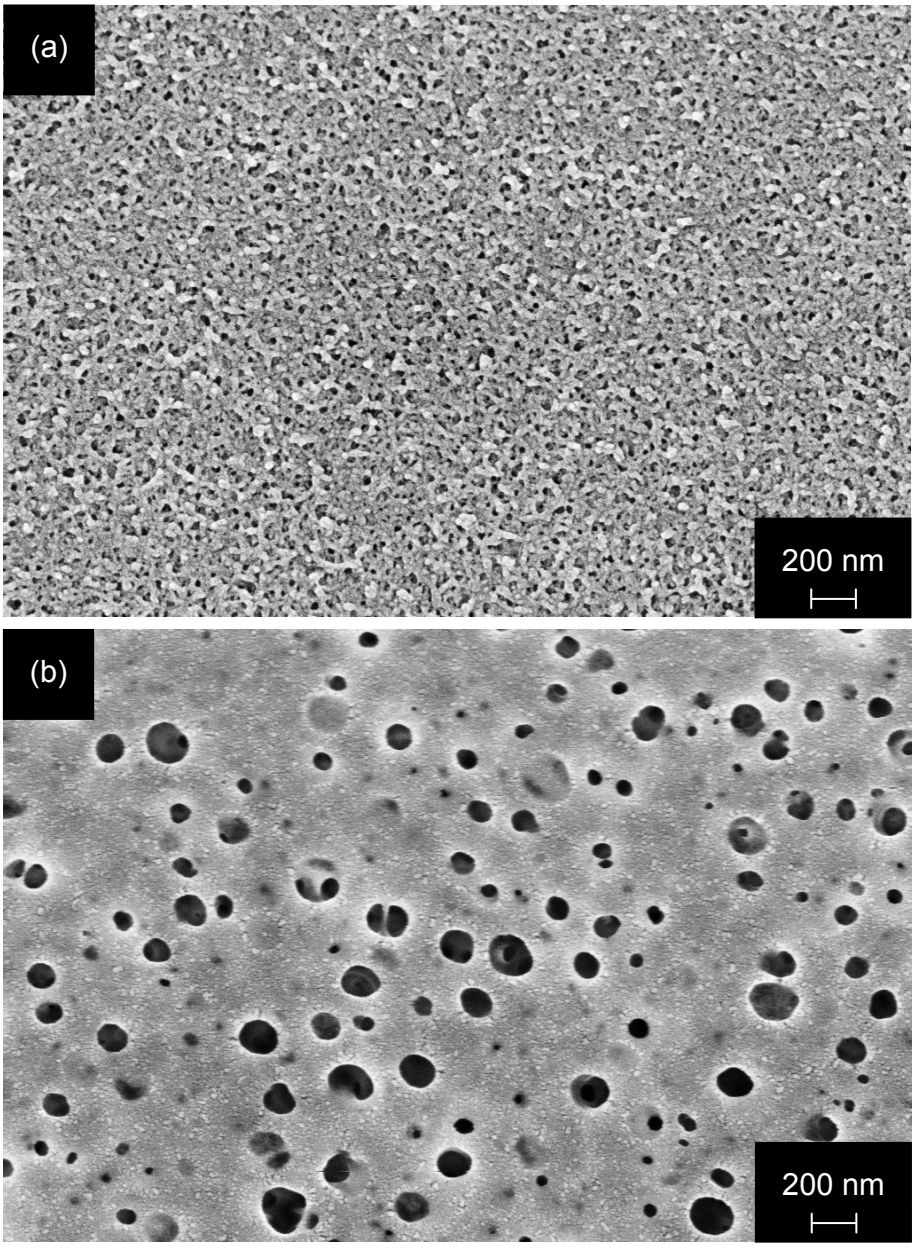

Figure 4.1 FESEM micrographs of the clean PES membranes (magnification 50,000×): (a) 100 kDa and (b) 200 kDa.

To quantify the number of pores per area and the mean pore size, images of the clean membranes were thresholded (using the same threshold range) and analyzed by ImageJ 1.37 software package (analyzing tool). This analysis showed that the pore density of the 100 kDa membrane was approximately 16 times higher compared to the 200 kDa

membrane. The mean pore size was 21 and 70 nm for the 100 and the 200 kDa membrane, respectively. The estimated porosity (pore area fraction) was, however, quite similar for both of the membranes, with the 100 kDa membrane having a somewhat higher porosity (9.7 %) than the 200 kDa membrane (8.6 %), which could explain the slightly higher permeability for the 100 kDa MWCO membrane.

4.3.2 Permeate flux profile

The permeate flux as a function of time for ultrafiltration of SPE 6 and SPE 9 to VCR 2.5 using the 100 kDa membrane is shown in **Figure 4.2**. The permeate flux profile for the 200 kDa membrane (data not shown) was indistinguishable from the one obtained for the 100 kDa membrane, which is likely attributable to the similar membrane porosities. As previously observed for the filtration of several different proteins (albumin, lysozyme, ribonuclease A, hemoglobin, and immunoglobulins) through the Omega PES membranes [55,56], the membrane-to-membrane variability of the clean membrane resistance, observed also in this work, had no effect on the subsequent permeate flux decline during filtration of the soy protein extracts.

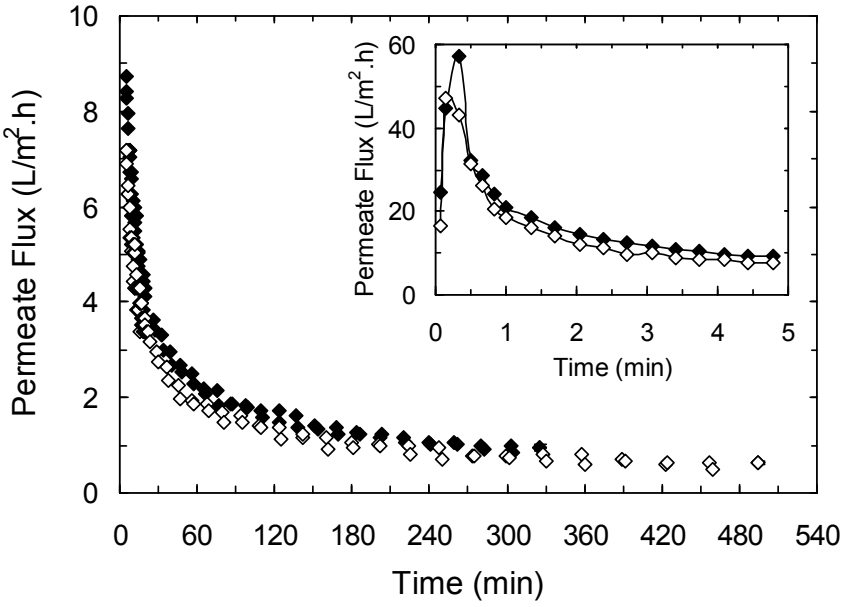

Figure 4.2 Permeate flux decline in ultrafiltration of SPE 6 (◇) and SPE 9 (◆) to VCR 2.5 using the 100 kDa membrane (n = 4), conditions: 30 psi and RT. Inset shows the first five minutes of the ultrafiltration runs.

The initial flux increase (to 40–60 L/m^2.h) due to pressurization of the cell to 30 psi was followed by a rapid flux decline (to ~20 L/m^2.h) in the first minute of the filtration (**Figure 4.2**, inset). The flux continued decreasing very rapidly in the first hour of the filtration and then relatively slowly in the following hours. As previously reported [34,51], the flux for the electroacidified feed (SPE 6) was always lower compared to the flux for the non-electroacidified feed (SPE 9), indicating more significant membrane fouling. The final flux was approximately 0.64 and 0.94 L/m^2.h for SPE 6 and SPE 9, respectively. As a result, ultrafiltration to VCR 2.5 was ~2.5 h longer for SPE 6 compared to SPE 9 (**Figure 4.3**).

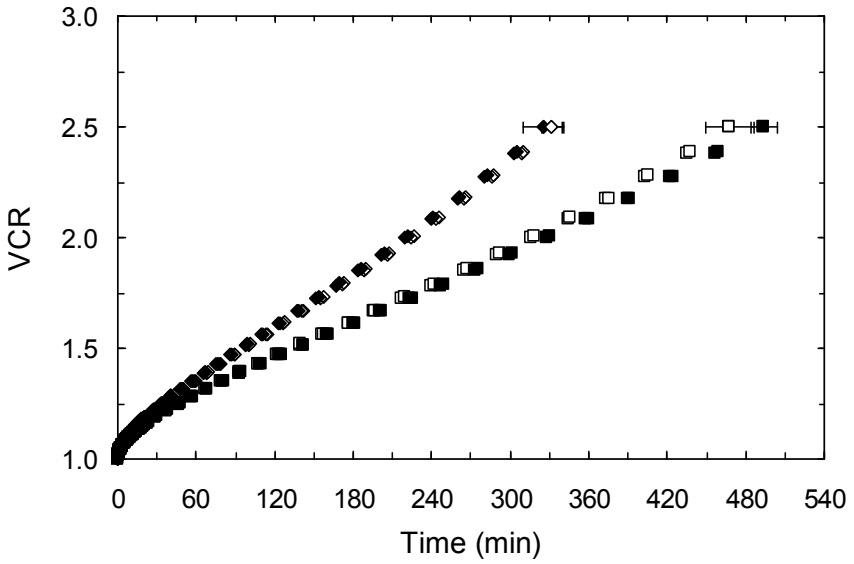

Figure 4.3 VCR as a function of time for ultrafiltration of SPE 6 (squares) and SPE 9 (diamonds) using the 100 kDa (closed symbols, n = 4) and the 200 kDa membranes (open symbols, n = 2), conditions: 30 psi and RT. Error bars (SE) along the time axis represent the variation in the filtration time to reach VCR 2.5.

The error bars along the time axis for the last data point in **Figure 4.3** represent the standard error in the filtration up to VCR 2.5. The difference between SPE 6 and SPE 9 for the 100 kDa membrane was significant ($p < 0.0003$, $n = 4$). However, there was no significant difference between the different MWCO membranes for a given feed.

4.3.3 Hydraulic resistance analysis

The relationship between t/V_P and V_P illustrated in **Figure 4.4** was approximately linear in agreement with the conventional cake filtration theory.

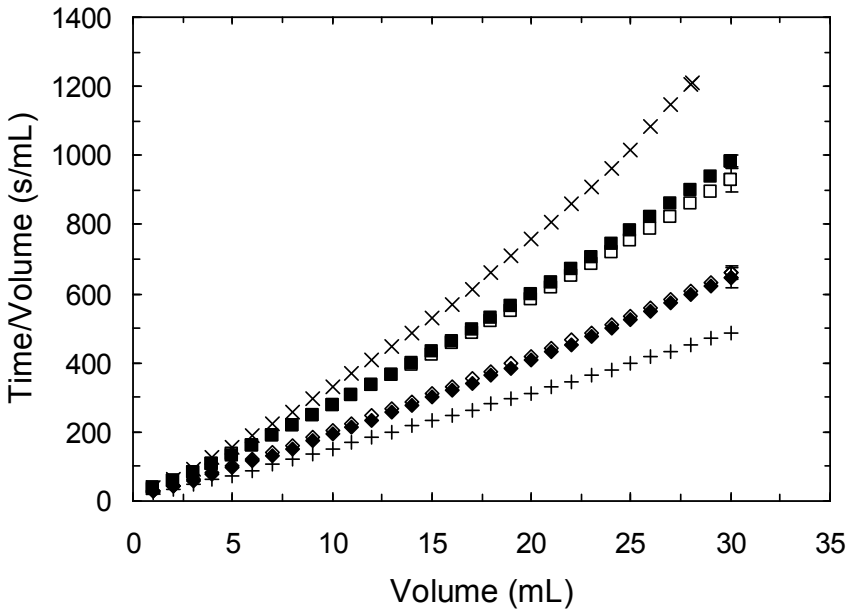

Figure 4.4 Plot of t/V_P versus V_P for ultrafiltration of SPE 6 (squares) and SPE 9 (diamonds) to VCR 2.5 using the 100 kDa (closed symbols, n = 4) and the 200 kDa membranes (open symbols, n = 2), conditions: 30 psi and RT. Error bars (SE) are shown at V_P = 30 mL. Data from ultrafiltrations of SPE 6 adjusted to pH 9 (+) and SPE 9 adjusted to pH 6 (×) using the 100 kDa membrane (same operating conditions).

The specific cake resistance (α) was estimated from the slope of the t/V_P versus V_P plot and Eq. (4-3). The slope was estimated by linear regression using all data points with R^2 values ranging between 0.989 and 0.999 for all curves in **Figure 4.4**. The specific cake resistances (α) obtained for SPE 6 were approximately 1.5 times higher than for SPE 9 and were independent of the membrane MWCO (**Table 4.1**). To investigate whether the membrane fouling was caused by the different pH of the feed, SPE 6 was adjusted to pH 9 (with 1 M NaOH) and SPE 9 to pH 6 (with 1 M HCl). The filtration was performed with the 100 kDa membrane under identical conditions as used for the pH unadjusted feeds. The specific cake resistance significantly increased for SPE 9 adjusted to pH 6 and inversely, it decreased for SPE 6 adjusted to pH 9. The curvature in t/V_P versus V_P profile for SPE 9 adjusted to pH 6 indicates that the specific cake resistance increases with time, which could be due to the consolidation of the cake layer. Although the t/V_P versus V_P profiles for the pH adjusted feeds were not exactly the same as the ones for the pH unadjusted feeds, it proved that the lower pH of SPE 6 was responsible for the observed higher membrane fouling.

Table 4.1 Specific cake resistance (α) evaluated from Eq. (4-3) and the fouling resistance (R_F) with the contribution of the reversible (R_R) and the irreversible (R_I) fouling for dead-end ultrafiltration to VCR 2.5

Feed	MWCO (kDa)	α x 10^{-15} (m/kg) [a]	R_F x 10^{-15} (m^{-1}) [a]	R_I x 10^{-15} (m^{-1})	R_R x 10^{-15} (m^{-1})
SPE 6	100	7.3 ± 0.1	1.32 ± 0.01	0.29	1.03
SPE 6	200	7.0 ± 0.3	1.26 ± 0.06	0.27	0.98
SPE 9	100	4.4 ± 0.2	0.92 ± 0.01	0.01	0.91
SPE 9	200	4.5 ± 0.1	0.89 ± 0.05	0.01	0.88
SPE 9 adjusted to pH 6	100	8.6	1.77	0.24	1.53
SPE 6 adjusted to pH 9	100	3.6	0.64	0.01	0.63

[a] n = 3 and n = 2 for 100 and 200 kDa, respectively.

Since no information could be found in the literature regarding the specific cake resistance for ultrafiltration of soy proteins, the estimates obtained for the specific cake resistance in this study were compared with literature values reported for ultrafiltration of solutions containing different protein types. The specific cake resistances for soy proteins (**Table 4.1**) are in good agreement with the reported estimates for BSA, in the range of 2×10^{15}–7×10^{15} m/kg [54], and for hemoglobin, BSA and gelatin, in the range of 7×10^{15}–8×10^{16} m/kg [68]. According to the Carman-Kozeny equation [69], developed for a packed bed of rigid spherical particles, the specific cake resistance (α) is a function of bed porosity (ε), particle diameter (d) and particle density (ρ) (Eq. (4-5)):

$$\alpha = \frac{180(1-\varepsilon)}{\rho d^2 \varepsilon^3} \tag{4-5}$$

Assuming an average porosity of 0.4 (typical value for randomly packed spherical particles of uniform size [69]), a particle density of 1000 kg/m^3 and using the estimates for α listed in **Table 4.1**, the particle diameter was estimated to be between 14–22 nm, which is a reasonable estimate of protein size. The use of Carman-Kozeny equation to estimate the porosity of the protein deposits is limited due to the assumption of rigid, non-interacting particles. Nevertheless, Carman-Kozeny equation shows that the magnitude of the specific cake resistance for soy proteins are what one would expect for particles in a protein size range.

After the filtration, the membranes were rinsed with water to remove loosely attached foulants (reversible fouling). The resistance of the rinsed membranes was evaluated from the water flux measured at 30 psi corresponding to the pressure at which the filtrations were performed. As shown in **Figure 4.5**, the water flux across the SPE 6 fouled membranes was always around 2–4 L/m^2.h and remained constant over the 10 min period. In contrast, the water flux through the membranes fouled by SPE 9 was much higher but decreased continuously from 200 to 60 L/m^2.h during the 10 min period (and kept on decreasing for longer time periods).

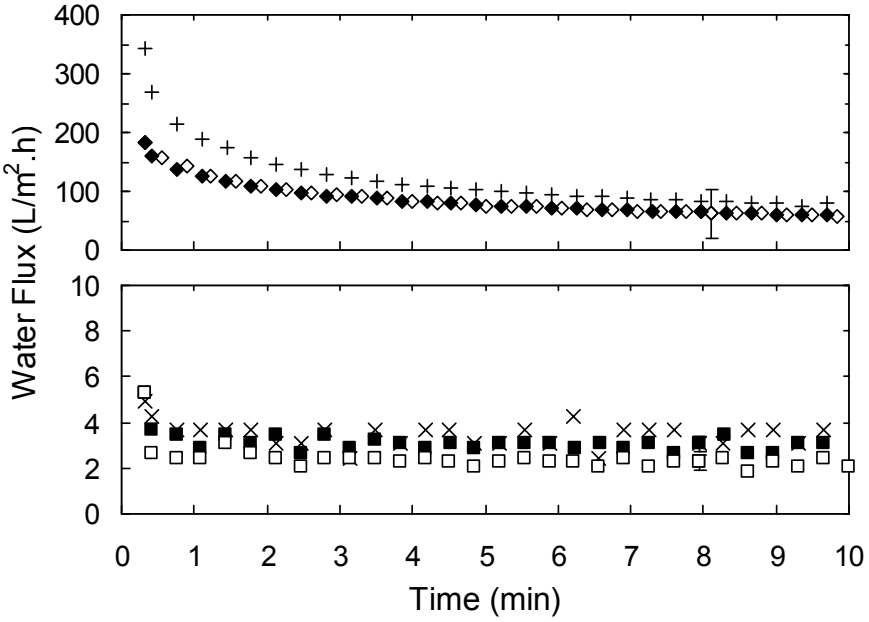

Figure 4.5 Water flux as a function of time across rinsed membranes after ultrafiltration of SPE 6 (squares) and SPE 9 (diamonds) to VCR 2.5 using the 100 kDa (closed symbols, n = 3) and the 200 kDa membranes (open symbols, n = 2), conditions: 30 psi and RT. Error bars (SE) are shown at t = 8 min. Data from ultrafiltrations of SPE 6 adjusted to pH 9 (+) and SPE 9 adjusted to pH 6 (×) using the 100 kDa membrane (same operating conditions).

The time-variable permeability for SPE 9 suggests that the fouling layer remaining on the membrane is less stable compared to that of SPE 6 and the exposure to the pressure and to the permeation flow causes its consolidation. It is also possible that exposing the fouled membrane to Nanopure water during the water flux measurements results in the consolidation of the fouling deposit due to the decrease in ionic strength. In contrast, the fouling layer of SPE 6 was likely more rigid and/or the drag force exerted by the low permeation flow was too low to induce any structural changes. The water flux of the

membrane fouled with SPE 9 adjusted to pH 6 was similar to the magnitude of the flux observed for the SPE 6 fouled membranes and remained constant over time (**Figure 4.5**). Similarly, the water flux for the membrane fouled with SPE 6 adjusted to pH 9 was consistent with the flux profile obtained for the SPE 9 fouled membranes.

These experiments show that the pH of the feed affects the permeability of the fouling layer. The water flux was averaged for the last 1.5 min (for each series) to determine the resistance due to irreversible fouling. Note that the fouling layer resistance (R_F) in **Table 4.1** was by four orders of magnitude higher than the clean membrane resistance for all filtrations. Regardless of the membrane MWCO, the irreversible fouling resistance (R_I) constituted about 22 % of the fouling layer resistance (R_F) for SPE 6 and was negligible (1 %) during ultrafiltration of SPE 9, indicating that the fouling was mostly reversible for SPE 9. As expected, the irreversible fouling increased when SPE 9 was adjusted to pH 6 and similarly, decreased when SPE 6 was adjusted to pH 9. These observations are in disagreement with a previous study by Mondor et al. [35] who estimated the irreversible fouling between 1 and 2 % for both SPE 6 and SPE 9. However, Mondor et al. [35] used agitation and regenerated cellulose hydrophilic membranes which could have minimized protein adsorption.

4.3.4 Morphology of the fouled membranes

The lower permeate flux observed during the filtration of SPE 6 resulted in a lower volume of the permeate collected over time when compared to SPE 9 even at early stages of the filtration (**Figure 4.6**).

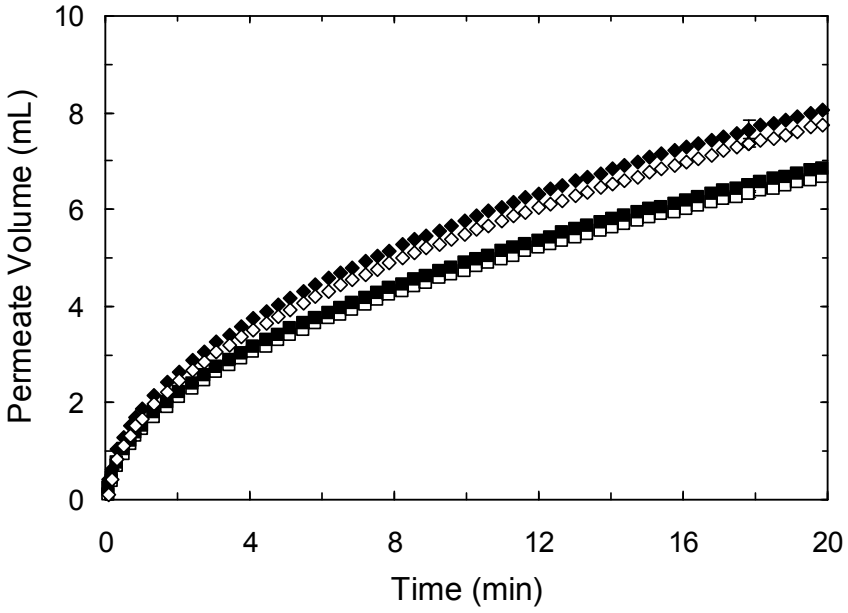

Figure 4.6 Permeate volume collected during ultrafiltration of SPE 6 (squares) and SPE 9 (diamonds) for 20 min using the 100 kDa (closed symbols) and the 200 kDa (open symbols) membranes (n = 7), conditions: 30 psi and RT. Error bars (SE) are shown at t = 18 min.

The fouling layer morphology was evaluated using FESEM to clarify the differences in the flux behavior. Samples of the fouled membranes after 20 min ultrafiltration analyzed by FESEM revealed some differences in the fouling layer structure. SPE 6 on the 100 kDa membrane had a dense but fine structure with a few filamentous strands and some large aggregates (~700 nm) on the top of the surface (**Figure 4.7** (a)). The fouling layer of SPE 9 (**Figure 4.7** (b)) had a light, more open structure with many filamentous strands covering the surface. Similar differences according to the feed type were also observed for the 200 kDa membrane (**Figure 4.8**). The fouling layer of SPE 6 (**Figure 4.8** (a)) consisted of aggregated fibers which appeared much thicker when compared to those of SPE 9 (**Figure 4.8** (b)). The deposits formed by SPE 9 looked alike on both MWCO membranes but some morphological differences became apparent for SPE 6 with respect to the membrane MWCO (**Figure 4.7** (a) and **Figure 4.8** (a)). It could be that the clean membrane acts as a template providing support for the formation of the initial fouling layers. The 100 kDa membrane with smaller and more uniformly distributed pores could give rise to a finer deposit than the 200 kDa membrane with large pores (**Figure 4.1**). However considering only the differences

between SPE 6 and SPE 9, it seems that soy proteins tend to form denser and more compact deposits with lower permeability at pH 6 than at pH 9, as also supported by the higher fouling resistance for solutions at pH 6 (**Table 4.1**). This can be attributed to the higher negative charge of the soy proteins at pH 9 compared to pH 6 where the proteins are closer to their pI (4.5–4.8) and the electrostatic repulsion forces are weaker, which permits denser protein packing on the membrane surface. This is consistent with the work of Mukai et al. [58] who showed for dead-end ultrafiltration of BSA that the cake porosity was minimal at the protein isoelectric point and increased with increasing protein charge.

Rinsing the membranes with water removed most of the fibrous material (**Figure 4.7** (c), (d) and **Figure 4.8** (c), (d)). Although the pores of the 100 kDa membranes were still mostly covered, a few openings became visible through the SPE 9 deposit (**Figure 4.7** (d)). More apparent differences were seen between the fouling deposits on the 200 kDa membranes according to the feed pH (**Figure 4.8** (c) and (d)). A considerable amount of material still covered the membrane used for the SPE 6 filtration, although in comparison to the non-rinsed membrane (**Figure 4.8** (a)), the network seemed less dense. The 200 kDa membrane with the SPE 9 deposit looked much cleaner after rinsing and many pores became uncovered (**Figure 4.8** (d)). Supporting the more significant irreversible fouling resistance obtained from the water flux for SPE 6 (**Table 4.1**), the fouling deposit observations with FESEM show that soy proteins may bind to the membrane surface more strongly at pH 6 than at pH 9. The reduction of the protein net charge as the pH approaches the pI is likely coupled with an increase in protein hydrophobicity, leading to higher protein-protein interactions and aggregation. This was confirmed by Mondor et al. [35] who found (using a light scattering technique) that SPE 6 reconstituted in double distilled water contained larger particles than SPE 9.

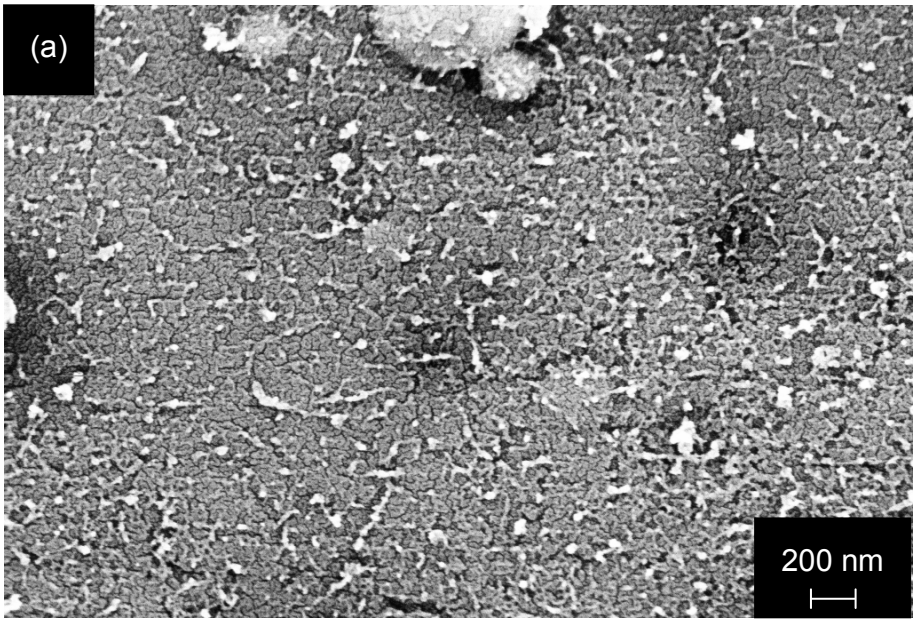
(a)
200 nm

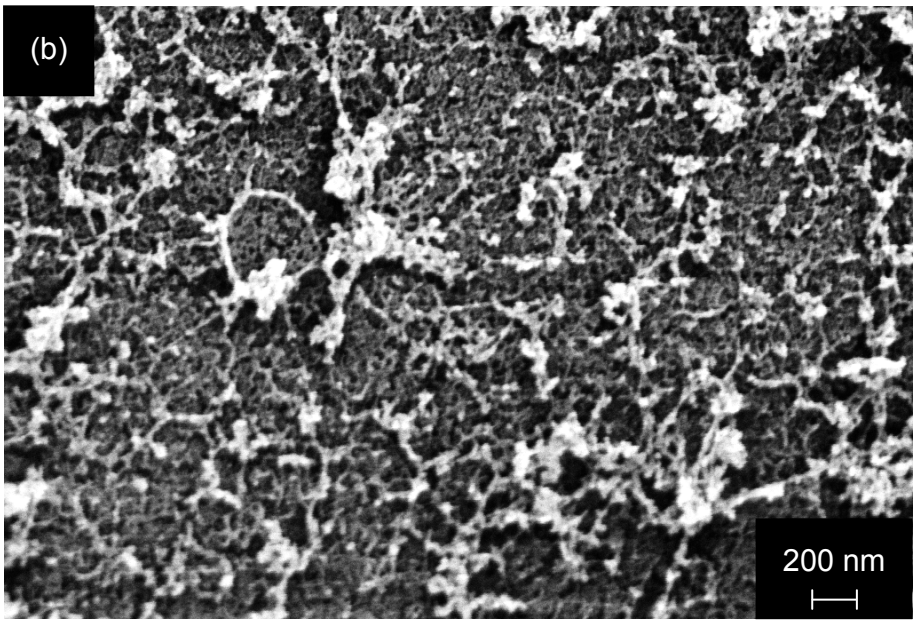
(b)
200 nm

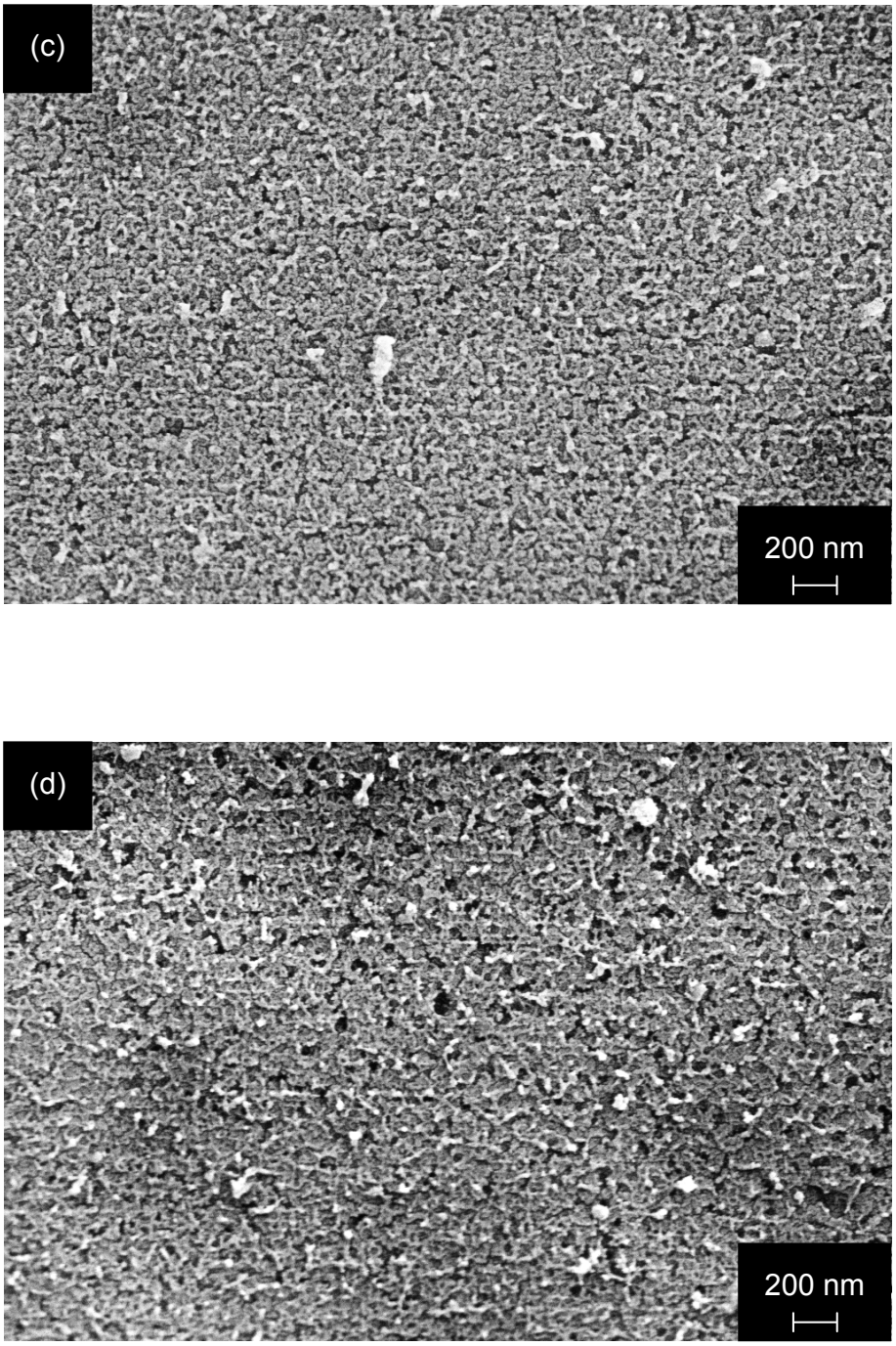

Figure 4.7 FESEM micrographs of the fouled and rinsed 100 kDa membranes after 20 min ultrafiltration (magnification 50,000×): (a) fouled, SPE 6; (b) fouled, SPE 9; (c) rinsed, SPE 6; (d) rinsed, SPE 9.

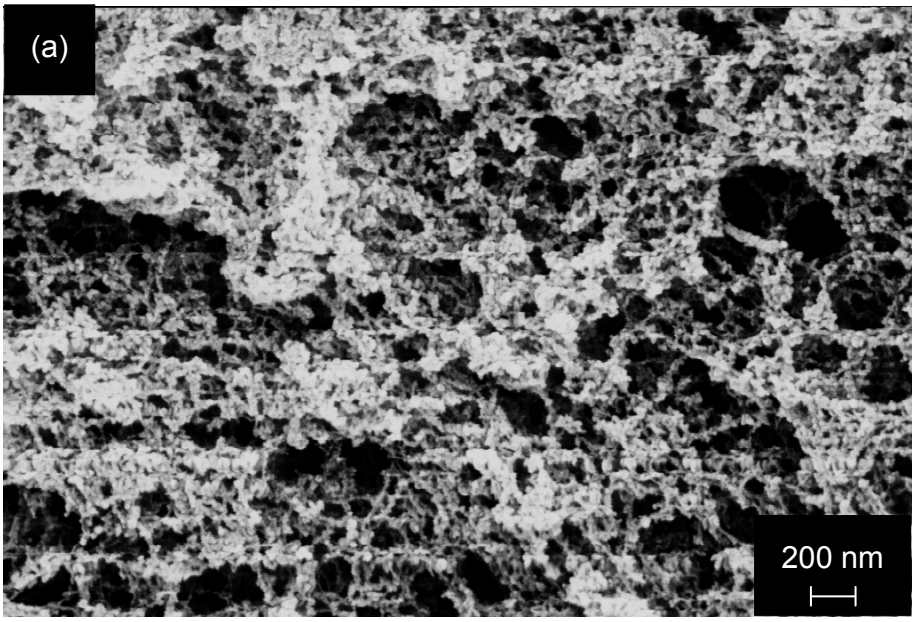
(a)
200 nm

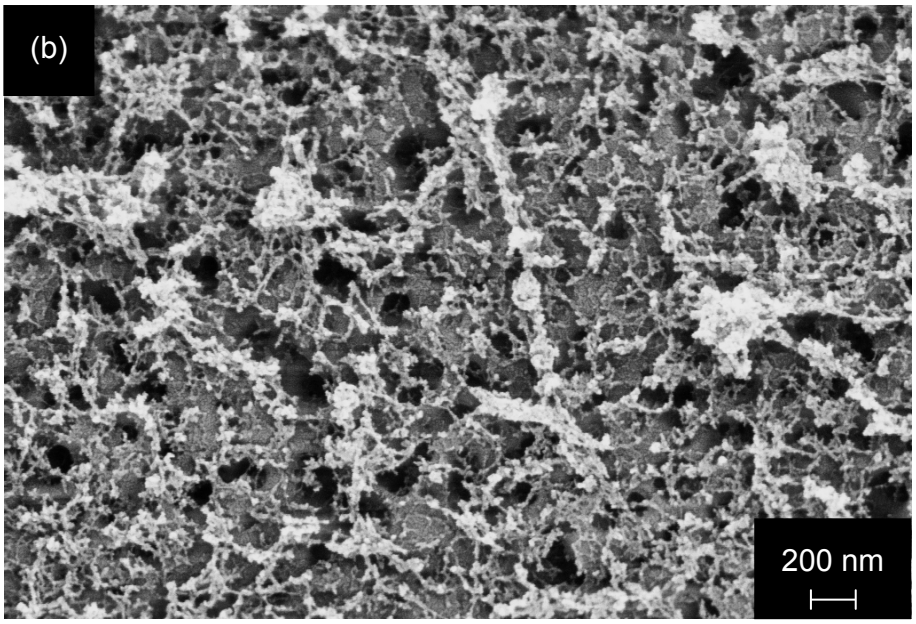
(b)
200 nm

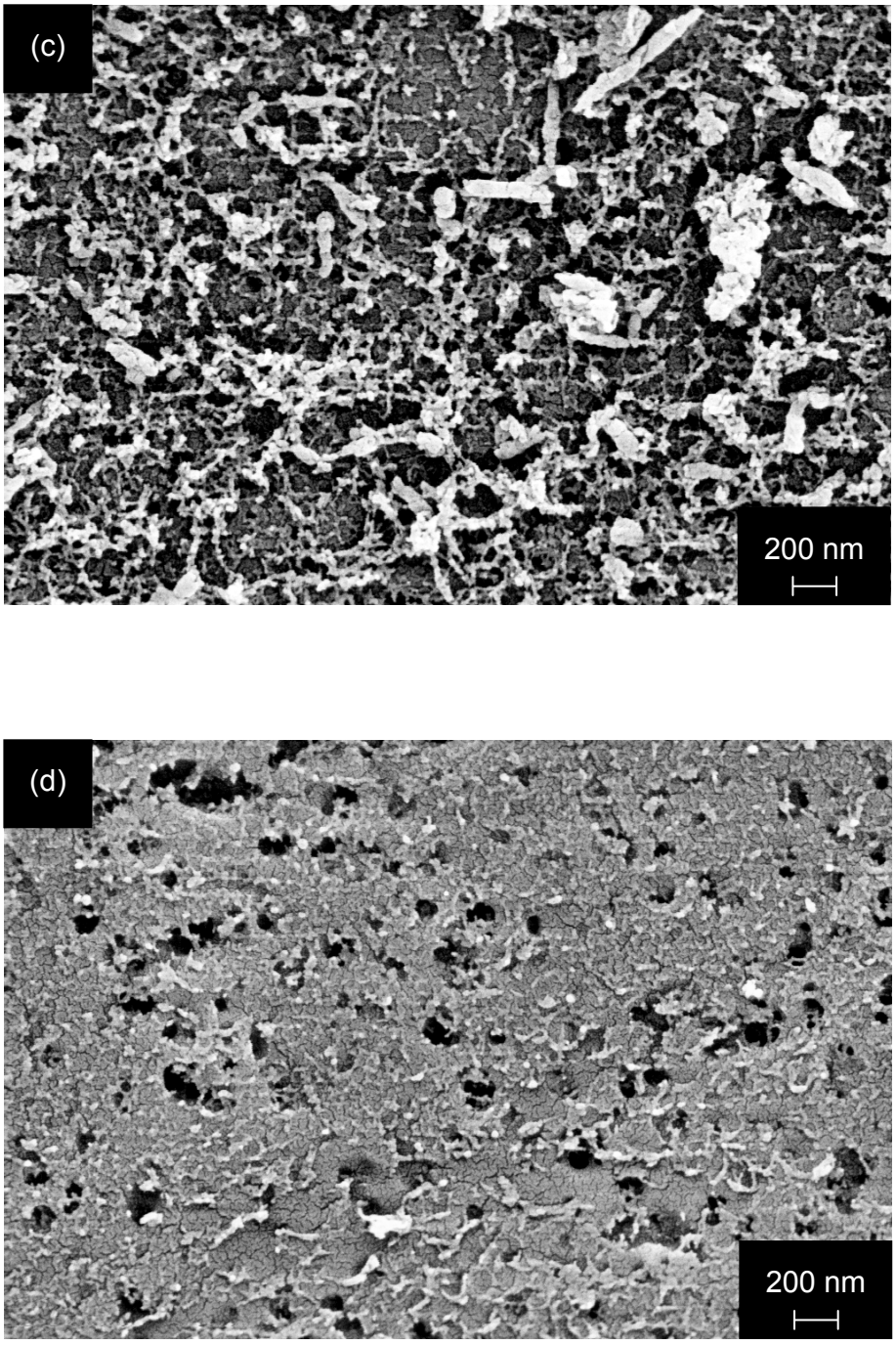

Figure 4.8 FESEM micrographs of the fouled and rinsed 200 kDa membranes after 20 min ultrafiltration (magnification 50,000×): (a) fouled, SPE 6; (b) fouled, SPE 9; (c) rinsed, SPE 6; (d) rinsed, SPE 9.

4.3.5 Estimation of protein content in irreversible/reversible fouling

Protein deposition on the membranes after 20 min ultrafiltration was estimated by soaking the membranes in 5 % SDS solution for 5 h and then measuring the protein concentration. It should be noted that the membranes were briefly rinsed with water before soaking them in the SDS solution and this was assumed to be sufficient to remove the reversible fouling. The protein deposits are, therefore, considered estimates of the proteins participating in the irreversible fouling layer. The amount of protein deposited on the 100 and the 200 kDa membrane was 290 ± 88 μg/cm^2 (n = 3) and 504 ± 164 μg/cm^2 (n = 2), respectively, for SPE 6. This was higher compared to the protein deposition for SPE 9, 82 ± 3 μg/cm^2 and 118 ± 10 μg/cm^2 using the 100 and the 200 kDa membrane (n = 2), respectively. Due to the high variation in the protein deposition estimates for the 20 min filtration (especially for SPE 6), we decided to perform ultrafiltration of SPE 6 and SPE 9 to VCR 2.5 (i.e., for several hours, see **Figure 4.3**) using the 100 kDa membrane to obtain a more pronounced difference between the two feeds. A visual inspection of the fouled membranes at the end of the filtration revealed that the deposit of SPE 6 was clearly thicker compared to that of SPE 9. The results of protein analysis showed that there was a 21-fold increase in protein deposition after ultrafiltration of SPE 6 (2700 μg/cm^2) compared to SPE 9 (130 μg/cm^2), which correlates with the difference seen in the irreversible fouling resistance observed for the two feeds (**Table 4.1**). Considering the membrane area (28.7 cm^2), the amount of protein involved in the irreversible fouling was 77.5 mg for SPE 6 and 3.7 mg for SPE 9. Although the feed solution was prepared in the same way for both extracts, the protein mass of the feed was 0.46 and 0.60 g for SPE 6 and SPE 9 (SE = 0.01 g, n = 6) respectively, due to the lower solubility and protein content of the SPE 6 extract. This indicates that 16.8 % (SPE 6) and 0.6 % (SPE 9) of the protein present initially in the feed became part of the irreversible fouling. Protein deposition estimated by Kim et al. [66] during one hour ultrafiltration of 0.1 % w/w BSA using various types of membranes were in the range of 34 to 133 μg/cm^2, which is comparable with the protein deposition obtained for SPE 9. The amount of protein deposited observed in this study during ultrafiltration of SPE 6 to VCR 2.5 was by an order of magnitude higher compared with the BSA study of Kim et al. [66].

The water used for rinsing the membranes after the filtration to VCR 2.5 was analyzed for the total solids (TS) and protein content (**Table 4.2**) to quantify the components contributing to the reversible fouling.

Table 4.2 Amount of total solids (TS) and protein in rinsing water and deposition of magnesium, calcium, and phosphorus (phytic acid) on membrane during ultrafiltration

Feed	MWCO (kDa)	TS mass [a] (mg/cm^2)	Protein (% of TS)	Mg [b] ($\mu g/cm^2$)	Ca [b] ($\mu g/cm^2$)	P [b] ($\mu g/cm^2$)
SPE 6	100	4.3 ± 0.1	93	2.75 ± 0.42	4.80 ± 1.25	5.36 ± 0.73
SPE 6	200	4.4 ± 0.1	93	2.45 ± 0.20	4.01 ± 0.05	4.88 ± 0.19
SPE 9	100	6.8 ± 0.4	100	0.24 ± 0.06	1.01 ± 0.18	0.80 ± 0.18
SPE 9	200	7.0 ± 0.2	102	0.15	0.77	0.76 ± 0.20
- [c]	100	-	-	0.04	1.04	0.23
- [c]	200	-	-	0.06	0.78	0.18

[a] Mass of total solids (TS) per membrane area (28.7 cm^2), n = 4. [b] n = 2. [c] Clean membrane (control).

The proteins accounted for most of the total solids (above 90 %) in the rinsing water for both SPE 6 and SPE 9. The total solids content and the corresponding protein estimates in **Table 4.2** were used to calculate the protein surface coverage (calculated per membrane area) for the 100 kDa membrane, 4.0 mg/cm^2 for SPE 6 which is significantly lower ($p < 0.005$, $n = 4$) when compared to SPE 9, 6.8 mg/cm^2. The estimated protein content in the rinsing water, associated with reversible fouling, is in agreement with the resistance-in-series estimates presented in **Table 4.1**. The relative contribution of the reversible fouling for SPE 6 was lower when compared to SPE 9. By looking at the analysis of the protein desorbed from the membrane and the analysis of the protein in the rinsing water, one can get an estimate of the contribution of the proteins to the overall fouling. The quantity of protein involved is similar for both SPE 6 (6.70 mg/cm^2) and SPE 9 (6.93 mg/cm^2) but nearly all of the protein coverage for SPE 9 was detected in the rinsing water corresponding to the reversible fouling while for SPE 6, the protein coverage was distributed between the rinsing water (reversible fouling) and the desorption analysis (irreversible fouling). However, with respect to the protein content of the feed solutions (i.e., 0.46 and 0.60 g for SPE 6 and SPE 9, respectively), the relative amount of protein accumulated on the membrane turns out to be higher for SPE 6 (42 %) than for SPE 9 (33

%). Since the quantity of protein (in mg/cm^2) involved in the overall membrane fouling is comparable for both SPE 6 and SPE 9, the higher permeate flux decline observed for the electroacidified feed (SPE 6) may be related to its more compact fouling structure as revealed by the FESEM micrographs (**Figure 4.7** and **Figure 4.8**). The role of the cake structure was also reported by Mourouzidis-Mourouzis et al. [70] for the microfiltration of whey proteins using ceramic membranes at pressures ranging from 2.5 to 10 psi. During the microfiltration of whey, the amount of protein deposited at the end of the filtration was higher at the lower pressure but a lower flux decline was observed, suggesting a more porous deposit at the lower pressure than at the higher pressure. The amount of whey protein deposited at the end of the filtration for the various pressures (15 to 30 mg) and the active membrane surface area (12.5 cm^2) indicate that the protein surface deposition, 1.2–2.4 mg/cm^2 [70], was of the same magnitude as the observations in this study for soy proteins (**Table 4.2**).

4.3.6 Mineral content of the fouled membranes

It was observed previously [34,51] that ultrafiltration of SPE 9 was associated with a high rejection of minerals (i.e., low removal) when compared to ultrafiltration of SPE 6 during the production of soy protein isolates. This was attributed to attractive electrostatic forces between cations (minerals) and negatively charged proteins, interactions which would be likely enhanced at pH 9 compared to pH 6. Therefore, the focus here was to evaluate whether or not minerals also contributed to the membrane fouling. The samples of the fouled membranes were obtained from the ultrafiltration of SPE 6 and SPE 9 to VCR 2.5 using the 100 and the 200 kDa membranes. It was decided to focus mainly on magnesium, calcium, and phosphorus (phytic acid) due to their known interactions with the soy proteins. After the filtration of SPE 9, only a minor increase in magnesium and phosphorus content and an insignificant difference in calcium were detected in the membrane with respect to the control membranes (**Table 4.2**). However, there was a significant increase in all three minerals after the filtration of SPE 6 for both MWCO membranes. No obvious differences were observed with respect to the membrane MWCO for any of the three minerals. The amount of minerals introduced onto the membrane by ultrafiltration of SPE 6 was 2.55 μg/cm^2 (Mg), 3.49 μg/cm^2 (Ca), and 4.92

μg/cm^2 (P) (control membranes subtracted). Higher amount of minerals within the fouling layer of SPE 6 most likely correlates with the higher amount of protein involved in the irreversible fouling. Although ultrafiltration of SPE 6 is characterized by relatively good mineral removal in comparison to SPE 9 [34,51], the minerals including phytic acid are (to some extent) bound to the protein and deposit with it on the membrane. This also suggests that the low removal of magnesium, calcium, and phytic acid observed in our previous study for the ultrafiltration of SPE 9 [51] is caused by the formation of the ternary complex (protein-mineral-phytic acid) rather than the precipitation of Mg/Ca phytate, because none of the selected minerals was detected in the fouled membranes of SPE 9. Since the amount of mineral deposition was quite low in comparison to the protein deposition (2700 μg/cm^2 estimated by SDS desorption for SPE 6 at VCR 2.5), it is likely that magnesium, calcium, and phytic acid do not significantly contribute to the membrane fouling for SPE 6 and the fouling is mostly due to the protein accumulation on the membrane surface.

4.4 Conclusion

This study investigated the formation of membrane fouling during the ultrafiltration of an electroacidified (SPE 6) and a non-electroacidified (SPE 9) feed in a dead-end system (without stirring) using 100 and 200 kDa polyethersulfone membranes. The membrane fouling was more significant for SPE 6, resulting in a lower permeate flux and considerably longer filtration times, when compared with SPE 9. Evaluation of the resistance components revealed that the irreversible fouling was higher for SPE 6 and accounted for 22 % of the total fouling resistance, compared to only 1 % for SPE 9. Experiments with SPE 9 adjusted to pH 6 and SPE 6 adjusted to pH 9 showed that the severity of the membrane fouling and the reversible/irreversible fouling distribution was mainly governed by the pH of the solution. The total amount of protein accumulated on the membrane surface at the end of the filtration, including the analysis of the rinsing water (for reversible fouling) and the protein desorption by SDS (for irreversible fouling), was similar for both feeds (6.70 and 6.93 mg/cm^2 for SPE 6 and SPE 9, respectively) but more protein participated in the irreversible fouling for SPE 6 (2.70 mg/cm^2), when compared with SPE 9 (0.13 mg/cm^2). Similar overall protein deposition for both feeds

indicated that the permeate flux is mainly controlled by the structure of the fouling layer. Indeed, FESEM examination of the fouled membranes revealed that SPE 6 forms rather denser and presumably less porous fouling layer than SPE 9, which can be attributed to lower electrostatic repulsion forces between the protein molecules at pH 6 (closer to pI), allowing for tighter packing on the membrane surface. Magnesium, calcium, and phosphorus (phytic acid) were detected in the fouled membranes for SPE 6 and only marginally in the fouled membranes for SPE 9. Higher mineral and protein deposition observed for SPE 6 suggests that calcium, magnesium, and phytic acid are (to some extent) associated with the protein and deposit with it on the membrane. Although association of magnesium, calcium, phosphorus, and the soy proteins is likely to be expected also at pH 9, the protein deposition for SPE 9 was low and the minerals in the fouling layer could not be detected. This study indicates that the major factor influencing the membrane fouling in ultrafiltration of the soy protein extracts is the pH of the feed. The effect of minerals on the membrane fouling did not seem to be important.

4.5 Appendix: Membrane fouling models

This section provides a description of the most common fouling models that can be used to identify the predominant fouling mechanism during a filtration process. Depending on the solute to pore size ratio, fouling can occur within the membrane pores or on the external surface of the membrane. The fouling models used to describe the fouling phenomena include standard blocking, complete blocking, intermediate blocking, and cake filtration (**Figure 4.9**).

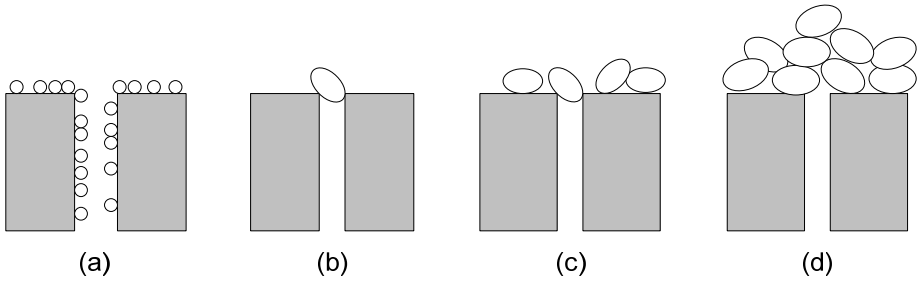

Figure 4.9 Illustration of membrane fouling mechanisms: (a) standard blocking, (b) complete blocking, (c) intermediate blocking, and (d) cake filtration. Adopted from Bowen et al. [71].

The standard blocking model (or pore constriction) occurs when the solutes are able to enter the membrane pores and adsorb on the pore walls, thus reducing the effective pore

diameter. In the complete blocking, some pores may become completely blocked by the depositing solutes, resulting in a reduced number of pores per area. Intermediate blocking is characterized by pore blockage but also deposition of the solutes on the external surface of the membrane. In the cake filtration, solutes deposit in multiple layers on the external surface, resulting in a cake build-up and increase in the effective membrane thickness. Understanding the fouling mechanisms can clarify the kinetics of the permeate flux decline and help in the selection of a suitable strategy for fouling minimization (increase in shear rate, backflushing).

Fouling models or blocking laws describing the four fouling mechanisms are summarized in **Table 4.3**, where J_P (m/s) is the time-variable permeate flux, J_0 (m/s) is the initial permeate flux (at time = 0), and k_1 to k_4 are constants.

Table 4.3 Fouling models and their linearized forms for the different fouling mechanisms

Mechanism	Model*	Linearized form	Plot
Standard blocking	$J_P = \frac{J_0}{(1+k_1 t)^2}$	$\frac{1}{\sqrt{J_P}} = \frac{1}{\sqrt{J_0}} + \frac{k_1}{\sqrt{J_0}} t$	$\frac{1}{\sqrt{J_P}}$ vs. t
Complete blocking	$J_P = J_0 \exp(-k_2 t)$	$\ln\frac{1}{J_P} = \ln\frac{1}{J_0} + k_2 t$	$\ln\frac{1}{J_P}$ vs. t
Intermediate blocking	$J_P = \frac{J_0}{(1+k_3 t)}$	$\frac{1}{J_P} = \frac{1}{J_0} + \frac{k_3}{J_0} t$	$\frac{1}{J_P}$ vs. t
Cake filtration	$J_P = \frac{J_0}{\sqrt{1+k_4 t}}$	$\frac{1}{J_P^2} = \frac{1}{J_0^2} + \frac{k_4}{J_0^2} t$	$\frac{1}{J_P^2}$ vs. t

* Model equations were obtained from Bowen et al. [71].

The linearized forms derived from the model equations can be used to quickly analyze the filtration data and determine the type of the fouling mechanism. For the unstirred dead-end ultrafiltration of the soy protein extracts, it is expected that the membrane fouling occurs primarily due to the cake build-up on the external surface of the membrane. However, at the beginning of the filtration, when the membrane area is uncovered, pore constriction or pore blocking may also occur. **Figure 4.10** shows the comparison of the various fouling models for the dead-end ultrafiltration of SPE 6 and SPE 9 to VCR 2.5 using the 100 kDa membrane. The relationship between $1/J_P^{-0.5}$ and

$\ln(1/J_P)$ and time (t) is not linear (**Figure 4.10** (a) and (b)), which indicates that standard and complete blocking models are not responsible for the permeate flux decline during ultrafiltration of both SPE 6 and SPE 9. This is expected, because proteins are the major foulants (Section 4.3.5) and the size of individual protein molecules and their aggregates is likely much larger compared to the size of the membrane pores. The intermediate blocking model (**Figure 4.10** (c)), which involves both pore blocking and solute deposition on the external surface of the membrane, provides a better overall fit to the filtration data than the previous two models, but does not describe the data well in the initial stages of the filtration (in the first 30 min). Despite the significant noise in the permeate flux, the cake filtration model (**Figure 4.10** (d)) provides the best fit to the filtration data over the entire experiment. This indicates that, for both SPE 6 and SPE 9, the cake layer starts forming on the external surface of the membrane from the beginning of the filtration and the permeate flux declines in proportion to the cake mass. These results support the selection of the cake filtration model (or theory) in Section 4.3.3 to estimate the specific cake resistance (α) when comparing the severity of membrane fouling for the electroacidified (SPE 6) and the non-electroacidified (SPE 9) feed.

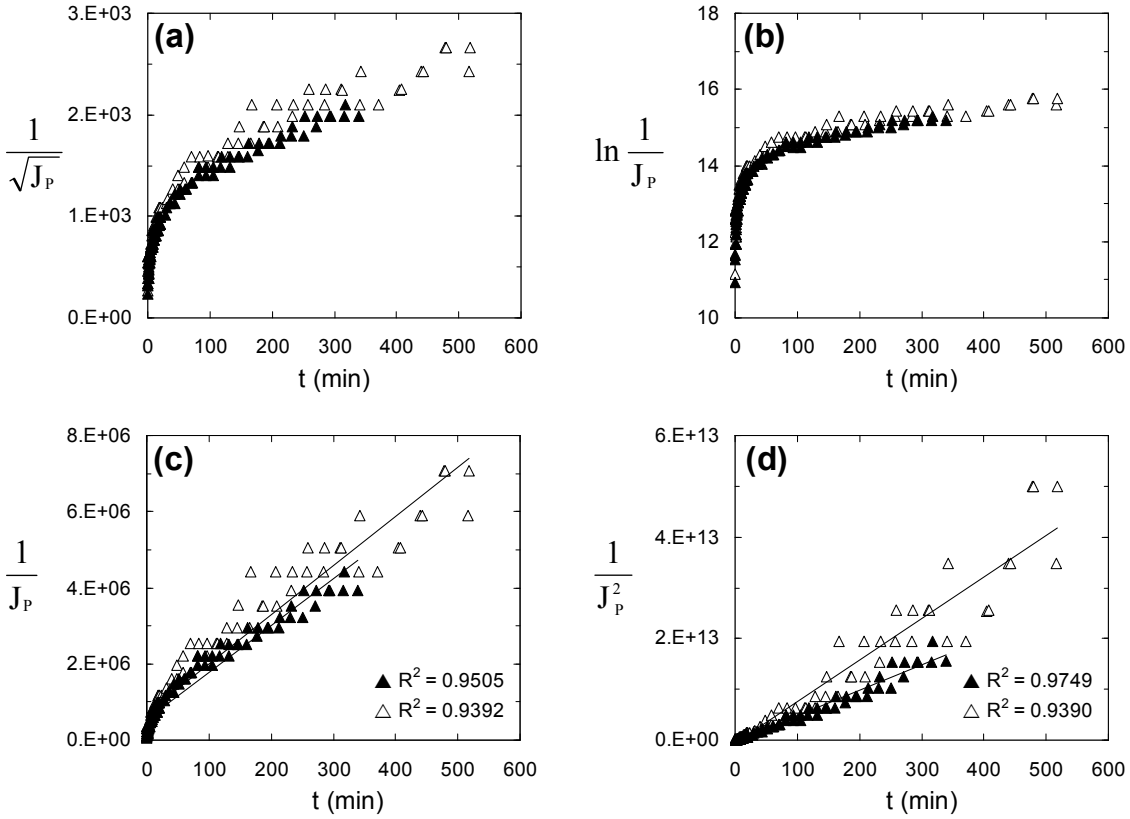

Figure 4.10 Comparison of fouling models for dead-end ultrafiltration of SPE 6 (△) and SPE 9 (▲) to VCR 2.5 using 100 kDa (PES) membrane: (a) standard blocking, (b) complete blocking, (c) intermediate blocking, and (d) cake filtration. Conditions: 30 psi and RT.

5

Effect of Electroacidification on Viscosity of Soy Protein Extracts and Concentrates Produced by Ultrafiltration

An axial pressure drop increase was observed during a hollow fiber ultrafiltration of an electroacidified (pH 6) and a non-electroacidified (pH 9) soy protein extract. Despite the similar composition of the concentrates, the viscosity of the non-electroacidified product was about twice as high compared to the electroacidified product, thus explaining a higher axial pressure drop observed during the ultrafiltration of the non-electroacidified extract. The zeta potential of the electroacidified extract was about 7 mV less negative than that of the non-electroacidified extract (-24 mV). The particle size distribution, determined by the dynamic light scattering, showed that most of particles (> 80 %) were found between 30 and 400 nm for the electroacidified extract and between 10 and 30 nm for the non-electroacidified extract. However, the differences in the zeta potential and the particle size distribution were unable to explain the different viscosity of the two extracts. The viscosity increased with higher protein content, i.e., lower mineral content, for the non-electroacidified concentrate, while no correlation between the viscosity and the composition was observed for the electroacidified concentrate. This was attributed to the higher negative zeta potential for the non-electroacidified extract and hence, stronger electrostatic interactions between the protein molecules at low mineral content. Using Einstein's equation and a shape factor derived from the molecular dimensions of glycinin reported in the literature, it was proposed that the higher viscosity of the non-electroacidified extract may be caused by higher degree of protein hydration compared to the electroacidified extract.

5.1 Introduction

Membrane ultrafiltration is increasingly used for the production of non-animal protein ingredients such as soy protein concentrates and isolates. Alkaline extraction of defatted soy flakes yields a soy protein extract, containing about 60 % protein, 30 % carbohydrates, and 10 % ash (minerals). The objective of ultrafiltration is to concentrate the protein and remove the carbohydrates and minerals. As the protein concentration in the retentate becomes higher, the viscosity will likely increase. To minimize the costs due to pumping or mixing, it is important to understand the relationship between the concentration and the viscosity and identify the factors that might influence the viscosity behavior.

The flow properties of food dispersions are strongly influenced by the nature of their components (proteins, carbohydrates, lipids, minerals) and their mutual interactions. In food applications, soy proteins are often used as functional ingredients to modify the texture and the consistency of the food products. The functional properties, including viscosity, are mostly affected by the properties of the soy proteins [15]. Based on the size of the protein molecules (in the low nanometer range), soy protein dispersions can be classified as colloidal systems, where the viscosity is controlled by a combination of hydrodynamic, colloidal, and Brownian forces [72]. The hydrodynamic forces are caused by the distortion of the flow field around the particles (particle-dispersant interactions) and interparticle interactions. At very low concentrations, where interparticle interactions are limited, the dynamic viscosity of the dispersion (η) increases linearly with the particle volume fraction (φ) according to Einstein's equation (5-1):

$$\eta = \eta_0 (1 + s\varphi) \tag{5-1}$$

where η_0 is the dynamic viscosity of the pure dispersant and s is a factor, which is dependent on the particle shape. For spherical particles, s has a value of 2.5 and higher than 2.5 for particles of other shapes [10]. At higher concentrations, interactions between the particles become more important and the viscosity increases more rapidly with the volume fraction than predicted by Einstein's equation. The relations, describing the viscosity behavior at higher volume fractions, have been reviewed by Rutgers [73]. The

colloidal and Brownian forces are characteristic for submicron particles. The former are related to the surface properties of the particles and determine the character of the interparticle interactions, and the latter result from the random movement of the particles due to collisions with the molecules of the dispersant [10].

Colloidal dispersions of rigid, spherical particles (e.g., silica, polymer) have been frequently used as model systems to study the flow behavior as a function of particle size, particle size distribution, and electrolyte concentration. At constant volume fraction, the viscosity of monodisperse systems increases with smaller particle size (as the number of particles in the system increases and the interparticle distance decreases). Mixtures containing particles of two different sizes exhibit lower viscosity than dispersions of monosized particles prepared at the same total volume fraction [74,75]. This effect, explained by a more efficient packing (smaller particles filling the interstices between the larger ones), may be dependent on the size ratio of the mixed particles [76]. In a polar medium, colloidal particles acquire a surface charge that is counterbalanced by the formation of an electrical double layer, resulting in a viscosity increase due to electroviscous effects. The primary effect is associated with the shear-induced deformation of the electrical double layer, the secondary effect results from the electrostatic repulsions between the charged particles (double layer overlap), and the tertiary effect describes the effect of pH and ionic strength on the conformation of charged polyelectrolytes [10]. Electrostatic interactions between the charged particles typically decrease with higher electrolyte concentration, because the surface charge (and the thickness of the double layer) is reduced, resulting in a viscosity decrease [77-79].

To study the effects of individual parameters (size, shape, charge, polydispersity) on the viscosity of protein dispersions is more difficult, because the parameters can not be controlled independently. Factors such as pH, ionic strength, electrolyte composition, and processing history have a strong influence on the protein properties, the type of intermolecular interactions, and the flow behavior [80,81]. The hydrodynamic volume and the conformation of the protein molecules in solution are dependent on the degree of hydration (water-binding capacity). Increased swelling and protein solubility (e.g., by increasing the pH above the isoelectric point) lead to larger hydrodynamic volume and therefore, higher viscosity [80-82]. Paulson et al. [83] correlated increasing apparent

viscosity of canola protein dispersions with increasing solubility and decreasing hydrophobicity. Incorporation of the repulsive hydration forces in the DLVO theory (balance between van der Waals attraction and electrostatic repulsion) improved the correlation between the interparticle interaction energy and the viscosity for a soy protein suspension [84] and cloudy apple juice [85], which indicated that the hydration forces can significantly contribute to the viscosity of colloidal dispersions. The effect of ionic strength on the viscosity of protein dispersions reported in the literature differs according to the concentration and type of added salt and the type of protein [80,86-88]. For soy protein dispersions, the viscosity decreased with increasing NaCl concentration, followed by a reversal at concentrations higher than 0.5 M [80]. On the other hand, the viscosity of 1–7 % soy protein suspensions was significantly enhanced after addition of 10–12.5 mM calcium, as a result of complex formation mediated by protein-calcium cross-links, and decreased at higher calcium concentrations [86]. The hydrodynamic volume, estimated for soy protein dispersions from the viscosity data as a function of ionic strength (adjusted by NaCl) and pH, was indirectly proportional to the ionic strength at 0–0.07 M and increased with pH between 6 and 8, followed by a decrease at higher pH values [89]. Increase of the hydrodynamic volume with higher pH and lower ionic strength was explained by changes in the thickness of the electrical double layer and electroviscous effects. Increasing particle size (in the micrometer range) was shown to decrease the viscosity of tomato purees [90] and whey protein dispersions [91], but was reported to increase the viscosity of soy protein dispersions [81]. The discrepancy in these findings indicates that the relationships between the viscosity and other dispersion characteristics are likely not valid for all protein or food dispersions, but depend on the specific properties of the dispersed phase.

In the present work, ultrafiltration of an electroacidified soy protein extract at pH 6 (SPE 6) and a non-electroacidified soy protein extract at pH 9 (SPE 9) was performed in a hollow fiber system. The axial pressure drop (between the inlet and the outlet pressures of the membrane cartridge) and the composition of the retentate were monitored during the filtration. An attempt was made to explain the viscosity behavior of the electroacidified and the non-electroacidified soy protein extracts and concentrates produced by ultrafiltration. The viscosity, measured by a Cannon-Fenske capillary

viscometer, was studied as a function of protein concentration, protein content, and pH. To characterize the properties of the soy protein extracts, particles size distribution and zeta potential were also determined.

5.2 Materials and methods

5.2.1 Preparation of soy protein extract dispersions

Soy proteins are mainly composed of storage globulins with an isoelectric point at pH 4.5–4.8 [15]. The main constituents of the storage globulins are β-conglycinin (180–210 kDa) and glycinin (300–350 kDa). Lyophilized soy protein extracts, SPE 6 (electroacidified) and SPE 9 (non-electroacidified), were provided by Agriculture and Agri-Food Canada (Saint-Hyacinthe, PQ, Canada). The soy protein extracts contained (on dry basis): SPE 6: 55.2 % protein, 36.8 % carbohydrates, and 8.0 % ash (minerals); SPE 9: 59.9 % protein, 29.7 % carbohydrates, 10.4 % ash. Details on the production of the soy protein extracts were provided by Mondor et al. [34]. Preweighed amounts of each soy protein extract were dissolved in Nanopure water (resistivity ~17.5 MΩ-cm, Barnstead water purification system, Dubuque, IA, USA) and mixed with a magnetic stirrer for 1–2 h to ensure complete rehydration. The samples were centrifuged at 15300 g for 20 min (Sorvall RC 5B Plus, Dupont, Mississauga, ON, Canada) to remove insoluble solids. The concentration of the total solids (TS) in the supernatant (measured gravimetrically) accounted for 85–90 % of the initial sample weight. The supernatant was used in the subsequent experiments.

5.2.2 Tangential flow ultrafiltration

Tangential flow ultrafiltration of the soy protein extracts was performed with a filtration system illustrated in **Figure 5.1**. A hollow fiber cartridge with a polysulfone membrane (GE Healthcare, Baie d'Urfe, QC, Canada) contained 50 fibers, 30 cm long and 1 mm in inner diameter (effective area 420 cm^2). The membrane had a nominal molecular weight cutoff (MWCO) of 100 kDa and therefore, should be fully retentive to soy proteins while permeable for carbohydrates and minerals. The axial pressure drop, defined as $\Delta P = P_{in} - P_{out}$, was monitored with two pressure transducers (Cole Parmer Canada Inc., Anjou, QC, Canada). Transmembrane pressure (TMP), defined as TMP =

(P_{in} + P_{out})/2 (permeate side opened to the atmosphere), was maintained constant at 6 psi (41.4 kPa) using a manual pinch valve. Samples of the retentate (2.5 mL) were collected at various times using a sampling valve. The flow rate was kept at 2.4 L/min, corresponding to a shear rate of 8000 s^{-1}. Reynolds number calculated using the fiber dimensions and viscosity of water was 1140, indicating a laminar flow regime. The feed was prepared as described in Section 5.2.1 by mixing 34 g of lyophilized SPE 6 or SPE 9 in 1700 g of Nanopure water, resulting in 1.7 % w/w total solids after centrifugation. The filtrations were carried out with a feed volume of 1.5 L in a concentration mode (retentate recycled and permeate withdrawn) until ~ 78 % of the initial water content was removed, corresponding to a volume concentration ratio (VCR) of 4.5. The temperature was maintained at 25 ± 1 °C.

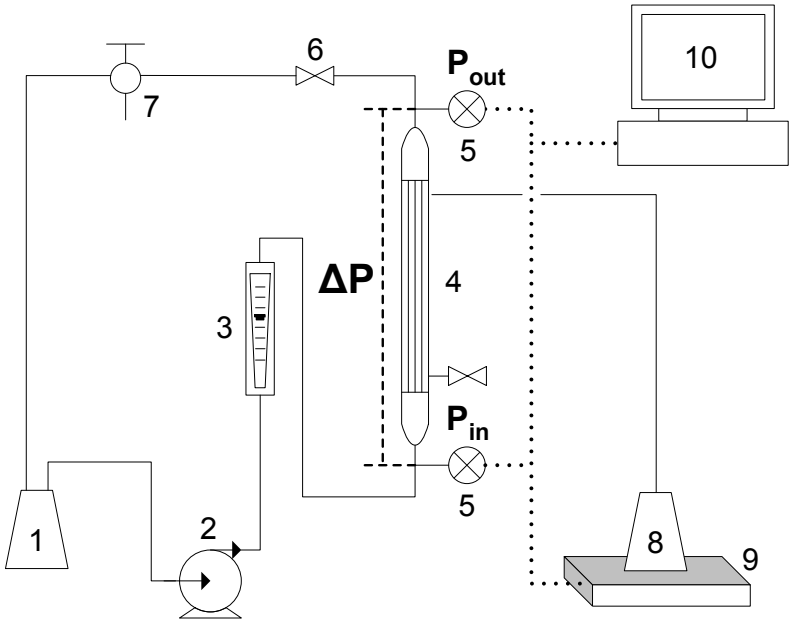

Figure 5.1 Schematic diagram of the filtration unit: 1-feed tank, 2-pump, 3-flowmeter, 4-membrane, 5-pressure transducers, 6-pinch valve, 7-sampling valve, 8-permeate container, 9-balance, and 10-PC/software.

5.2.3 Total solids and protein analyses

Total solids were determined gravimetrically by drying the samples (1 mL) at 100 °C overnight. Protein concentration was measured by Bradford protein assay (Standard Procedure for Microtiter Plates, Bio-Rad Laboratories, Mississauga, ON, Canada) against bovine serum albumin (BSA) as a protein standard and the protein content was expressed as protein to TS concentration ratio × 100. The concentration of soy proteins was,

however, always about 20–25 % lower than expected from the known protein content in the soy protein extracts, between 55 and 60 % for both SPE 6 and SPE 9 [34]. This was attributed to variable protein to dye binding efficiency for different proteins and confirmed by constructing a calibration curve for BSA and purified β-conglycinin and glycinin (provided by M. Corredig, University of Guelph, ON, Canada), combined in a 1:1.4 ratio based on their distribution in the soy proteins [15]. As shown in **Figure 5.2**, the slope for the soy proteins was about 77 % of the slope obtained with BSA, consistent with the difference between expected and actual protein concentrations determined using the BSA standard. Therefore, the protein content in the retentate and permeate samples was scaled with respect to the initial protein content in the feed, which was assumed 60 % for both SPE 6 and SPE 9.

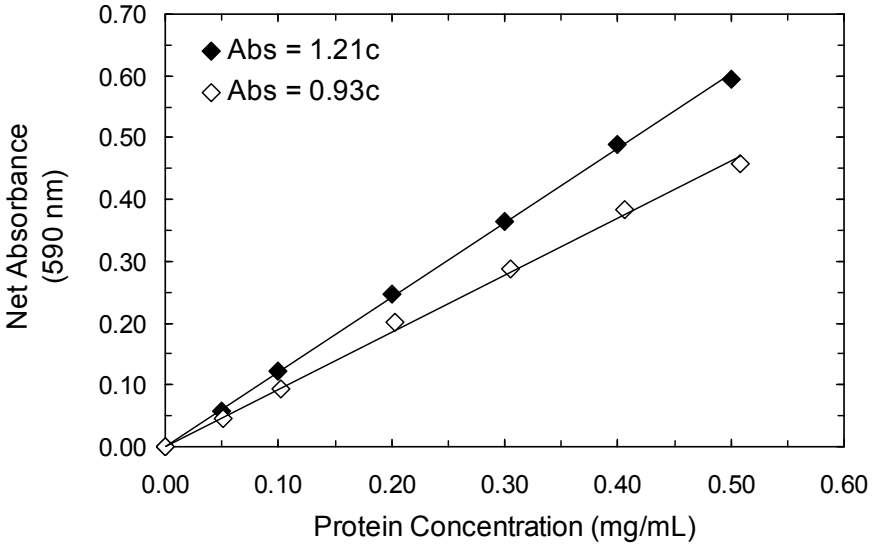

Figure 5.2 Typical calibration curves for BSA (◆) and purified soy proteins (◇).

5.2.4 Viscosity measurements

The viscosity was studied with the dispersions prepared from the lyophilized soy protein extracts at TS concentrations ranging from 0.9 to 7.0 % w/w (after centrifugation). The effect of pH on the viscosity of soy protein dispersions was determined by adjusting the pH of SPE 6 to 9 and SPE 9 to 6. In these experiments, 7 % w/w soy protein dispersion was adjusted to the desired pH with 2 M NaOH or 2 M HCl and diluted with Nanopure water to a final concentration of 6 % w/w (verified by TS analysis). The viscosity of the pH adjusted and non-adjusted soy protein extracts was

compared at the same TS concentration. To find out whether the removal of carbohydrates and minerals during the ultrafiltration of the soy protein extracts had any influence on the viscosity behavior, the final retentate at VCR 4.5 was back diluted with Nanopure water or with the permeate. The viscosity was measured with a capillary Cannon-Fenske routine viscometer (size 50), mounted in a water bath at 25 °C. Each sample was allowed at least 10 min in a water bath for the temperature equilibration and passed once through the capillary without taking a measurement. The flow time was then measured at least four times for each sample. The viscometer was cleaned with 2 M HCl, thoroughly rinsed with deionized water and acetone, and blow dried with clean air.

The kinematic viscosity (μ) can be converted into the dynamic viscosity (η) using the density of the fluid (ρ), according to Eq. (5-2). Since the density of the soy protein dispersions was very close to the density of water, the dynamic viscosity was calculated using the measured kinematic viscosity and the density of water at 25 °C (997 kg/m^3).

$$\eta = \mu\rho \tag{5-2}$$

According to Hermansson [80], the soy protein dispersions prepared from a soy protein isolate displayed a Newtonian behavior up to a concentration of 6 % (% based dry weight). Since in this work, the viscosity of the soy protein dispersions was studied in a similar concentration range (7 % w/w maximum), a Newtonian behavior was assumed for all samples.

5.2.5 Zeta potential and particle size distribution

The zeta potential and the particle size distribution of the soy protein extracts were determined by light scattering techniques in a Zetasizer Nano ZS (Malvern Instruments, Worcestershire, UK). Evaluation of the zeta potential is based on measuring the mobility of the dispersed particles in an applied electric field by laser Doppler velocimetry. The particle size distribution is obtained from the rate of the scattered light intensity fluctuations, which is related to the Brownian motion of the dispersed particles and their size. To avoid multiple scattering effects, the measurements were performed with dilute solutions of the soy protein extracts. A stock solution of SPE 6/SPE 9 was prepared at a concentration of 1 % w/w and centrifuged at 15300g for 20 min. The supernatant with a

final TS concentration of approximately 0.9 % w/w was diluted to 0.045 % w/w with a 0.01 M phosphate buffer (mono- and dibasic sodium phosphate) at the respective pH of the soy protein extracts (i.e., pH 6 for SPE 6 and pH 9 for SPE 9). The phosphate buffer (pH 6 and pH 9) is used to keep the pH of the diluted soy protein solutions at 6 and 9 for SPE 6 and SPE 9, respectively. The measurements were performed at 25 °C. Each sample was measured at least four times and two independent experiments were performed for each extract.

Statistical analysis was carried out according to Montgomery [50] using a two-sample t-test (two tailed) assuming an unequal variance to determine significant differences between the results obtained for SPE 6 and SPE 9. The results are reported as mean ± standard error (SE) and the number of independent experiments (n) is indicated.

5.3 Results and discussion

5.3.1 Pressure drop profile in tangential flow ultrafiltration

Ultrafiltration of the soy protein extracts to VCR 4.5 was associated with a gradual increase in the axial pressure drop (ΔP). For better comparison between the experiments, the pressure drop was normalized with respect to its initial value (ΔP_0). A linear relationship between the pressure drop and VCR was observed for both soy protein extracts (**Figure 5.3**). However, the pressure drop increase was about 2.5 times higher for the non-electroacidified feed (SPE 9) compared to the electroacidified feed (SPE 6). Such an observation was unexpected because the ultrafiltration of SPE 6 was always characterized by higher membrane fouling and a faster permeate flux decline than the ultrafiltration of SPE 9 [51].

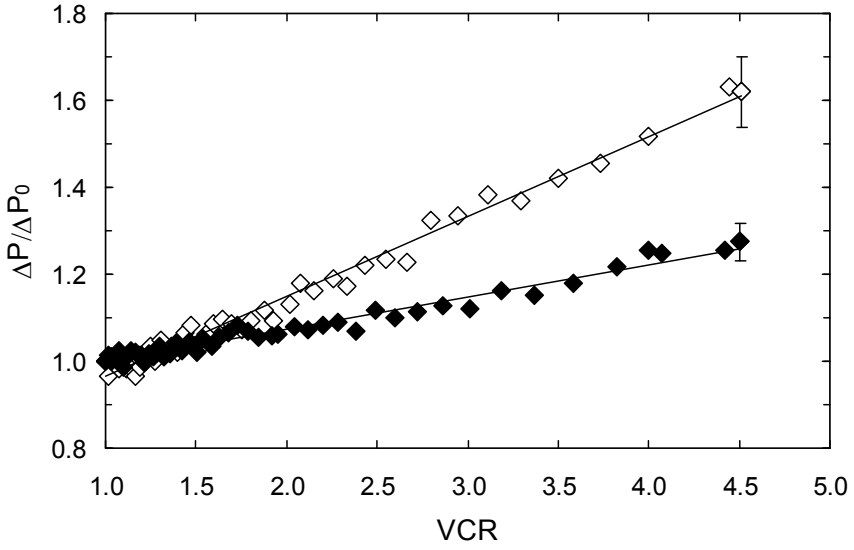

Figure 5.3 Axial pressure drop (ΔP) normalized to its initial value (ΔP_0) as a function of VCR during ultrafiltration of SPE 6 (◆) and SPE 9 (◇) to VCR 4.5. Standard error is shown at VCR 4.5 (n = 2). MWCO = 100 kDa, shear rate = 8000 s^{-1}, TMP = 6 psi, T = 25 °C.

In a hollow fiber configuration, the flow conditions can be described as those of a nonporous circular pipe, when the permeate flow rate is much smaller compared to the retentate flow rate. The flow of a fluid along the fiber length will induce an axial pressure drop characterized by the Hagen-Poiseuille equation (for laminar flow regime), which is a function of the flow velocity (v), the fiber length (l) and diameter (d), and the dynamic viscosity (η) of the fluid:

$$\Delta P = \frac{32 v l \eta}{d^2} \tag{5-3}$$

The increased deposition of protein along the membrane walls would reduce the fiber diameter, resulting in a higher axial pressure drop. However, the pressure drop was always higher for the less fouling feed (SPE 9), suggesting that the viscosity might increase faster during the ultrafiltration of SPE 9 compared to SPE 6. As the concentration of protein and total solids (TS) in the retentate increased linearly with increasing VCR during ultrafiltration of both soy protein extracts [51], it was decided to compare the axial pressure drop profile with the protein and the TS concentrations. As expected, a linear relationship between the axial pressure drop and the respective concentrations was observed. The pressure drop increased more rapidly for SPE 9

compared to SPE 6 (**Figure 5.4**). Since the protein accounts for a major part of the total solids, the slope of the pressure drop increase was similar with respect to the protein or the TS concentration for a given feed.

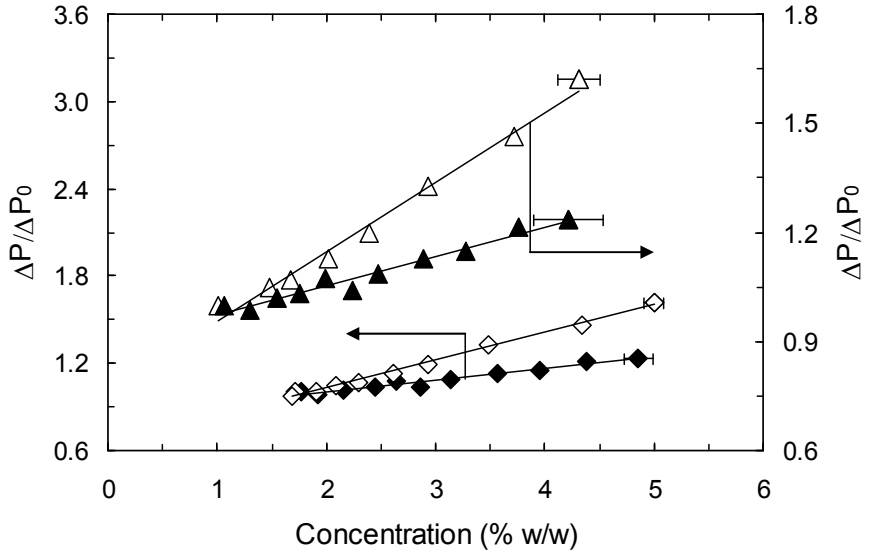

Figure 5.4 Normalized pressure drop ($\Delta P/\Delta P_0$) as a function of TS (diamonds, left axis) and protein concentration (triangles, right axis) during ultrafiltration of SPE 6 (closed symbols) and SPE 9 (open symbols) to VCR 4.5. Standard errors are shown for the final concentration (n = 2). MWCO = 100 kDa, shear rate = 8000 s^{-1}, TMP = 6 psi, T = 25 °C.

During the ultrafiltration, the protein and the TS concentration increased from approximately 1.0 to 4.0 % w/w and 1.7 to 5.0 % w/w, respectively. Such an increase corresponds to a protein content (protein to TS ratio × 100) increase from 60 % in the feed to at least 80 % in the final retentate for both soy protein extracts (**Figure 5.4** and **Table 5.1**). The dynamic viscosity for the feed showed only a small but significant difference ($p < 0.006$, $n = 2$) between SPE 6 (1.03 mPa·s) and SPE 9 (1.23 mPa·s). The viscosity of the final retentate was 1.81 mPa·s for SPE 6, which was about half of the viscosity for SPE 9 (3.69 mPa·s), thus explaining the higher axial pressure drop observed during the ultrafiltration of SPE 9. The difference between the viscosity of the SPE 6 and SPE 9 retentate was significant at $p < 0.12$ ($n = 2$), which is satisfactory, considering the retentate samples were produced by two independent ultrafiltration experiments. Since the final retentate samples had a similar composition, the higher viscosity observed for the non-electroacidified extract was unclear. The correlation between the pressure drop and the protein concentration suggests that proteins and their properties play a significant

role. The most evident difference between the two soy protein extracts is their pH, which likely affects the protein surface charge, the particle size distribution, and the intermolecular interactions between the proteins and the other components in the mixture (minerals, carbohydrates, and water as a dispersant). The objective of the subsequent work was to characterize the physicochemical properties of the soy protein extracts and clarify the difference in their viscosity.

5.3.2 Zeta potential and particle size distribution

To evaluate the effect of the protein net charge on the viscosity, the zeta potential of the soy protein extracts was determined. From the isoelectric point of the soy proteins (pH 4.5–4.8), one would expect the proteins to have a negative net charge in both the electroacidified (pH 6) and the non-electroacidified (pH 9) soy protein extracts. However, the proteins will likely carry a more negative charge at pH 9, being further away from the isoelectric point. This was confirmed by measuring the zeta potential, which was -16.6 and -24.0 mV for SPE 6 and SPE 9, respectively ($p < 0.017$, $n = 2$). These values are about 50 % lower than those reported by Malhotra et al. [92] for a soy protein isolate (approximately -30 mV at pH 6 and -50 mV at pH > 7), which could be due to the difference in the production and composition of the soy protein isolate and the soy protein extracts used in this work and the method of pH adjustment for the zeta potential measurements (acid, base, or buffer).

The analysis of the particle size distribution revealed that both soy protein extracts contained two classes of particles with sizes ranging between 10–30 and 30–400 nm (**Figure 5.5** (a)). The maximum molecular dimension of soy glycinin reported in the literature, around 11–18 nm [93-95], suggests that the first peak corresponds to individual proteins, while the second peak may represent protein aggregates. The size distribution by intensity was similar for both extracts, although it could be seen that SPE 9 contained a larger fraction of smaller particles than SPE 6. Since the intensity of the scattered light increases rapidly with the particle size, the intensity distribution is weighted in favor of larger particles. Transformation to a volume distribution (**Figure 5.5** (b)) provides a better estimate about the quantity of the large and the small particles in the sample. The volume distribution of SPE 6 remained bimodal with the first peak (10–30 nm) accounting for

about 20 % of the total particle volume and the second peak (30–400 nm) accounting for the remaining 80 %. On the other hand, the volume distribution of SPE 9 contained a single peak at 10–30 nm, representing about 88 % of the total particle volume and the peak tail in the range of 30 to 400 nm particles accounted for the remaining 12 %. The higher proportion of the larger particles in SPE 6 is in agreement with the less negative surface charge of the soy proteins at pH 6, reducing the repulsive electrostatic forces between the protein molecules and resulting in a higher degree of protein aggregation.

The observed viscosity differences of the soy protein extracts can be explained by both the zeta potential and the particle size distribution characteristics. The higher negative charge of the protein for SPE 9 will cause stronger electrostatic repulsion between the protein molecules as well as higher degree of protein hydration, both leading to enhanced viscosity. In addition, the higher proportion of the smaller particles in SPE 9 indicates that at the same mass concentration, the number of particles in the system will be higher for SPE 9 than for SPE 6, resulting in shorter interparticle distances, more frequent particle collisions, and therefore a viscosity increase.

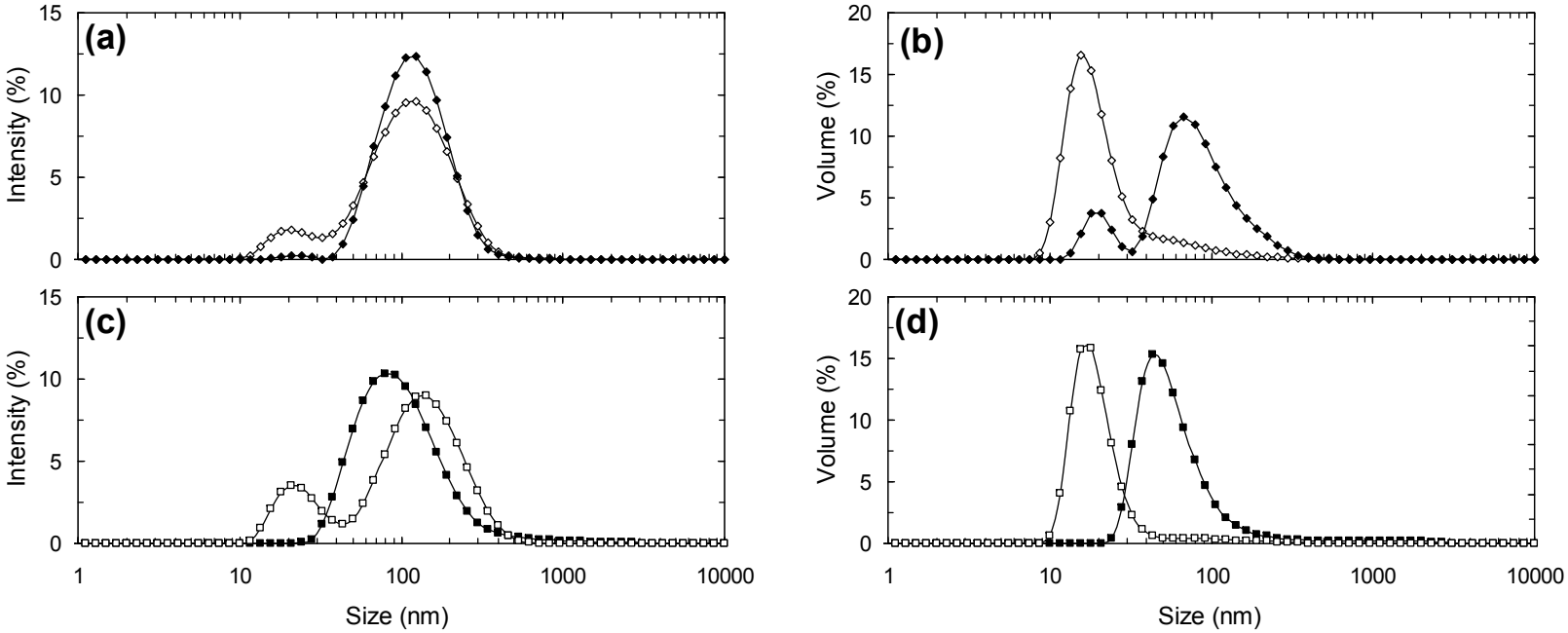

Figure 5.5 Particle size distribution according to intensity and volume for pH non-adjusted, (a) and (b), and pH adjusted, (c) and (d), soy protein extracts: SPE 6 (◆), SPE 9 (◇), SPE 6 adjusted to pH 9 (□), and SPE 9 adjusted to pH 6 (■). The data were averaged from at least two independent experiments for both extracts.

5.3.3 The effect of pH on viscosity and particle size distribution

To further investigate whether the protein net charge is responsible for the different viscosity behavior, the pH of the soy protein extracts was adjusted from 6 to 9 for SPE 6 and vice versa for SPE 9 using concentrated NaOH or HCl. The viscosity increased from 1.55 to 1.69 mPa·s (SE = 0.02 mPa·s, n = 2) for SPE 6 adjusted to pH 9 and decreased from 2.28 to 2.07 mPa·s (SE = 0.01 mPa·s, n = 2) for SPE 9 adjusted to pH 6, which is expected, considering the electrostatic repulsion forces are likely enhanced in the former while reduced in the latter. However, in both cases, the change in viscosity was only 9 % with respect to the pH non-adjusted extracts, and SPE 9 at pH 6 still had a higher viscosity than SPE 6 at pH 9, suggesting that the protein net charge may not be a governing factor for the viscosity of the soy protein extracts. From the similar viscosity for the pH adjusted and non-adjusted soy protein extracts, one was expecting also a similar particle size distribution, if a correlation existed between the viscosity properties and the particle size. To determine the particle size distribution, the samples of the pH adjusted soy protein extracts were diluted 100-fold with 0.01 M phosphate buffer at their respective pH values. **Figure 5.5** (c) and (d) shows that in contrast to the viscosity, the particle size distribution was greatly influenced by the pH adjustment. The intensity distribution for SPE 6 adjusted to pH 9 displayed two distinct peaks (10–40 nm and 40–500 nm) while only one peak (30–500 nm) appeared for SPE 9 adjusted to pH 6. Although the proportion of small to large particles and the position of the peaks were slightly different, qualitatively, the size distributions according to pH compared quite well with the distributions obtained for the pH non-adjusted soy protein extracts (**Figure 5.5** (a)). A very good agreement was found between the volume distributions for SPE 9 and SPE 6 adjusted to pH 9 (**Figure 5.5** (b) and (d)). The volume distribution obtained for SPE 9 adjusted to pH 6 displayed one peak, which position was between the two peaks observed in the volume distribution for SPE 6. Since the viscosity of the soy protein extracts was not significantly affected by the pH adjustment or related to differences in the particle size distribution, one can suggest that the electroacidification pretreatment has an impact on some other properties of the soy protein extracts that affect the viscosity.

5.3.4 The effect of composition on viscosity characteristics

The viscosity behavior was also studied as a function of TS concentration with dispersions of the lyophilized soy protein extracts prepared at a concentration ranging between 0.3 and 7.0 % w/w. **Figure 5.6** shows that the viscosity increased linearly with the TS concentration and the rate of viscosity increase was higher for SPE 9 than for SPE 6, which correlates with the axial pressure drop profile observed during the ultrafiltration of the soy protein extracts. Note that for the non-filtered soy protein extracts, the protein content (protein to TS ratio × 100) does not change and the protein concentrations are always about 60 % of the TS concentrations (upper axis in **Figure 5.6**), unlike for the concentrates (after ultrafiltration), where the protein content was at least 80 %.

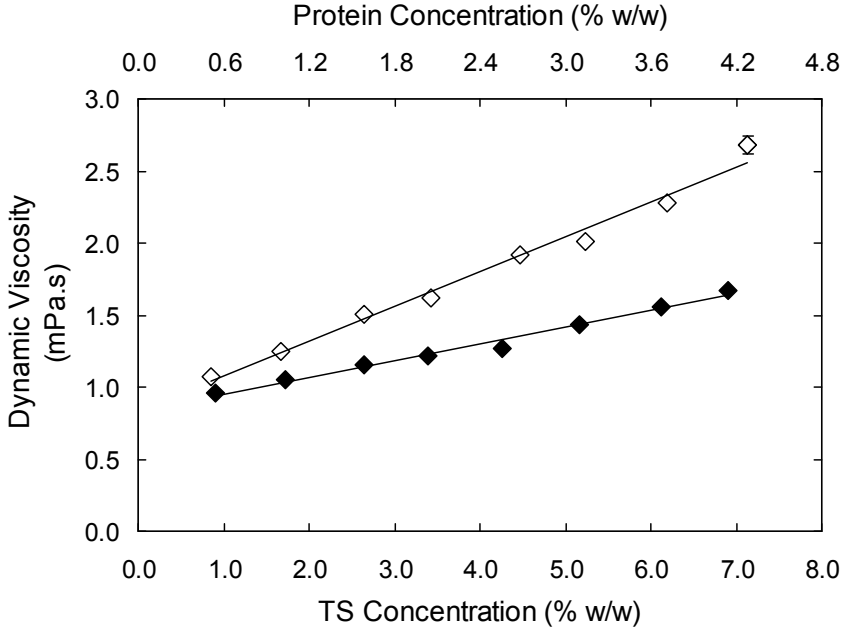

Figure 5.6 Dynamic viscosity as a function of TS and protein concentration (calculated as 60 % of TS concentration): SPE 6 (◆) and SPE 9 (◇). Standard error is shown at 7 % w/w for SPE 9 (n = 2).

The viscosity obtained for the concentrate (final retentate) can be compared with the non-filtered soy protein extracts either according to the total solids or the protein concentration. A comparison at the same TS concentration (i.e., 5 % w/w) shows that the viscosity of the non-filtered soy protein extracts was 1.43 and 2.01 mPa·s for SPE 6 and SPE 9, respectively, which was 1.3 and 2.0 times lower than the viscosities obtained for the final retentate samples. Better agreement was obtained when the viscosity of the

filtered and the non-filtered samples was compared at the same protein concentration (i.e., ~ 4 % w/w), indicating that the flow properties of the soy protein extracts are affected primarily by the protein concentration in contrast to the TS concentration. In fact, the viscosity of the non-filtered SPE 6 extract (1.67 mPa·s) was very similar to the viscosity of the SPE 6 final retentate (1.81 mPa·s), but the viscosity of the non-filtered SPE 9 extract was still about 1.4 times lower than that of the SPE 9 final retentate (3.69 mPa·s). The discrepancy between the viscosity of the filtered and non-filtered SPE 9 samples suggests that the protein content (or the removal of carbohydrates and minerals during the ultrafiltration) has some impact on the viscosity of the non-electroacidified extract (SPE 9).

To further investigate the effect of the composition, the final retentate samples for both SPE 6 and SPE 9 were diluted to various protein concentrations with water or with their respective permeates, containing carbohydrates and minerals separated from the soy proteins during the ultrafiltration. The resulting protein and TS concentrations for the feed, final retentate, and the diluted retentate samples are reported in **Table 5.1**. Note that the protein content does not change if the diluent is water but varies for the permeate diluted samples, because the permeate contains minerals and carbohydrates. Due to the very low protein of the permeate samples, the protein concentrations for a given dilution remain constant regardless of the diluent.

Table 5.1 Concentration of protein and total solids (TS) in final retentate, diluted retentate with water and permeate, and feed for SPE 6 and SPE 9.

Extract	Stream	Diluent	Dilution	Protein concn (g/L)	TS concn (g/L)	Protein content (%)
SPE 6	Feed	-	1.0	10.6	17.6	60.0
	Retentate	-	1.0	39.1	47.3	82.6
	Retentate	H_2O	1.2	32.5	39.4	82.6
		H_2O	1.6	24.4	29.6	82.6
		H_2O	2.3	17.0	20.6	82.6
		H_2O	4.0	9.8	11.8	82.6
		Permeate*	1.2	32.6	40.8	79.9
		Permeate	1.6	24.5	32.6	75.2
		Permeate	2.3	17.1	25.1	68.1
		Permeate	4.0	9.9	17.9	55.6
SPE 9	Feed	-	1.0	10.2	17.0	60.0
	Retentate	-	1.0	41.1	50.6	81.2
	Retentate	H_2O	1.2	34.3	42.2	81.2
		H_2O	1.6	25.7	31.6	81.2
		H_2O	2.3	17.9	22.0	81.2
		H_2O	4.0	10.3	12.7	81.2
		Permeate**	1.2	34.3	43.3	79.1
		Permeate	1.6	25.8	34.2	75.3
		Permeate	2.3	18.0	25.9	69.3
		Permeate	4.0	10.4	17.8	58.2

* TS and protein concentrations were 8.0 and 0.22 g/L respectively. ** TS and protein concentrations were 6.9 and 0.13 g/L respectively.

The viscosity obtained for the samples listed in **Table 5.1** is presented as a function of the protein concentration in **Figure 5.7** (a) and (b). The electroacidified extract (SPE 6) showed no difference in the viscosity for the retentate samples diluted with water or the permeate, which means that the viscosity of SPE 6 is only affected by the protein concentration and not by the protein content or the removal of carbohydrates and minerals that occurs during the ultrafiltration. This conclusion is further supported by

comparing the viscosity of the diluted retentate and the non-filtered SPE 6 samples at various protein concentrations (replotted from **Figure 5.6**), which fall approximately on the same line. The non-electroacidified extract (SPE 9) displayed a higher viscosity for the retentate diluted with water compared to the permeate diluted samples **Figure 5.7** (b). The ratio between the viscosities for the two types of diluents decreased with increasing dilution (from 0.95 to 0.87 for a dilution factor of 1.2 and 4.0, respectively). Diluting the retentate four times yielded a similar protein concentration as for the feed, but only the sample diluted four times with the permeate displayed a comparable protein content and viscosity as the feed. From the comparison between the retentate (diluted with water or the permeate) and the non-filtered SPE 9 samples with a protein content of ~60 % (replotted from **Figure 5.6**), it becomes apparent that the protein content has a greater effect on the viscosity at higher protein concentrations.

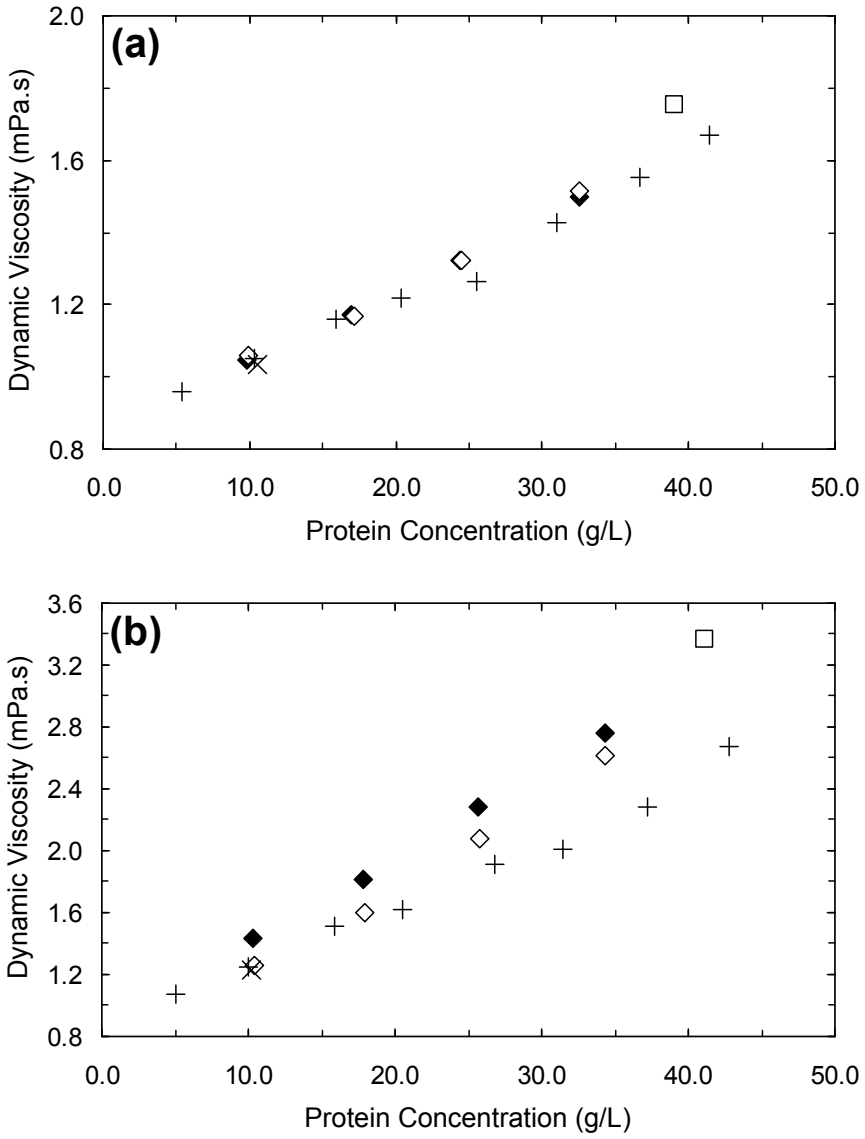

Figure 5.7 Viscosity of feed (×), final retentate (□), diluted retentate with water (◆) and the permeate (◇) plotted as a function of protein concentration for SPE 6 (a) and SPE 9 (b). The results are compared with the dynamic viscosities of non-filtered soy protein extracts (+), replotted from **Figure 5.6**.

Diluting the retentate with the permeate results in the addition of carbohydrates and minerals back to the soy proteins. It is assumed that carbohydrates do not interact with the soy proteins to reduce the viscosity but the addition of minerals increases the ionic strength, thus neutralizing the protein net charge and reducing the electrostatic repulsion between the protein molecules. This effect would be likely more pronounced for SPE 9

because of its higher negative zeta potential than for SPE 6, clarifying the distinct viscosity behavior with respect to the protein content for the electroacidified (SPE 6) and the non-electroacidified (SPE 9) soy protein extracts.

5.3.5 The effect of volume fraction on viscosity

The viscosity of colloidal dispersions is controlled by the effective volume fraction rather than the mass concentration of the dispersed particles. The hydrodynamic volume of a protein molecule depends on its geometrical shape and the degree of hydration, which are difficult to determine experimentally [81,82,89]. The relationship between the viscosity and the concentration in **Figure 5.6** can be described by a linear function (Eq. (5-4)):

$$\eta = \eta_0 \left(1 + Ac_B\right) = \eta_0 \left(1 + s\upsilon_h c_B\right) \tag{5-4}$$

where η and η_0 have the same meaning as in Eq. (5-1) and c_B is the concentration of the dispersed phase. The proportionality constant (A) is a product of the particle shape, characterized by the shape factor (s), and the specific hydrodynamic volume (υ_h). The volume fraction (φ) is obtained from the product of the mass concentration and the specific hydrodynamic volume (yielding Eq. (5-1)). The constant A was obtained by plotting the relative dynamic viscosity (η/η_0) minus unity against the protein concentration (**Figure 5.8**) using the data in **Figure 5.6** for the non-filtered soy protein extracts. It is assumed that only proteins account for the volume fraction and the contribution of other components (carbohydrates and minerals) is negligible. Under this assumption, constant A is given by the slope of the curves in **Figure 5.8** and has a value of 19.6 and 43.2 mL/g for SPE 6 and SPE 9, respectively.

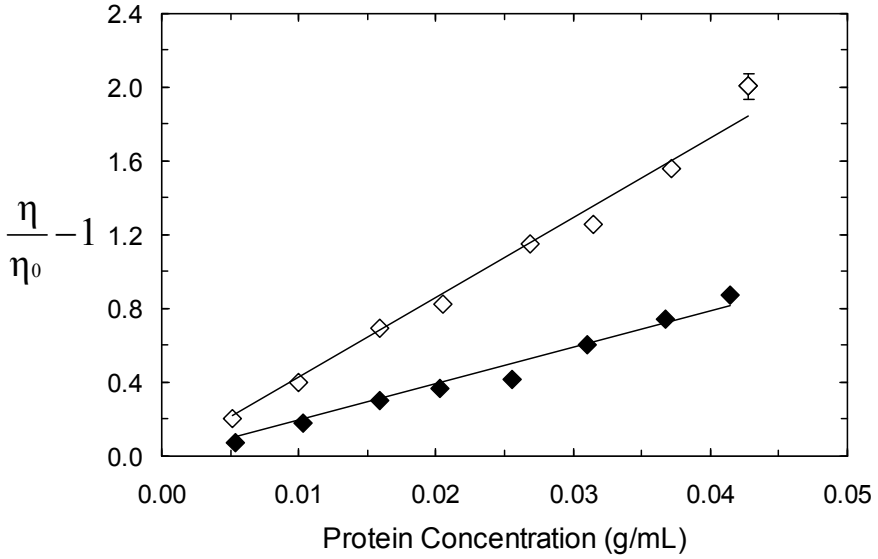

Figure 5.8 Relative dynamic viscosity (η/η_0) minus unity plotted against protein concentration for SPE 6 (◆) and SPE 9 (◇).Standard error is shown at 0.043 g/mL for SPE 9 (n = 2).

The specific hydrodynamic volume can be determined when the geometrical shape of the dispersed particles is known. Molecular and shape characteristics were obtained from the literature for glycinin [93-95], which is the most abundant soy protein constituent. The shape for the molecule of glycinin is an oblate ellipsoid with a wide range of reported molecular dimensions. The axial ratio (AR), defined as the ratio of major and minor axes, thus ranges between 1.25 and 8. The shape factor (s) is given as 2.5 for spherical particles (AR = 1) and increases with increasing axial ratio [10]. Simha [96] provided a relation, which allows the shape factor to be calculated as a function of AR for oblate and prolate ellipsoids of revolution. Based on this relation, the reported axial ratios of 1.25–8 for the glycinin molecule correspond to a shape factor of 2.57–6.70 (for oblate), respectively [97]. Using the shape factor (s) and constant A, one can calculate the specific hydrodynamic volume (υ_h = A/s) per gram of dry protein (**Table 5.2**). Specific hydrodynamic volume multiplied by the mass concentration provides an estimate of the effective volume fraction of the soy proteins in the dispersions. The volume fractions (φ) calculated from the range of the protein concentrations in **Figure 5.8** and the specific hydrodynamic volume are listed in **Table 5.2**. Since the viscosity increased with the protein concentration about two times faster for SPE 9 than for SPE 6, the same ratio is also found between their specific hydrodynamic volumes and volume fractions. It can be

seen from **Table 5.2** that the volume fractions corresponding to the shape factor of 2.57 (nearly spherical molecules) are too high for the relatively low viscosity of the dispersions. The maximum volume fraction for SPE 9 (0.709) exceeds the maximum volume fraction for randomly packed rigid, spherical particles (0.64). For this reason, the volume fractions estimated from the shape factor of 6.70 seem more reasonable for both SPE 6 and SPE 9. In addition, the estimated specific hydrodynamic volume (2.9 and 6.4 mL/g for SPE 6 and SPE 9, respectively) are in a good agreement with the estimates reported by Boulet et al. [89] for a dispersion of soy protein isolate at pH 6 (4–5 mL/g) and pH 9 (9–10 mL/g) and ionic strength of 0.05 M.

Table 5.2 Specific hydrodynamic volume and volume fractions for SPE 6 and SPE 9 derived from the viscosity data obtained for the non-filtered soy protein dispersions and molecular parameters for glycinin from the literature.

Extract	A (mL/g)	AR	s	υ_h (mL/g)	φ**
SPE 6	19.6	1.25	2.57	7.6	0.038–0.319
		8	6.70	2.9	0.015–0.122
SPE 9	43.2	1.25	2.57	16.8	0.084–0.706
		8	6.70	6.4	0.032–0.269

* AR = axial ratio. ** For protein concentrations of 0.005–0.042 g/mL.

This suggests that the proteins are less hydrated in the electroacidified extract (SPE 6) than in the non-electroacidified extract (SPE 9), and that the degree of hydration does not change significantly upon pH adjustment (SPE 6 to pH 9 and SPE 9 to pH 6) as indicated by the small difference in the viscosity for the pH adjusted and non-adjusted soy protein extracts. Although the pH adjustment was associated with changes in the particle size distribution (**Figure 5.5**), it is proposed that the protein aggregates in the non-electroacidified extract have a more open structure, that may be permeable to the solvent, while the protein aggregates in the electroacidified extract have a closed and rigid structure that reduces the hydration. However, the difference in the protein hydration for the soy protein extracts needs to be yet clarified. It is possible that electroacidification has some impact on the surface hydrophilicity/hydrophobicity of the soy proteins.

5.4 Conclusion

The tangential flow ultrafiltration (to VCR 4.5), when used for the concentration of the soy protein extracts with an electroacidification pretreatment (SPE 6) and no electroacidification pretreatment (SPE 9), revealed different axial pressure drop profiles. The axial pressure drop increased linearly with increasing total solids and protein concentration for both SPE 6 and SPE 9, but the rate of increase was 2.5 times higher for SPE 9. The viscosity measurements for the feed and the concentrate (final retentate) revealed that the viscosity increased 1.8- and 3.0-fold for SPE 6 and SPE 9, respectively, thus clarifying the axial pressure drop profile. As the composition of the soy protein extracts was similar and the concentration of the protein and the total solids increased at the same rate during the ultrafiltration of both soy protein extracts, the cause for the higher viscosity of the non-electroacidified extract remained unclear. The zeta potential was -16.6 and -24.0 mV for SPE 6 and SPE 9, respectively. Analysis of the particle size distribution according to volume revealed that at least 80 % of particles were in the size range of 10–30 nm for SPE 9 and 30–400 nm for SPE 6. To verify whether the higher viscosity for SPE 9 was caused by its higher pH or the smaller particle size, the pH of the soy protein extracts was adjusted from 9 to 6 for SPE 9 and from 6 to 9 for SPE 6. Although, the particle size distribution was greatly influenced by the pH adjustment, the viscosity of the soy protein extracts changed only marginally, indicating that the particle size distribution and the pH were not responsible for the higher viscosity of SPE 9. The viscosity increased linearly with the protein concentration for both soy protein extracts, with a more rapid increase for SPE 9 than for SPE 6. Measurements of the viscosity for the final retentate diluted with water or the permeate revealed that the viscosity of SPE 9 was dependent on the composition and decreased with higher mineral content (lower protein content), whereas the composition had no influence on the viscosity of SPE 6. It was assumed that the minerals reduced the viscosity of SPE 9 through neutralization of the protein surface charge and the reduction in electrostatic repulsive forces. It is proposed that higher degree of protein hydration (water-binding capacity) may be responsible for the higher viscosity of SPE 9 compared to SPE 6, however, a further verification of this assumption is needed.

6

Conclusion

A combined process of electroacidification and membrane ultrafiltration was investigated as an alternative to the conventional production of soy protein isolates for food applications. Ultrafiltration performance was compared for the electroacidified (SPE 6) and the non-electroacidified (SPE 9) soy protein extract.

Ultrafiltration of the soy protein extracts in the hollow fiber and the dead-end system was accompanied by membrane fouling and a permeate flux decline. The membrane fouling was always more significant for SPE 6, resulting in at least a 1.5-fold increase in the total fouling resistance (decrease in the permeate flux) compared to SPE 9. The analysis of the membrane fouling in the dead-end system showed that the irreversible fouling was higher for SPE 6 and accounted for 22 % of the total fouling resistance, compared to only 1 % for SPE 9. The amount of protein desorbed from the membrane surface (irreversible fouling) was 2.70 mg/cm^2 for SPE 6 and 0.13 mg/cm^2 for SPE 9, which correlated well with the estimates of the irreversible fouling resistance. The overall protein deposition, consisting of the protein collected in the rinsing water (reversible fouling) and the protein desorbed from the membrane surface, was 6.70 and 6.93 mg/cm^2 for SPE 6 and SPE 9, respectively. The higher observed total fouling resistance but the similar overall protein deposition for the two extracts was explained by a lower porosity of the fouling deposit for SPE 6. This was confirmed by the scanning electron micrographs of the fouled membranes, which showed that the fouling deposits appeared denser and more compact for SPE 6 than those for SPE 9. The formation of denser fouling deposits for SPE 6 was attributed to weaker electrostatic repulsion between the protein molecules due to the lower protein net charge at pH 6 (closer to pI) than at pH 9. Experiments with SPE 9 adjusted to pH 6 and SPE 6 adjusted to pH 9 revealed that the pH of the soy protein extract had a strong impact on the extent of membrane fouling and the proportions of reversible and irreversible fouling. The zeta potential (electrical potential in the vicinity of a charged surface) was -17 and -24 mV for SPE 6 and SPE 9, respectively, which confirmed that the soy proteins were less negatively charged at pH 6 than at pH 9. The lower protein net charge at pH 6 also resulted in a higher degree of protein aggregation for SPE 6, as indicated by the higher proportion of larger particles (30–400 nm) in the particle size distribution, estimated by the dynamic light scattering.

The protein aggregates may be strongly bound to the membrane surface due to multiple attachments and thus contribute to the higher irreversible fouling for SPE 6.

The composition of the soy protein isolates produced by the direct ultrafiltration to VCR 4.5 and the two-stage discontinuous diafiltration (VCR 2, dilution, and VCR 4) in the hollow fiber system was determined by independent analytical methods for total solids, proteins, carbohydrates, and minerals. The composition was always determined for the feed, the retentate, and the permeate streams in order to calculate the mass balance. A three-way sample valve installed on the retentate line allowed for sample collections throughout the course of ultrafiltration. Concentration profiles as a function of the volume concentration ratio provided an insight into the retention characteristics of the soy protein extract components. From the constant carbohydrate concentration in the retentate, it was concluded that the carbohydrates were able to freely permeate through the membrane despite the membrane fouling. The removal of carbohydrates was 78 and 89 % for the direct ultrafiltration to VCR 4.5 and the two-stage discontinuous diafiltration, respectively, which is consistent with the theoretical predictions for freely permeable solutes. In contrast, the minerals were partially retained by the membrane, especially for the electroacidified extract. The mineral removal during the direct ultrafiltration to VCR 4.5 was 64 and 58 % for SPE 6 and SPE 9, respectively, which was enhanced to 72 and 64 % during the discontinuous diafiltration. Mineral analysis revealed that the removal of magnesium, calcium, and phosphorus (phytic acid) was 63, 55, and 50 % for SPE 6, compared to only 41, 21, and 11 % for SPE 9 during the direct ultrafiltration to VCR 4.5. The discontinuous diafiltration enhanced the removal of all three minerals by at least 7 % for SPE 6 but no improvement was obtained for SPE 9. The lower removal of these selected minerals at alkaline pH was attributed to the ternary complex formation between the soy proteins, the divalent minerals, and the phytic acid and/or the precipitation of mineral-phytates. The protein content of the soy protein isolates produced by the hollow fiber ultrafiltration was at least 88 % (dry basis), regardless of whether the soy protein extract was electroacidified or non-electroacidified.

The observed retention of minerals by the membrane, despite their much lower size than the membrane pores, led to the investigation of the role of minerals in the formation of membrane fouling. The fouled membranes recovered after ultrafiltration of the soy protein extracts in the dead-end system were analyzed for magnesium, calcium, and phosphorus. Despite the higher membrane retention of all three minerals for SPE 9, none of these minerals could be detected in significant amounts in the fouled membranes for this type of extract. This suggests that the minerals were retained by the membrane due to the ternary complex formation rather than the precipitation of mineral-phytates. The removal of magnesium, calcium, and phosphorus during the hollow fiber ultrafiltration was higher for SPE 6 than for SPE 9, but still lower than predicted for freely permeable solutes. This indicates that the protein-mineral-phytic acid interactions also occur in SPE 6 but to a lower extent than in SPE 9. Higher protein deposition associated with the irreversible fouling and the protein-mineral-phytic acid interactions were likely responsible for the higher levels for all three minerals in the fouled membranes for SPE 6. Since the mineral deposition was insignificant compared to the protein deposition, it was concluded that the minerals had a minor contribution to the membrane fouling.

The concentration of the soy protein extracts in the hollow fiber ultrafiltration system was also associated with an axial pressure drop increase, which was more significant for SPE 9 compared to SPE 6. Despite the similar composition of the final retentate samples for both extracts, the viscosity was about two times higher at pH 9 compared to pH 6, which explained the higher axial pressure drop observed during the ultrafiltration of SPE 9. It was initially believed that the higher viscosity for SPE 9 could be related to its higher zeta potential, which would enhance the viscosity due to stronger electrostatic interactions between the protein molecules (electroviscous effects). Also, the dynamic light scattering analysis revealed a higher proportion of smaller particles (10–30 nm) for SPE 9, which could also contribute to the higher observed viscosity, because at the same mass concentration, the number of particles in the system would be higher for SPE 9 compared to SPE 6. However, the contributions of the pH and the particle size distribution were excluded, because adjusting the pH of SPE 6 to 9 and the pH of SPE 9 to 6 significantly affected the particle size distribution but had no effect on the viscosity

of the pH adjusted extracts. The use of Einstein's equation with the molecular dimensions for glycinin, the most abundant of the soy proteins, suggests that the differences in viscosity between SPE 6 and SPE 9 could be caused by a difference in the protein hydration and the compactness (permeability) of the protein aggregate. It is possible that the electroacidification treatment affects the hydration characteristics of the soy proteins. The viscosity of the electroacidified soy protein concentrates was not affected by both the protein and the mineral content, while the viscosity of the non-electroacidified soy protein concentrates increased with decreasing mineral content (or increasing protein content). The effect of minerals on the viscosity of the soy protein dispersions at pH 9 was attributed to the higher zeta potential (i.e., protein net charge). With increasing mineral content, the protein net charge is reduced, resulting in the compression of the electrical double layer and reduction of the electroviscous effects.

The presented study demonstrated the feasibility of combining electroacidification and membrane ultrafiltration for the production of soy protein isolates. The understanding of the effect of electroacidification on the formation of membrane fouling and the physicochemical properties of the soy protein extracts has been improved. The superior composition of the final soy protein isolate (lower ash and phytic acid content) and its lower viscosity, which reduces the axial pressure drop in the hollow fiber ultrafiltration system (and consequently the pumping costs) could compensate for the lower permeate flux obtained during the ultrafiltration of the electroacidified extract. The efficiency of the mineral and phytic acid removal could be enhanced by operating first in a continuous diafiltration mode, followed by ultrafiltration of soy proteins in a concentration mode. The potential of this novel processing technology should be investigated further.

Based on the presented findings, the future work should include:

1. Investigation of a continuous diafiltration to enhance the mineral and phytic acid removal.

2. Identification of the membrane fouling mechanisms in the hollow fiber ultrafiltration to determine effective methods for membrane fouling minimization (e.g., backflushing, creating a pulsatile feed flow).

3. Examination of different membrane materials that would be less prone to protein fouling.

4. Investigation of the interactions (e.g., hydrophobic, disulfide bonding) between the protein subunits of β-conglycinin and glycinin to find out about the role of these interactions in membrane fouling.

5. Study of the temperature effect on the ultrafiltration performance during the ultrafiltration of the soy protein extracts.

6. Evaluation of the surface hydrophobicity and the hydration properties of the soy proteins and their relation to the viscosity of the electroacidified and the non-electroacidified soy protein extract.

7. Characterization of the functional properties for the soy protein isolates produced by electroacidification and membrane ultrafiltration.

8. Detailed cost analysis taking into account operating, maintenance, and membrane cleaning costs and also the quality of the soy protein isolates (protein purity, functionality, and yield).

7

References

[1] M. Cheryan, Ultrafiltration handbook, Lancaster, Technomic, 1986.

[2] R. Ghosh, Protein bioseparation using ultrafiltration : Theory, applications and new developments, London, Imperial College Press, 2003.

[3] G. Belfort, R.H. Davis, and A.L. Zydney. The behavior of suspensions and macromolecular solutions in cross-flow microfiltration. J.Membr.Sci., 96 (1994) 1.

[4] A.D. Marshall, P.A. Munro, and G. Tragardh. The effect of protein fouling in microfiltration and ultrafiltration on permeate flux, protein retention and selectivity: A literature review. Desalination, 91 (1993) 65.

[5] M. Nystrom. Fouling of unmodified and modified polysulfone ultrafiltration membranes by ovalbumin. J.Membr.Sci., 44 (1989) 183.

[6] D. Mockel, E. Staude, and M.D. Guiver. Static protein adsorption, ultrafiltration behavior and cleanability of hydrophilized polysulfone membranes. J.Membr.Sci., 158 (1999) 63.

[7] M. Wahlgren, T. Arnebrant. Protein adsorption to solid-surfaces. Trends Biotechnol., 9 (1991) 201.

[8] D.J. Nichols, M. Cheryan. Production of soy isolates by ultrafiltration: Factors affecting yield and composition. J.Food Sci., 46 (1981) 367.

[9] K. Wilson, J.M. Walker, Protein and enzyme techniques, in Principles and techniques of practical biochemistry, Cambridge, Cambridge University Press, 1994, pp. 167.

[10] D.H. Everett, Basic principles of colloid science, London, Royal Society of Chemistry, 1988.

[11] R.J. Hunter, The calculation of zeta potential, in Zeta potential in colloid science: Principles and applications, London ; Toronto, Academic Press, 1981, pp. 59-124.

[12] ASA, World statistics, in SoyStats 2007: A reference guide to important soybean facts and figures, Saint Louis, MO, The American Soybean Association, 2007. Available at: www.SoyStats.com (Retrieved Nov 4 2007).

[13] K. Liu, Soybeans : Chemistry, technology and utilization, Gaithersburg, MD, Aspen Publisher Inc., 1999.

[14] G.J. Endres, Protein quality and human nutrition, in Soy Protein Products: Characteristics, Nutritional Aspects and Utilization, Champaign, IL, AOCS Press, 2001, pp. 10-19.

[15] M.C. Garcia, M. Torre, M.L. Marina, and F. Laborda. Composition and characterization of soyabean and related products. Crit.Rev.Food Sci.Nutr., 37 (1997) 361.

[16] V.H. Thanh, K. Shibasaki. Major proteins of soybean seeds: Reversible and irreversible dissociation of beta-conglycinin. J.Agric.Food Chem., 27 (1979) 805.

[17] D.D. Maenz, Enzymatic characteristics of phytases as they relate to their use in animal feeds, in M.(. Bedford and G. Partridge (Ed.), Enzymes in farm animal nutrition, Oxon, UK, CABI Pub., 2001, pp. 61-84.

[18] L. Oatway, T. Vasanthan, and J.H. Helm. Phytic acid. Food Rev.Int., 17 (2001) 419.

[19] E.W. Lusas, M.N. Riaz. Soy protein products: Processing and use. J.Nutr., 125 (1995) S573.

[20] A.M. Nash, W.F. Kwolek, and W.J. Wolf. Denaturation of soybean proteins by isoelectric precipitation. Cereal Chem., 48 (1971) 360.

[21] M.P. Hojilla-Evangelista, D.J. Sessa, and A. Mohamed. Functional properties of soybean and lupin protein concentrates produced by ultrafiltration-diafiltration. J. Am. Oil Chem. Soc., 81 (2004) 1153.

[22] A. Rao, H.E. Shallo, A.P. Ericson, and R.L. Thomas. Characterization of soy protein concentrate produced by membrane ultrafiltration. J.Food Sci., 67 (2002) 1412.

[23] C.L. Lah, M. Cheryan. Protein solubility characteristics of an ultrafiltered full-fat soybean product. J.Agric.Food Chem., 28 (1980) 911.

[24] N.S.K. Kumar, M.K. Yea, and M. Cheryan. Soy protein concentrates by ultrafiltration. J.Food Sci., 68 (2003) 2278.

[25] O. Omosaiye, M. Cheryan. Low-phytate, full-fat soy protein product by ultrafiltration of aqueous extracts of whole soybeans. Cereal Chem., 56 (1979) 58.

[26] M. Cheryan, F.W. Anderson, and F. Grynspan. Magnesium-phytate complexes: Effect of pH and molar ratio on solubility characteristics. Cereal Chem., 60 (1983) 235.

[27] F. Grynspan, M. Cheryan. Calcium phytate: Effect of pH and molar ratio on in vitro solubility. J. Am. Oil Chem. Soc., 60 (1983) 1761.

[28] A.G. Appurao, M.S.N. Rao. Binding of Ca(II) by 11S fraction of soybean proteins. Cereal Chem., 52 (1975) 21.

[29] A.G.A. Rao, M.S.N. Rao. Binding of Mg(II) by 11S fraction of soybean proteins. J.Agric.Food Chem., 23 (1975) 657.

[30] G.W. Wallace, L.D. Satterlee. Calcium-binding and its effect on properties of several food protein-sources. J.Food Sci., 42 (1977) 473.

[31] F. Grynspan, M. Cheryan. Phytate-calcium interactions with soy protein. J. Am. Oil Chem. Soc., 66 (1989) 93.

[32] L. Bazinet, F. Lamarche, R. Labrecque, and D. Ippersiel. Effect of KCl and soy protein concentrations on the performance of bipolar membrane electroacidification. J.Agric.Food Chem., 45 (1997) 2419.

[33] L. Bazinet, F. Lamarche, and D. Ippersiel. Comparison of chemical and bipolar-membrane electrochemical acidification for precipitation of soybean proteins. J.Agric.Food Chem., 46 (1998) 2013.

[34] M. Mondor, D. Ippersiel, F.O. Lamarche, and J.I. Boye. Production of soy protein concentrates using a combination of electroacidification and ultrafiltration. J.Agric.Food Chem., 52 (2004) 6991.

[35] M. Mondor, D. Ippersiel, F. Lamarche, and J.I. Boye. Effect of electro-acidification treatment and ionic environment on soy protein extract particle size distribution and ultrafiltration permeate flux. J.Membr.Sci., 231 (2004) 169.

[36] Z. Alibhai, M. Mondor, C. Moresoli, D. Ippersiel, and F. Lamarche. Production of soy protein concentrates. Desalination, 191 (2006) 351.

[37] B. Vaughan, High shear cross flow filtration of electroacidified soy protein extracts, MASc thesis, Department of Chemical Engineering, University of Waterloo, 2005.

[38] M. Friedman. Nutritional value of proteins from different food sources. A review. J.Agric.Food Chem., 44 (1996) 6.

[39] AAFC, Soybeans: Situation and outlook, in Bi-Weekly Bulletin, Winnipeg, Manitoba, Agriculture and Agri-Food Canada, 2005.

[40] M.C.L. Deogara, M.D. Delayno, A.M. Pilosof, and R.A. Macchi. Functional-properties of soy protein isolates as affected by heat-treatment during isoelectric precipitation. J. Am. Oil Chem. Soc., 69 (1992) 184.

[41] E.L. Arrese, D.A. Sorgentini, J.R. Wagner, and M.C. Anon. Electrophoretic, solubility, and functional-properties of commercial soy protein isolates. J.Agric.Food Chem., 39 (1991) 1029.

[42] O. Omosaiye, M. Cheryan, and M.E. Matthews. Removal of oligosaccharides from soybean water extracts by ultrafiltration. J.Food Sci., 43 (1978) 354.

[43] B.F. Harland, E.R. Morris. Phytate - A good or a bad food component. Nutr.Res., 15 (1995) 733.

[44] I.A. Al-Wahsh, H.T. Horner, R.G. Palmer, M.B. Reddy, and L.K. Massey. Oxalate and phytate of soy foods. J.Agric.Food Chem., 53 (2005) 5670.

[45] O. Adeola, J.S. Sands. Does supplemental dietary microbial phytase improve amino acid utilization? A perspective that it does not. J. Anim. Sci., 81 (2003) E78.

[46] M.I. Molina, J.R. Wagner. The effects of divalent cations in the presence of phosphate, citrate and chloride on the aggregation of soy protein isolate. Food Res.Int., 32 (1999) 135.

[47] J.D. Fox, J.F. Robyt. Miniaturization of three carbohydrate analyses using a microsample plate reader. Anal. Biochem., 195 (1991) 93.

[48] AOAC, Official method 923.03 and 925.09, in P. Cunniff (Ed.), Official Methods of Analysis, Washington, DC, AOAC International, 1995.

[49] P.T. Slack, Determination of total phosphorus (phospho-vanado-molybdate colorimetric method), in Analytical Methods Manual, Leatherhead, UK, Leatherhead Food Research Association, 1987.

[50] D.C. Montgomery, Simple comparative experiments, in W. Anderson, S. Russell and E. Aiello (Ed.), Design and Analysis of Experiments, New York, NY, Wiley, 2001, pp. 21-59.

[51] J. Skorepova, C. Moresoli. Carbohydrate and mineral removal during the production of low-phytate soy protein isolate by combined electroacidification and high shear tangential flow ultrafiltration. J.Agric.Food Chem., 55 (2007) 5645.

[52] W. Norde, F. MacRitchie, G. Nowicka, and J. Lyklema. Protein adsorption at solid-liquid interfaces: Reversibility and conformation aspects. J. Colloid Interface Sci., 112 (1986) 447.

[53] E. Matthiasson. The role of macromolecular adsorption in fouling of ultrafiltration membranes. J.Membr.Sci., 16 (1983) 23.

[54] A. Suki, A.G. Fane, and C.J.D. Fell. Flux decline in protein ultrafiltration. J.Membr.Sci., 21 (1984) 269.

[55] S.P. Palecek, A.L. Zydney. Intermolecular electrostatic interactions and their effect on flux and protein deposition during protein filtration. Biotechnol.Prog., 10 (1994) 207.

[56] S.P. Palecek, A.L. Zydney. Hydraulic permeability of protein deposits formed during microfiltration: Effect of solution pH and ionic strength. J.Membr.Sci., 95 (1994) 71.

[57] I.H. Huisman, P. Pradanos, and A. Hernandez. The effect of protein-protein and protein-membrane interactions on membrane fouling in ultrafiltration. J.Membr.Sci., 179 (2000) 79.

[58] Y. Mukai, E. Iritani, and T. Murase. Effect of protein charge on cake properties in dead-end ultrafiltration of protein solutions. J.Membr.Sci., 137 (1997) 271.

[59] M.K. Menon, A.L. Zydney. Effect of ion binding on protein transport through ultrafiltration membranes. Biotechnol.Bioeng., 63 (1999) 298.

[60] A.D. Marshall, P.A. Munro, and G. Tragardh. Influence of ionic calcium concentration on fouling during the cross-flow microfiltration of beta-lactoglobulin solutions. J.Membr.Sci., 217 (2003) 131.

[61] C. Vetier, M. Bennasar, and B.T. Delafuente. Study of the fouling of a mineral microfiltration membrane using scanning electron-microscopy and physicochemical analyses in the processing of milk. J.Dairy Res., 55 (1988) 381.

[62] R. Chan, V. Chen. Characterization of protein fouling on membranes: Opportunities and challenges. J.Membr.Sci., 242 (2004) 169.

[63] D.N. Lee, R.L. Merson. Examination of cottage cheese whey proteins by scanning electron-microscopy: Relationship to membrane fouling during ultrafiltration. J.Dairy Sci., 58 (1975) 1423.

[64] S.K.S. Razavi, J.L. Harris, and F. Sherkat. Fouling and cleaning of membranes in the ultrafiltration of the aqueous extract of soy flour. J.Membr.Sci., 114 (1996) 93.

[65] J. Yu, R.W. Lencki. Effect of enzyme treatments on the fouling behavior of apple juice during microfiltration. J.Food Eng., 63 (2004) 413.

[66] K.J. Kim, A.G. Fane, C.J.D. Fell, and D.C. Joy. Fouling mechanisms of membranes during protein ultrafiltration. J.Membr.Sci., 68 (1992) 79.

[67] E.M. Tracey, R.H. Davis. Protein fouling of track-etched polycarbonate microfiltration membranes. J.Colloid Interface Sci., 167 (1994) 104.

[68] M. Shirato, T. Murase, E. Iritani, and S. Nakatsuka. Experimental analysis of flux decline mechanism of batch ultrafiltration (filtration characteristics of gel layer). Filtr. Sep., 28 (1991) 104.

[69] P.C. Carman. Fundamental principles of industrial filtration (A critical review of present knowledge). Trans. Inst. Chem. Eng., 16 (1938) 168.

[70] S.A. Mourouzidis-Mourouzis, A.J. Karabelas. Whey protein fouling of microfiltration ceramic membranes: Pressure effects. J.Membr.Sci., 282 (2006) 124.

[71] W.R. Bowen, J.I. Calvo, and A. Hernandez. Steps of membrane blocking in flux decline during protein microfiltration. J.Membr.Sci., 101 (1995) 153.

[72] D.B. Genovese, J.E. Lozano, and M.A. Rao. The rheology of colloidal and noncolloidal food dispersions. J.Food Sci., 72 (2007) R11.

[73] I.R. Rutgers. Relative viscosity and concentration. Rheol. Acta, 2 (1962) 305.

[74] R.L. Hoffman. Factors affecting the viscosity of unimodal and multimodal colloidal dispersions. J.Rheol., 36 (1992) 947.

[75] B.E. Rodriguez, E.W. Kaler, and M.S. Wolfe. Binary-mixtures of monodisperse latex dispersions: 2. Viscosity. Langmuir, 8 (1992) 2382.

[76] A.T.J.M. Woutersen, C.G. Dekruif. The viscosity of semidilute, bidisperse suspensions of hard-spheres. J.Rheol., 37 (1993) 681.

[77] A.A. Zaman, B.M. Moudgil. Role of electrostatic repulsion on the viscosity of bidisperse silica suspensions. J.Colloid Interface Sci., 212 (1999) 167.

[78] F.M. Horn, W. Richtering. Viscosity of bimodal charge-stabilized polymer dispersions. J.Rheol., 44 (2000) 1279.

[79] H. Kimura, H. Niimi, A. Tsuchida, and T. Okubo. Importance of the electrical double layers for the rheological properties of colloidal liquids. Colloid Polym.Sci., 283 (2005) 1079.

[80] A.M. Hermansson. Functional properties of proteins for foods – Flow properties. J. Texture Stud., 5 (1975) 425.

[81] C.H. Lee, C. Rha, Rheological properties of proteins in solution, in P. Sherman (Ed.), Food texture and rheology, London, Academic press, 1979, pp. 245-264.

[82] C. Tanford, J.G. Buzzell. The viscosity of aqueous solutions of bovine serum albumin between pH 4.3 and 10.5. J.Phys.Chem., 60 (1956) 225.

[83] A.T. Paulson, M.A. Tung. Rheology and microstructure of succinylated canola protein isolate. J.Food Sci., 53 (1988) 821.

[84] C.L.A. Berli, J.A. Deiber, and M.C. Anon. Connection between rheological parameters and colloidal interactions of a soy protein suspension. Food Hydrocoll., 13 (1999) 507.

[85] D.B. Genovese, J.E. Lozano. Contribution of colloidal forces to the viscosity and stability of cloudy apple juice. Food Hydrocoll., 20 (2006) 767.

[86] C.H. Lee, C. Rha. Thickening of soy protein suspensions with calcium. J. Texture Stud., 7 (1977) 441.

[87] G.T. Meng, C.Y. Ma. Flow property of globulin from red bean (Phaseolus angularis). Food Res.Int., 34 (2001) 401.

[88] A.J. Carr, P.A. Munro, and O.H. Campanella. Effect of added monovalent or divalent cations on the rheology of sodium caseinate solutions. Int.Dairy J., 12 (2002) 487.

[89] M. Boulet, M. Britten, and F. Lamarche. Voluminosity of some food proteins in aqueous dispersions at various pH and ionic strengths. Food Hydrocoll., 12 (1998) 433.

[90] B. Yoo, M.A. Rao. Effect of unimodal particle-size and pulp content on rheological properties of tomato puree. J.Texture Stud., 25 (1994) 421.

[91] C.R. Daubert, H.M. Hudson, E.A. Foegeding, and P. Prabhasankar. Rheological characterization and electrokinetic phenomena of charged whey protein dispersions of defined sizes. Lwt-Food Sci. Technol., 39 (2006) 206.

[92] A. Malhotra, J.N. Coupland. The effect of surfactants on the solubility, zeta potential, and viscosity of soy protein isolates. Food Hydrocoll., 18 (2004) 101.

[93] I. Koshiyama, D. Fukushima. Physicochemical studies on 11S globulin in soybean seeds: Size and shape determination of molecule. Int.J.Pept.Protein Res., 8 (1976) 283.

[94] R.A. Badley, D. Atkinson, H. Hauser, D. Oldani, J.P. Green, and J.M. Stubbs. Structure, physical and chemical properties of soy bean protein glycinin. Biochim.Biophys.Acta, 412 (1975) 214.

[95] P. Plietz, G. Damaschun, J.J. Muller, and K.D. Schwenke. The structure of 11-S globulins from sunflower and rape seed: A small-angle X-Ray-scattering study. Eur. J. Biochem., 130 (1983) 315.

[96] R. Simha. The influence of Brownian movement on the viscosity of solutions. J.Phys.Chem., 44 (1940) 25.

[97] S.E. Harding. On the hydrodynamic analysis of macromolecular conformation. Biophys.Chem., 55 (1995) 69.

8

Appendix

8.1 Chemical structures of membrane materials

8.1.1 Polysulfone

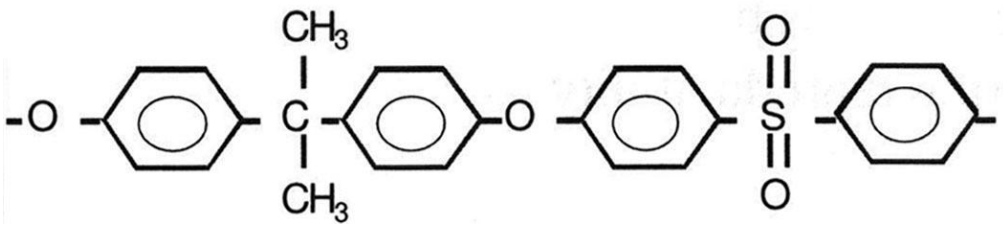

8.1.2 Polyethersulfone

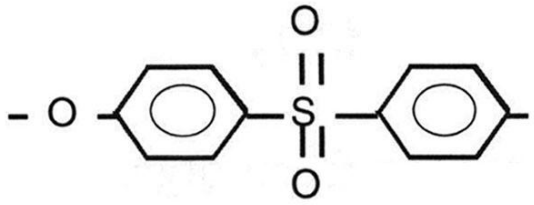

8.2 Chemical structure of phytic acid

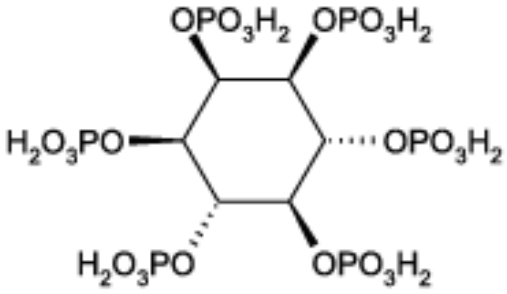

8.3 Mass balance for dead-end ultrafiltration

Samples from each filtration stream (feed, F; retentate, R; permeate, P) and the rinsing water (RW) were analyzed for TS and protein concentration. Knowing the volume (V) and the solute concentration (c_i) for each stream, one can calculate the mass balance according to Eq. (8-1):

$$\Delta = c_F V_F - \left(c_R V_R + c_P V_P + c_{RW} V_{RW}\right) \tag{8-1}$$

i.e. accumulation (Δ) = mass in – mass out. Ideally, there is no accumulation in the system (Δ = 0) which means total mass recovery. Accumulation in the system (Δ > 0) may occur due to adsorption and deposition of the solutes on the membrane surface. Therefore, the mass balance calculations can provide a quantitative estimate of protein deposition in the irreversible membrane fouling and can verify the results obtained from the protein desorption by soaking the membrane in SDS solution (see Section 4.2.4). The mass balance for the total solids calculated according to Eq. (8-1) is presented in **Table 8.1** (column d). For SPE 6, the mass accumulated in the system was around 1–2 % of the total TS mass in the feed. However, there is a discrepancy for SPE 9, because negative Δ values were obtained. This means there would have to be generation of mass in the system, corresponding to approximately 7.5 % of the initial TS mass, which is impossible.

Table 8.1 Mass balance calculations for ultrafiltration of SPE 6 and SPE 9 to VCR 2.5 using the 100 and the 200 kDa membrane.

Feed; MWCO	Stream	TS mass (g) [a]	Δ TS mass (g) [b]	TS mass (g) [c]	Δ TS mass (g) [b.c]	Protein mass (g)
SPE 6; 100 kDa	Feed	0.854 ± 0.009	0.009		0.081	0.454 ± 0.010
	Retentate	0.438 ± 0.004		0.366		0.242 ± 0.005 [c]
	Permeate	0.283 ± 0.006				0.008 ± 0.001
	Rinsing water	0.124 ± 0.003				0.115 ± 0.001
SPE 6; 200 kDa	Feed	0.850 ± 0.007	0.018		0.089	0.469 ± 0.012
	Retentate	0.428 ± 0.012		0.357		0.242 ± 0.012 [c]
	Permeate	0.279 ± 0.015				0.007 ± 0.003
	Rinsing water	0.125 ± 0.004				0.117 ± 0.000
SPE 9; 100 kDa	Feed	0.935 ± 0.011	-0.070		-0.008	0.613 ± 0.002
	Retentate	0.549 ± 0.013		0.487		0.399 ± 0.010 [c]
	Permeate	0.251 ± 0.002				0.014 ± 0.001
	Rinsing water	0.205 ± 0.010				0.206 ± 0.014
SPE 9; 200 kDa	Feed	0.926 ± 0.014	-0.071		-0.009	0.588 ± 0.009
	Retentate	0.543 ± 0.007		0.481		0.385 ± 0.015 [c]
	Permeate	0.252 ± 0.003				0.014 ± 0.001
	Rinsing water	0.202 ± 0.006				0.203 ± 0.009

[a] Mean ± standard error, at least to independent experiments. [b] Δ TS calculated according to Eq. (8-1). [c] Considering water evaporation rate at 0.41 mL/h.

As shown in **Figure 8.1** (a) for individual experiments, the Δ values are always negative for filtrations at pH 9 (SPE 9 and SPE 6 adjusted to pH 9) and tend to be positive for pH 6 filtrations (SPE 6 and SPE 9 adjusted to pH 6). There is no correlation with respect to the membrane MWCO.

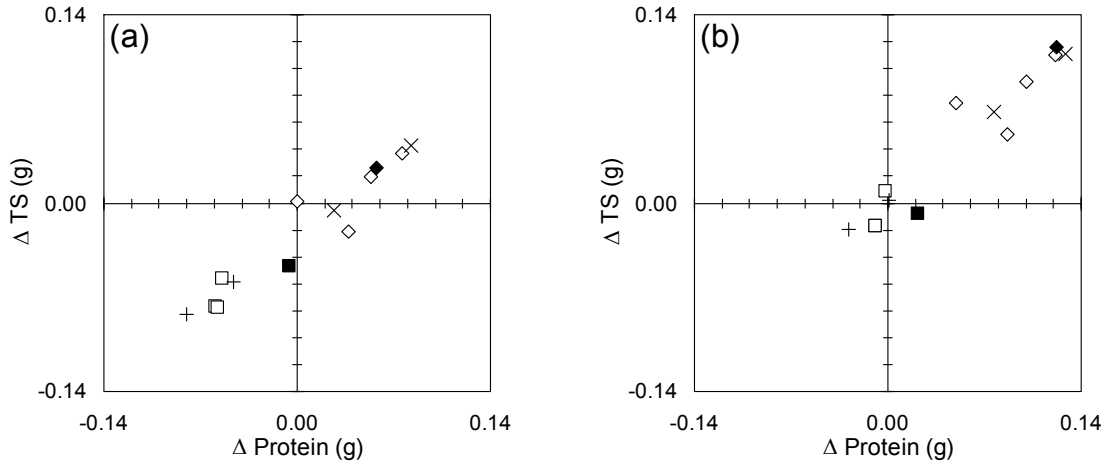

Figure 8.1 Mass balance calculations using the original data (A) and taking into account the evaporation rate of 0.41 mL/h (B) for ultrafiltration of SPE 9 to VCR 2.5 using the 100 kDa (□) and the 200 kDa (+) membrane, SPE 6 adjusted to pH 9 (■), SPE 6 using the 100 kDa (◇) and the 200 kDa (×), and SPE 9 adjusted to pH 6 (◆).

A possible explanation for this discrepancy could be water evaporation from the permeate during the experiments. The filtration is performed with a known volume of the feed solution. During the filtration, the permeate is collected in an open beaker, standing on a scale, its mass recorded, and converted to volume using the density of water. The retentate volume is determined by the difference between the feed and the permeate volume. The filtration is stopped when a given volume of permeate is collected (i.e., at a given VCR). Water evaporation over the course of the experiment would lead to over-collection of the permeate and underestimation of the retentate volume. Performing the filtrations up to VCR 2.5 took approximately 4.0, 5.5, 8.0, and 10.0 hours for SPE 6 adjusted to pH 9, SPE 9, SPE 6, and SPE 9 adjusted to pH 6, respectively. With such long filtration times, water evaporation seems likely to occur. To estimate the evaporation rate, a beaker was filled with water and the mass of water was recorded over a 10-hour period. The evaporation rate was estimated at 0.14 mL/h. Considering this evaporation rate and re-calculating the mass balance, the Δ values for the pH 9 filtrations in **Figure 8.1** (a) shifted closer to the origin of the coordinates but remained still negative. It is difficult to

determine the evaporation rate retrospectively, because it is a function of the temperature, the relative humidity, and the air-water interface area. The evaporation rate could have been higher during the filtrations, because the permeate drips slowly from a narrow tubing. Assuming, there is no mass accumulation in the system for SPE 9 filtrations, we can estimate that the evaporation rate would have to be as high as 0.41 mL/h. This would reduce the TS mass in the retentate by 16 and 11 % for the SPE 6 and SPE 9 filtrations, respectively (**Table 8.1**, column e). Re-calculating the mass balance according to Eq. (8-1) yields Δ values close to zero for SPE 9 filtrations and positive Δ values for SPE 6 filtrations **Table 8.1** (column f), indicating TS accumulation in the system for SPE 6. The results are also illustrated in **Figure 8.1** (b). The Δ values for protein calculated from the protein mass in column g, **Table 8.1** and Eq. (8-1) are 0.089, 0.103, -0.006, and -0.014 g for SPE 6 (100 kDa), SPE 6 (200 kDa), SPE 9 (100 kDa) and SPE 9 (200 kDa), respectively.

Protein deposition estimated by soaking the fouled membrane in SDS solution was 2.7 and 0.13 mg/cm^2 for SPE 6 and SPE 9, respectively (see Section 4.3.5), which corresponds to 77.5 and 3.7 mg (considering the membrane area of 28.7 cm^2). The protein deposition for SPE 9 is quite low and probably quite difficult to detect with the mass balance, considering the experimental error associated with the determination of TS and protein concentrations. On the other hand, the protein deposition for SPE 6 seems to be in a good agreement with the value obtained by the mass balance (i.e. 89 mg).

8.4 Bradford assay with purified soy proteins as standards

The calibration curves obtained by Bradford protein assay (Standard Procedure for Microtiter Plates, Bio-Rad Laboratories, Mississauga, ON, Canada) for BSA and purified soy proteins are compared in **Figure 8.2**. A mixture of β-conglycinin and glycinin was prepared by mixing the purified proteins in a 1:1.4 ratio, respectively. The slope of the calibration curves obtained for β-conglycinin, glycinin, and the mixture of the two proteins was 18, 27, and 23 %, respectively, lower than the slope obtained for BSA.

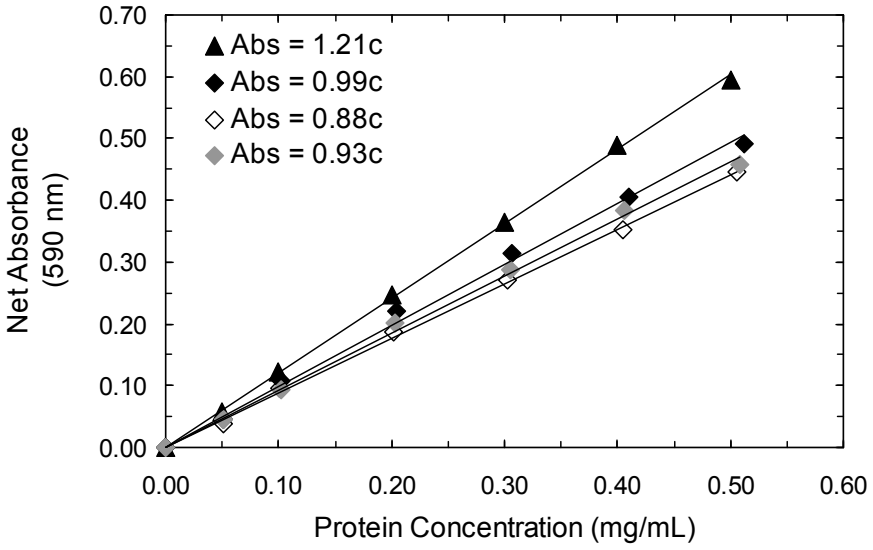

Figure 8.2 Calibration curves for BSA (▲), β-conglycinin (◆), glycinin (◇), and a mixture of β-conglycinin and glycinin (◆) combined in a 1:1.4 ratio.

8.5 Conductivity of soy protein extract solutions

The conductivity of the soy protein dispersions prepared at a TS concentration between 0.3 and 7 % w/w is shown in **Figure 8.3**. The conductivity of SPE 9 was always lower than that of SPE 6, which can be explained by the higher ash content for SPE 9 (10.4 %) compared to SPE 6 (8.0 %).

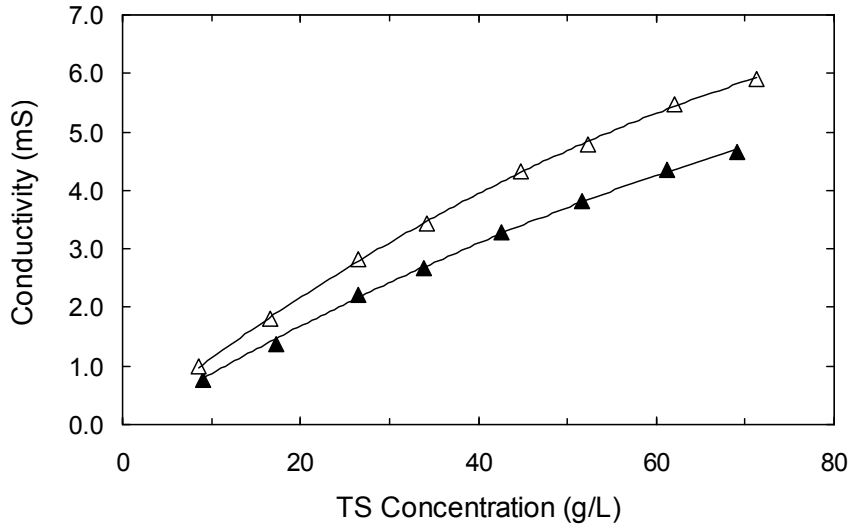

Figure 8.3 Conductivity of soy protein extract dispersions (25 ± 1 °C): SPE 6 (▲) and SPE 9 (△).

The conductivity measured for KCl solutions prepared at various molar concentrations is shown in **Figure 8.4**.

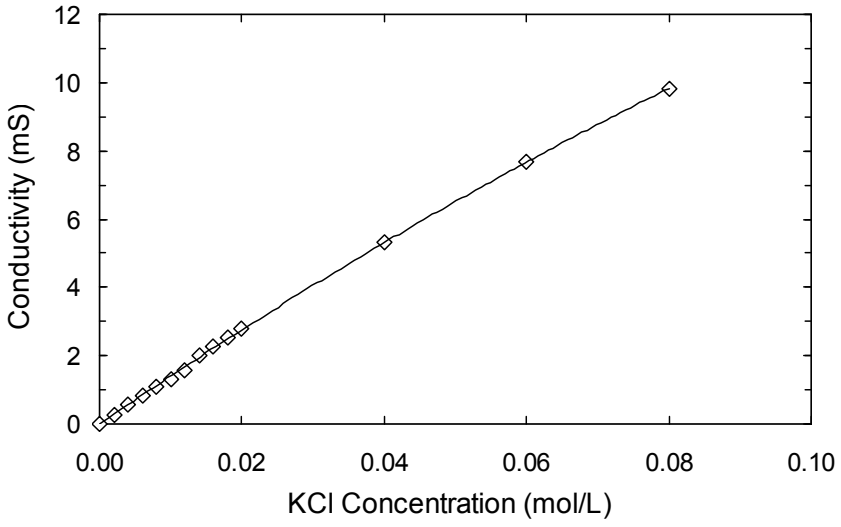

Figure 8.4 Conductivity of KCL solutions (25 ± 1 °C).

The conductivity of the feed, retentate and permeate samples obtained during direct UF to VCR 4.5 and two-stage discontinuous diafiltration in the hollow fiber system is shown in **Table 8.2**.

Table 8.2 Conductivity of feed, retentate and permeate samples collected during ultrafiltration experiments in the hollow fiber system.

Experiment	Conductivity (mS)			
	Feed	Retentate	Permeate	
SPE 6 Direct UF 1[a]	1.403	1.510	1.331	
SPE 6 Direct UF 2[a]	1.433	1.575	1.427	
SPE 9 Direct UF	1.990	2.280	1.830	
	Feed	Retentate	Permeate 1[b]	Permeate 2[b]
SPE 6 DDF	1.393	1.006	1.273	0.759
SPE 9 DDF	1.912	1.576	1.648	1.003

[a] Two replicate experiments. [b] Permeate 1 and 2 collected in DDF during stage 1 and 2, respectively. Conductivity measured at 25 ± 1 °C.